UNIVERSITY OF CALIFORNIA,
IRVINE

Innate and Adaptive Immunity in Aging and Alzheimer's Disease

DISSERTATION

submitted in partial satisfaction of the requirements
for the degree of

DOCTOR OF PHILOSOPHY

in Biological Sciences

by

Jaclyn Beck

Dissertation Committee:
Professor Mathew Blurton-Jones, Chair
Professor Marcelo Wood
Professor Leslie Thompson
Assistant Professor Vivek Swarup

2022

DEDICATION

To all of my fellow graduate students who struggled to keep going
while the world fell apart in 2020.

To Willow. I miss you every day.

TABLE OF CONTENTS

LIST OF FIGURES

Page

LIST OF TABLES

ACKNOWLEDGMENTS

I would like to thank my partner David, who moved across the country with me so I could pursue my PhD. You've supported me this whole time and I couldn't have made it through this without you.

Thank you to my committee members, past and present: Dr. Marcelo Wood, Dr. Leslie Thompson, Dr. Vivek Swarup, Dr. Karina Cramer, and Dr. Brian Cummings. You have all provided great insight and advice about my ERCC1 project, as well as encouragement and support when I doubted myself.

Thank you to my advisor, Dr. Mathew Blurton-Jones, for pulling me into the fascinating world of neuroimmunology.

Thank you to my fellow lab members Jessica Sanchez, Jean Paul Chadarevian, Sepideh Kiani Shabestari, and Christina Tu. Jessica, for including me on this T cell project, which turned out to be the most challenging and interesting research I have ever worked on. Jean Paul, Sepideh, and Christina for stepping up and providing a lot of help on the ERCC1 project when I really needed it.

A huge thank you to Manuella Yassa and the CNLM Ambassadors. You enabled me to discover my love of teaching in the most fun way possible, and volunteering with you all gave me my happiest memories of my time at UCI.

This work was funded by NIH-R01-AG056303 and NI-RF1-AG055524.

VITA

Jaclyn Beck

EDUCATION

PhD, Neurobiology and Behavior **2022**

M.Sc., Neurobiology and Behavior **2020**
University of California, Irvine, CA

M.Sc., Computer Sciences **2012**
University of Wisconsin, Madison, WI

B.S., Computer Science **2010**
Northern Michigan University, Marquette, MI

RESEARCH EXPERIENCE

The role of T cells in Alzheimer's Disease **2021–2022**

Advisor: Dr. Mathew Blurton-Jones, UCI

Analyzed single-cell RNA sequencing data obtained from several mouse models of AD pathology. Characterized different subpopulations of T cells that may interact with amyloid and tau pathology.

Aged Microglia and Alzheimer's Disease **2018–2022**

Advisor: Dr. Mathew Blurton-Jones, UCI

Created and validated a model of rapid aging in iPSC-derived microglia using a combination of cell culture, mice, and RNA sequencing analysis.

TEACHING EXPERIENCE

Head Teaching Assistant, Bio Sci 93 **2021**
University of California, Irvine

Teaching Assistant, Bio Sci 93 **2020**
University of California, Irvine

Instructor, UCI Brain Camp **2019**
University of California, Irvine

AWARDS

John Haycock Award, UCI Center for the Neurobiology of Learning and Memory **2022**

Division of Teaching Excellence and Innovation Summer Graduate Fellowship, University of California, Irvine **2021**

CERTIFICATES AND TRAINING

Certificate in Inclusive Hybrid Teaching, UCI School of Biological Sciences **2021**

Improv for Teaching, Activate to Captivate **2020**

Mentoring Excellence Program, UCI Graduate Division **2020**

Certificate in Course Design, UCI Division of Teaching Excellence and Innovation **2020**

Associate Level, Center for the Integration of Research, Teaching and Learning, UCI Division of Teaching Excellence and Innovation **2020**

SERVICE

CNLM Abassadors, Member **2018–2022**

Irvine Brain Bee Committee, Member **2021–2022**

CNLM Ambassador Communications Committee, Chair **2019**

Brain Explorer Academy, Mentor **2019**

Irvine Brain Bee, Mentor **2019–2020**

JOURNAL PUBLICATIONS

Coburn, MA, England, W, Hasselmann, J, McQuade, A, Picard, K, Lau, V, Silva, J, **Beck, J**, Shabestari, SK, Tremblay, MÉ, Spitale, RC, Davtyan, H, Blurton-Jones, M. (2022). Human microglia differentially respond to beta-amyloid, tau and combined Alzheimer's Disease Pathologies in vivo. EMBO, *In Review.*

Bolton, JL, Short, AK, Othy, S, Kooiker, CK, Shao, M, Gunn, BG, **Beck, J**, Bai, X, Law, SM, Savage, JC, Lambert, JJ, Belelli, D, Tremblay, MÉ, Cahalan, MD, Baram, TZ. (2022). Impaired developmental microglial pruning of excitatory synapses on CRH-expressing hypothalamic neurons exacerbates stress responses throughout life. *Cell Reports*. https://doi.org/10.1016/j.celrep.2022.110600

ABSTRACT OF THE DISSERTATION

Innate and Adaptive Immunity in Aging and Alzheimer's Disease

By

Jaclyn Beck

Doctor of Philosophy in Biological Sciences

University of California, Irvine, 2022

Professor Mathew Blurton-Jones, Chair

Alzheimer's Disease is the most common form of dementia and is the fifth-leading cause of death in people age 65 and older. Unfortunately, no cure currently exists, and the few treatment options may temporarily relieve symptoms but have limited long-term effectiveness. Recent genome-wide association studies (GWAS) have unearthed a strong link between immune-related genes and AD risk. Both the innate and adaptive immune system have been implicated in the progression of AD, and much of the neuroinflammation that exists in this disease is thought to be related to an age-related decline in immune function. Microglia, the innate immune cells of the brain, become a large source of dysfunctional inflammation as they become chronically activated by the amyloid-beta (Aβ) plaques and tau tangles that aggregate in the AD brain. The protective functions of microglia are known to decline with age, yet it is still unclear what separates healthy and pathogenic aging of these cells. T cells, which typically exist in small numbers in the healthy brain, infiltrate the parenchyma in large numbers in response to AD-related inflammation. The mechanisms that recruit T cells to the brain and the effects that these cells have on pathology remain understudied, especially for $CD8^+$ and γδ T cell subpopulations.

Chapter 1 of this dissertation explores the interaction of infiltrating T cells with amyloid plaques and tau tangles in AD model mice. In this study, we examined T cells from bone marrow transplantation studies and from immune-intact AD model mice using flow cytometry, immunohistochemistry, and single-cell RNA sequencing. We found evidence of significant infiltration of multiple T cell phenotypes in AD model mice, with $CD8^+$ effector memory T cells forming the largest population.

We also found clonal expansion of T cells from mice that developed Aβ pathology or Aβ and tau pathology, but not in mice with tau pathology alone, suggesting that early recruitment and clonal expansion of T cells is primarily amyloid-driven. These experiments provide an important resource for future investigations into the role of $CD8^+$ T cells in AD.

Chapter 2 of this dissertation describes the creation of a model of premature aging in human iPSC-derived microglia, which was developed to facilitate research into human-specific age-related dysfunction in microglia. To create an aged phenotype in iPSCs, we induced homozygous genetic knockout of ERCC1, a critical DNA repair enzyme that causes progeroid diseases in patients with near-total loss of ERCC1 expression. *In vitro* assays and single-cell RNA sequencing of xenotransplanted microglia reveal signs of immune dysfunction, early senescence, and an increase in pro-inflammatory interferon signaling in ERCC1 KO microglia that may indicate a more aged phenotype. While further examination of this model is required, ERCC1 KO in iPSCs provides a platform for testing age-related microglial dysfunction in AD and other neuroinflammatory diseases.

INTRODUCTION

Alzheimer's Disease (AD) is a neurodegenerative disease that affects over 6 million people in the United States. AD is also the most common cause of age-related dementia, and patients with AD can suffer from an array of cognitive symptoms including memory loss, confusion, difficulties with decision making, and personality changes [1]. As this disease progresses and additional brain regions become affected, patients also lose the ability to care for themselves or even move around, giving rise to other serious health issues including malnutrition, blood clots, and infections. AD is eventually fatal and is currently the fifth leading cause of death for people 65 and older [1].

Unfortunately, the prevalence of AD represents a growing crisis, as the largest risk factor for AD is age. About 3% of people ages 65-74 are living with AD, but this number increases drastically with age such that 32% of people over 85 years of age have AD [1]. A large segment of the U.S. population, the "baby boomer" generation, is now between the ages of 55 and 75 and as this generation continues to age, the incidence of AD will likewise continue to rise. By 2050, it is projected that the amount of people living with AD will more than double, to about 14 million people suffering from the disease in the US alone [1]. Therefore it is becoming increasingly urgent that we learn how to detect, prevent, and treat AD before symptoms severely impact people's lives.

Biological Changes Underlying Alzheimer's Disease

Two key neuropathological changes within the brain are thought to underlie the development and progression of AD. The first of these "hallmark" pathologies is the accumulation of amyloid-β (Aβ), a misfolded 40-42 amino acid peptide that forms insoluble extracellular aggregates termed amyloid plaques. The second is a buildup of hyper-phosphorylated tau (pTau) protein within neurons, which forms "neurofibrillary tangles" (NFT) that interfere with neuronal function and axonal transport [2, 3]. Importantly, AD patients also commonly exhibit amyloid buildup within the brain vasculature, which may reduce blood flow to the brain or increase permeability of the protective blood brain

barrier (BBB) [3]. Together, Aβ and pTau cause neuronal dysfunction, synaptic loss, and, eventually, the death of large numbers of neurons. Interestingly, both pathologies build up over years, with Aβ plaques beginning to accumulate as much as 20 years prior to the onset of dementia [1, 3–5]. In fact, some models suggest that Aβ plaque load may peak or plateau prior to cognitive decline [5]. This makes AD difficult to treat, as by the time patients or their families notice cognitive impairment, their brain has already been degenerating for several years. Unfortunately, the only currently available medications manage symptoms for a relatively short period of time but fail to modify pathology or disease progression [1, 2], and late-stage clinical trials targeting removal of Aβ have largely failed [3, 6]. In order to effectively treat this disease, it is necessary to better understand what causes Aβ and pTau to accumulate with age.

Genetics and environment both contribute to Alzheimer's Disease

A small set of dominantly-inherited genetic mutations are known to definitively cause AD in humans. Yet, these "familial mutations" are rare and these patients only account for between 1 and 5% of all AD cases [1–3]. Nevertheless, a great deal has been learned from the identification of the three genes that underlie "early onset" or familial AD (FAD). Specifically, mutations in amyloid precursor protein (APP), presenilin 1 (PSEN1), or presenilin 2 (PSEN2) result in either overproduction of Aβ or a shift in the ratio of Aβ species toward an increase in the more neurotoxic 42 amino acid form ($A\beta_{42}$). In addition, patients with trisomy 21, or Down's Syndrome, are also at high risk of developing AD. APP is located on chromosome 21, and thus Down's Syndrome patients harbor an extra copy of APP, resulting in increased Aβ production throughout life and a high incidence of early-onset AD in this population [1].

In contrast to these dominantly-inherited forms of AD, the vast majority (around 95%) of AD cases are sporadic, or "late onset" AD (LOAD), and have no single genetic cause. However, twin studies have shown that LOAD is approximately 60–80% heritable, indicating a polygenic influence [7]. That is, while no single gene is responsible for LOAD, combinations of variants in multiple genes can drive increased risk of developing AD. Recent genome-wide association studies (GWAS) have identified over 170 risk loci associated with LOAD [8–10]. Variants in genes associated with these

loci either increase or decrease risk of developing the disease, however possession of a risk allele does not guarantee disease development or severity. Similarly, people without any known risk variants may develop AD. One study of patients from ROSMAP, a combined data set consisting of the Religious Orders Study and the Rush Memory and Aging Project, found that all known AD risk variants accounted for less than 10% of the variance in AD plaque and tangle severity and cognitive decline between patients [11]. Clearly, some other environmental, lifestyle, or biological factors play a significant role in the development and severity of AD.

In fact, several environmental and societal risk factors have been identified. For example, twice as many women as men have AD, though it is not clear if this is strictly due to biological sex or to differences in longevity, healthcare, and other socioeconomic factors between men and women [1]. In addition, lifestyle factors such as diet and exercise, and the presence of co-morbidities including heart disease, obesity, and diabetes, can all affect the cumulative risk of developing AD [1]. Regardless of these other factors, age still remains the largest risk factor for LOAD, so it is critical to study how the aging process may contribute to neurological disease.

Microglia in Alzheimer's Disease

Aberrant aging of one cell type in particular has recently become a major focus within the field. Microglia are the brain's resident innate immune cells. They play a role in both brain development and maintenance by pruning synapses, removing debris and dying cells, and clearing misfolded proteins [2–4, 12–15]. Unlike many terminally differentiated cells, microglia are capable of self-renewal, and will proliferate in response to injury [2, 6, 12, 16, 17].

In the healthy brain, microglia exist along a spectrum from homeostatic to activated. Homeostatic microglia typically exhibit a ramified morphology with long, thin, branching processes that monitor neurons and the brain environment for changes [2, 4, 13–15]. They are dispersed homogeneously throughout the brain, with each cell having a "territory" to survey with their constantly-moving processes [15]. Microglia also secrete a variety of anti-inflammatory cytokines and growth factors including IL-10, TGFβ1, and BDNF, which can help mediate injury repair or synaptic remodeling

[2, 16, 17]. However, microglia can also become "activated" by various factors including signals from injured neurons, misfolded proteins, and foreign pathogens. When activated, they adopt a more amoeboid shape and will migrate their processes and even their whole cell body to the site of injury [2, 12, 13, 15]. Activated microglia tend to secrete a different set of proteins, including pro-inflammatory cytokines such as TNFα, IL-1β, and IL-6. Activated microglia can also upregulate phagocytosis machinery and reactive oxygen species (ROS) production to respond to injury or debris [2–4]. In AD, both the accumulation of Aβ and neuronal dysfunction caused by pTau can trigger an activated microglial response [2–4, 12, 13], which makes their function or dysfunction in AD a critical area of study.

Microglia initially protect the brain from disease

In early disease stages, general microglial activation could be protective. In patients with mild cognitive impairment (MCI), greater microglial activation, as measured by TSPO PET imaging, corresponded with higher Mini-Mental State Examination (MMSE) scores, larger gray matter volume, and slower rate of cognitive decline [18]. A similar study found that microglial activation decreased over time in MCI patients, which corresponded to an increase in amyloid deposition [19].

One activation profile in particular may be helpful in combating pathology. In both humans and mice, microglia cluster around Aβ plaques and express markers of activation like CD11c and HLA-DR [2]. The cells form a physical protective barrier around the plaques, compacting them to reduce their contact with neurons [20]. These plaque-surrounding cells make up a unique population, known as "disease-associated microglia" (DAMs) [21]. DAMs in mice upregulate several known AD risk genes involved in Aβ clearance, such as *Apoe* and *Trem2*. Loss of this DAM population resulted in worsened pathology in AD-model mice [21], suggesting that this specific response to Aβ plaques may be an essential protective function of microglia. Interestingly, while a DAM population can be seen in human microglia xenotransplanted into 5xFAD mice [22], microglia from AD patient tissue only weakly display the DAM phenotype [23]. Instead, they take on a transcriptomic profile the authors designate as "HAM" (human Alzheimer's microglia), characterized by enhanced

changes in genes related to aging. It is unclear whether this change is due to differences in brain environment between species, or if this perhaps indicates a failure of protective DAM mobilization in LOAD [23].

Dysfunctional microglia in the AD brain

One of the hallmarks of AD is chronic neuroinflammation, and continuously-activated microglia may switch from being protective to harmful during the course of the disease. Although the phagocytic DAM phenotype seems to be protective, there is evidence that microglia are not efficient at clearing Aβ in AD conditions. Two microglia ablation studies showed that elimination of microglia in AD mice for several weeks had no effect on plaque number or size, or on amount of soluble or insoluble Aβ in the brain [24, 25]. Additionally, microglial elimination actually resulted in improved cognition [24]. This suggests that microglia are not effectively removing Aβ from the AD brain, and may in fact contribute to neurotoxicity. This deficiency may be a result of aging, as young microglia are effective at Aβ uptake but lose efficiency in adulthood [26, 27]. The presence of excess Aβ may also exacerbate this by creating a feedback loop of suppression, as microglia from AD-model mice down-regulate Aβ-binding receptors and Aβ degrading enzymes while still producing pro-inflammatory cytokines. The secreted cytokines, especially TNFα and IL-1β, may result in further downregulation of Aβ clearance-related systems and synaptic dysfunction [27, 28].

Any remaining clearance function in these cells appears to shift from protective to toxic in the AD brain. Microglia from AD tissue have Aβ fibrils in their endoplasmic reticulum and cell membrane instead of in lysosomes, which may be due to either buildup of unprocessed fibrils or to production of fibrils from monomeric or oligomeric Aβ [29, 30]. These studies hypothesized that in addition to being unable to clear Aβ, microglia may actually a source of plaques in the brain. In support of this, several studies have noted that the acidic environment of lysosomes is conducive to fibril formation, whereas the extracellular brain space is not [30–32]. One study in human tissue and young AD mice found fibril Aβ accumulating in microglia that were not near any plaques, ruling out existing plaques as a source of the fibrils [32]. The same study showed that with lifelong microglial elimination in AD mice, plaques do not form in the brain except near surviving microglia.

In contrast, a study of an AD mouse model with genetically-deleted microglia (5X-FIRE mice) found that without microglia to compact them, plaques still form, however they are more diffuse, and the majority of Aβ shifts to blood vessels instead of brain tissue [33]. Another time-lapse study in mice observed that over-accumulation of Aβ in the lysosomes of microglia eventually caused cell death and the release of compacted Aβ, which may act as a "seed" for a new plaque [31].

There is also evidence that microglia increase tau tangle pathology and neurodegeneration. Microglia play a key role in propagating tau tangles from neuron to neuron, by engulfing tau fibrils and then excreting them for other neurons to take up [34]. Chronic exposure to tau pathology appears to cause microglial activation as well as loss of structural integrity, resulting in microglia that are fragmented [35]. In turn, microglial inflammasome activation seems to exacerbate pTau formation in neurons. One study found that knockout of *Nlrp3* in Tau22 mice results in a decrease in tau pathology and cognitive decline [36]. Another study was able to induce pTau formation in young 3xTg-AD mice with injection of lipopolysaccharide (LPS), a potent inflammasome activator [37]. The authors suggest that pTau formation may be triggered by IL-1β, which is secreted by activated microglia. Activated microglia also secrete IL-1α, TNFα, and C1q, which has been shown to induce astrocytes to an activated (A1), neurotoxic state [38]. In addition to astrocyte neurotoxicity, exposure to tau can directly induce microglial phagocytosis of neurons [39], which may contribute to neurodegeneration and cognitive decline.

Collectively, these studies suggest that there may be a degenerative feedback loop between pathology accumulation, microglial activation, neurotoxicity, and microglial dysfunction. Both Aβ and tau pathology begin accumulating during middle age, so it is critical to understand the interplay between healthy and dysfunctional microglial aging if we are to understand how AD develops.

Aged Microglia in Health and Disease

Many traits of AD-associated microglia are also present in microglia from "healthy" aged brains. Some of these commonalities include lowered phagocytic function, increased inflammasome

function, morphological changes, and dysfunctional immune signaling characterized by an increase in both pro- and anti-inflammatory cytokines [12, 28, 40–42].

RNA sequencing analysis of aged human microglia revealed a general down-regulation of genes related to homeostasis and microglia-neuron interaction (CX3CR1, P2RY12, P2RY13, and CSF1R) coupled with an increase in pro-inflammatory genes (SPP1, APOE, LPL, and LIPA) and an increase in interferon signaling [43–45]. Many of these changes are reflected in studies of aged mice, although there are some differences between species [42, 46–49].

Morphological studies have shown that both mouse and human microglia become less ramified with age, exhibiting shorter and less complex branching [6, 50, 51], however the majority of observed cells do not resemble amoeboid, classically activated microglia. Aged human, but not mouse, microglia also have dystrophic processes characterized by swelling, fragmentation, or a beaded appearance, along with loss of structural integrity of the cell body [6, 12, 35, 52]. This change seems to correlate with exposure to pTau and an age-related accumulation of intracellular iron, which causes oxidative stress [52–54]. In mice, aged microglia also exhibit increases in soma volume and movement [55], decreased process motility, and a decrease in territory covered by processes [50]. Microglial number and density appear to increase with age, and cell distribution becomes less even and more clustered throughout the brain [50, 51, 55].

Functional and histological studies in mice have helped shed light on aged microglial behavior which is not feasible to study in human tissue. Microglia in aged mice adopt a "primed" phenotype in which they are not especially neurotoxic at rest but will produce a prolonged and exaggerated inflammatory response to immune insults when compared to activated young microglia [47, 56]. They will also migrate to injury sites and remain aggregated in the area significantly longer than young microglia [50]. Despite this exaggerated response, aged microglia are less efficient at Aβ phagocytosis [42], and accumulate myelin basic protein (MBP) that they are seemingly unable to break down [57]. Aged microglia also harbor a greater number of cell inclusions overall, which may contain lipid droplets, cellular debris, and lysosomal debris [51], again indicating a failure in clearance function. Some of these inclusions even appear to contain axon terminals and spines, suggesting an increased role in neuronal stripping with age [51].

Neuronal stripping is further supported by the presence of "dark microglia", which are so named due to their electron-dense interior giving them a dark appearance in electron microscopy images [58]. These microglia appear to be highly phagocytic and display signs of oxidative stress. Importantly, they are often seen encircling synapses, axon terminals, spines, and blood vessels, and they become more prevalent in both aged and AD-model mice [58].

Taken together, these studies show a shift away from homeostais toward inflammation and neurotoxicity with increased age. Aging microglia exhibit a dysfunctional combination of both increased and decreased immune signaling, over-reactive but less effective responses to immune insults, and decreased communication and self-regulation [12, 56]. Age-related microglial dysfunction largely parallels AD-related dysfunction (Table 1), and it may be that small perturbations to an already stressed system are enough to drive the brain toward neurodegeneration.

Human and murine microglia age differently

Despite what mouse studies have shown about microglial aging, caution must be used when translating this knowledge to human aging. Laboratory mice are kept in relatively sterile conditions, which limits immune challenges and diseases that may affect murine microglia. Humans, on the other hand, are exposed to many immune challenges and over a much longer lifespan, which affects microglial health, behavior, and turnover [59]. Accordingly, many differences between aged human and murine microglia have already been found across a range of studies.

Comparisons of RNA transcriptomes from human and mouse microglia highlight drastic differences between species during aging. One study found 572 genes changed with age in human microglia, however only 40 of those genes overlap with changes seen in aged murine microglia [43, 49]. Further, only about half of those 40 genes had altered expression in the same direction between the two species. This leaves only 2% of gene changes in aged murine microglia that correspond with human microglial changes [43]. It is important to note, however,

that microglia display region-dependent transcriptome profiles [49], which may affect comparisons between human and mouse data sets.

Few studies have examined the role of microglia-specific cytokine and chemokine signatures in aging, as most studies analyze whole brain tissue or mixed glia cultures. Where such cell-specific data exists, human and mouse measurements often conflict. For example, while several studies of mouse microglia have shown an increase with age in expression of pro-inflammatory cytokines [42, 47, 48], RNA sequencing data from human cohorts does not show a significant change in these cytokines with age [43, 44]. Human studies of whole brain tissue have observed an increase in both pro- and anti-inflammatory cytokines, however it is not clear how much of this contribution is due to microglia and how much is from astrocytes or other cell types [40, 41].

Morphological differences also exist between aged human and mouse microglia. Microglia in human tissue have a much larger decrease in branching complexity with age than those in mice, and the dystrophic processes seen in human tissue are not seen in aged WT or AD-model rodents [6, 12]. To date, no studies have examined whether dark microglia are over-represented in the aging human brain as they are in the murine brain, and studies comparing morphology and inflammatory markers at different ages in human tissue are also lacking. This makes it challenging to determine whether these characteristics of aged mouse microglia parallel human microglia.

Given these differences and lack of studies comparing young and aged human tissue, several key aspects of human microglial aging remain unclear, including cytokine production, immune function, and interaction with neurodegenerative conditions [59]. This disparity highlights the need for more studies of human microglia and better models of human aging, which could in turn benefit neurodegeneration research and drug discovery.

Feature	Aging		AD		Sources
	Hu	Ms	Hu	Ms	
Gene Changes					
Immune Response (APOE, SPP1, MHC II/HLA)	↑	↑	↑	↑	[21, 23, 37, 44–47, 60, 61]
Immune Response (TREM2)	↑↓	↑↓	↑	↑	[21, 44, 46, 47, 60, 62]
Immune Response (TLRs)	↓	↑	ns	↑↓	[23, 43, 44, 46, 47, 61, 62]
Priming (CLEC7A, MRC1, MSR1)	↓	↑	ns	↑	[21, 23, 44, 46, 47, 61, 63]
Priming (AXL, ITGAX/CD11c, LGALS3)	ns	↑	ns	↑	[21, 23, 43, 44, 46, 47, 60, 61, 63]
Cytokines (IL-1β, TNFα, IL-6)	ns	↑	ns	↑	[23, 28, 42–44, 46–48, 61, 64]
Homeostasis (P2RY12, P2RY13, CX3CR1)	↓	↓	ns	↓	[21, 23, 43–47, 49, 61, 63]
Morphology and Function					
Cell Clustering	↑	↑	↑	↑	[28, 35, 51, 53, 55]
Ramification, Branching Complexity	↓	↓	↓	↓	[35, 50, 55, 65]
Number and Density	?	↑	?	↑	[50, 51, 57, 65]
Dark Microglia	?	↑	?	↑	[58]
Dystrophic Processes	↑	ns	↑	ns	[6, 35, 53]
Motility	?	↓	?	↓	[27, 43, 49, 50]
Aβ Clearance	?	↓	?	↓	[24–28, 42]

Table 1: Key changes seen in microglia with aging and AD in human and mice. Arrows indicate direction of change from young to aged and age-matched to AD microglia, respectively. Legend: (ns): The associated gene was not significantly up- or down-regulated in the referenced data sets. (↑↓): The referenced data sets conflict on direction of change. (?): This feature has not been adequately studied in the referenced species.

T Cells in Alzheimer's Disease

Microglia have become a popular area of study in AD research since the discovery that many AD risk variants, such as TREM2, MS4A6A, and CD33, are highly or exclusively expressed by microglia in the brain [2–4, 8, 9, 14]. However, recent studies have also shown significant infiltration of T cells into the brain in multiple neurodegenerative diseases, with both beneficial and harmful effects [66–72]. Yet, the role of T cells in AD remains understudied, and research on this topic is complicated by these cells' adaptability and the multiple T cell sub-types that can exhibit vastly different behaviors.

T cell development creates a highly flexible immune response

To understand how T cells migrate into the brain and how different phenotypes influence AD, it is important to discuss T cell development. Lymphocyte progenitors form in the bone marrow but then migrate to the thymus, an immune organ located in the upper chest just above and in front of the heart, to mature into T cells. Once in the thymus, each progenitor commits to the T cell lineage and begins rearranging pieces of its genome to create a unique T cell receptor (TCR) sequence [73, 74].

Each cell's signature receptor is created from a combination of either TCRα and TCRβ genes, creating an $\alpha\beta$ TCR, or TCRγ and TCRδ genes, resulting in a $\gamma\delta$ TCR. The number of possible combinations of rearranged $\alpha\beta$ or $\gamma\delta$ genes ensures that each developing T cell has a unique TCR with the potential to recognize an enormous range of antigens. These genome rearrangements permanently alter the T cell's DNA, so any future proliferation of a given T cell will result in clones with identical TCRs to the original [73–75].

T cell receptors cannot recognize free-floating antigen. Rather, they require other cells to "present" antigens on their surface, usually via major histocompatibility complex (MHC) class I or II molecules [73, 74]. T cells that express the co-receptor CD8 are restricted to binding to MHC class I molecules for antigen recognition. MHC I molecules are expressed by most nucleated

cells in the body, allowing infected cells of any type to present pieces of internal pathogens for T cells to recognize. T cells that express CD4 can only bind to antigens presented on MHC class II molecules. MHC II molecules are selectively expressed by antigen-presenting immune cells (APCs) like dendritic cells, macrophages, and B cells. A small population of T cells remain double-positive for CD4 and CD8, and can therefore recognize both types of MHC molecules.

Nearly all $CD4^+$ and $CD8^+$ cells are $\alpha\beta$ T cells, while most $\gamma\delta$ cells are $CD4^-CD8^-$ and can bind to a variety of molecules other than classical MHC I or II complexes, many of which are still unknown. The majority of T cells in both humans and mice have $\alpha\beta$ TCRs, with only a small percentage carrying $\gamma\delta$ TCRs [76–78].

Naive T cells

T cells which have fully formed but have not yet recognized their antigen are called "naive" T cells. Naive cells circulate through the lymphatic system and lymphoid organs until they either encounter an antigen they recognize or die from lack of stimulation [79].

Effector T cells

When a naive T cell recognizes its antigen, typically in the thymus or lymph nodes, it will become activated and rapidly proliferate to produce clones with identical TCRs. These clones, or effector T cells (T_{Eff}), have varying functions that are determined by expression of specific co-receptors and by cytokines in the surrounding environment [80, 81]. Most $CD4^+$ cells will become "helper" T cells, of which there are at least 7 distinct sub-types that secrete cytokines that recruit, activate, or otherwise affect other immune cells. $CD8^+$ cells will generally become cytotoxic "killer" T cells, which induce apoptosis in infected cells bearing the recognized antigen. A small population of $CD4^+$ or $CD8^+$ cells will become regulatory T cells (T_{reg}) with immunosuppressive functions. $\gamma\delta$ T cells take on several different phenotypes that can be helper-like or cytotoxic. After 4-5 days of proliferation, effector cells leave the thymus or secondary lymphoid organ and follow a gradient of chemokines to the site of infection. Once there they secrete their type-specific effector cytokines, which have a range of effects including recruitment of other immune cells, induction of apoptosis in infected cells, and reinforcement of immune cell survival [80].

Memory T cells

When the infection is resolved, T_{Eff} cells undergo "clonal contraction" to reduce the population of expanded clones. Loss of IL7R on activated effectors reduces their responsiveness to the survival cytokine IL-7, and prolonged loss of this signal eventually induces apoptosis. A small number of T_{Eff} cells retains or re-expresses IL7R, however, and these survive as "memory" T cells to guard against future re-infection. These cells can survive for decades and have a lower threshold for activation than naive T cells, allowing them to quickly proliferate into effectors if they encounter their antigen again [82].

Memory T cells typically take on one of three phenotypes. Central memory (T_{CM}) cells are naive-like and express CD62L/SELL and CCR7, which allows them to re-enter the lymphatic system to circulate. Effector memory (T_{EM}) cells are $CD62L^{-}CCR7^{-}$ and express receptors for inflammatory cytokines that allow them to rapidly respond to re-infection. Finally, resident memory (T_{RM}) cells express CD69, and are also $CD62L^{-}CCR7^{-}$ but do not circulate at all [80–82].

T cells infiltrate the brain in response to neuroinflammation

The central nervous system has multiple protective barriers to prevent activated (and potentially neurotoxic) immune cells from reaching the brain. Both the blood-brain-barrier (BBB) and the blood-leptomeningeal-barrier (BLMB) consist of blood vessels and capillaries that are surrounded by pericytes and astrocytes, which physically block immune cells from entering the CNS [83, 84]. However, a small number of T cells and other components of the adaptive immune system do enter and populate the CNS under normal "healthy" conditions [83–86]. Studies have found T cells in the cerebral spinal fluid (CSF), meninges, and, to a lesser extent, the brain parenchyma itself in healthy brain tissue [83, 85]. One possible entry point is the choroid plexus, which produces cerebral spinal fluid (CSF) and may act as a "gate" to allow T cells through. The environment of cytokines and surface proteins in the choroid plexus skews T cells toward a neuro-protective phenotype, which would ensure that infiltrating T cells are largely non-cytotoxic under normal conditions [83, 84]. Indeed, the majority of T cells in the CSF and meninges appear to be CD4+

memory T cells, while the majority of parenchymal T cells are CD8+ memory cells which are neither activated, proliferating, nor senescent [86].

However, under inflammatory conditions, the BBB and BLMB can become permeable to activated immune cells due to dysregulation of the physical barrier provided by pericytes and astrocytes [83]. The number of T cells in the brain drastically increases in multiple neurodegenerative diseases, including Multiple Sclerosis (MS), Parkinson's Disease (PD), and Alzheimer's Disease (AD) [66–72, 87]. In all three diseases, massively clonally expanded $CD8^+$, $CD4^+$, and $\gamma\delta$ cells have been found in patient blood, cerebral spinal fluid (CSF), and/or brain tissue, some of which target self-antigens like myelin components and α-synuclein [66–69, 72, 88]. Although CD4 T cells are more well-studied in these diseases, the majority of brain-infiltrating T cells appear to be $CD8^+$ [68–70, 72, 87, 89].

In AD, amyloid and tau pathology appear to encourage T cell recruitment to the brain, although the exact mechanisms remain unclear. A study of AD model mice that developed amyloid pathology, but not tau tangles, showed increased numbers of $CD8^+$ T cells specifically in amyloid-burdened areas of the brain [89], and $CD8^+$ T cells have been observed adjacent to Aβ plaques in AD patients [69]. Similarly, tau pathology alone resulted in significant infiltration of $CD8^+$ T cells in tau model mice [90], although another study found that T cells were not significantly spatially associated with $pTau^+$ neurons in these mice [70]. Increased numbers of $CD8^+$ T cells were also seen in patients with frontotemporal dementia associated with the P301L tau mutation, which causes aggregation of tau protein in the brain [90]. Interestingly, a study of AD patient hippocampus tissue found that, in late stages of AD, the number of T cells in the hippocampus correlated with the amount of tau pathology but not with the amount of amyloid pathology [71]. It is clear from these studies that Aβ and tau can separately play a role in recruitment of T cells to the brain parenchyma, but that more complicated dynamics are involved when both pathologies are present.

Microglia and T cell interactions influence disease severity

The innate and adaptive immune system heavily reinforce each other, and there is evidence of both beneficial and harmful communication between T cells and microglia in neurodegeneration. T cells have been observed adjacent to microglia in the hippocampus of AD patients and near MS lesions [66–68], and have been observed aiming cytotoxic granules at macrophages and microglia in MS [68].

T cells are able to directly interact with microglia via surface signaling. Microglia express both MHC I and MHC II proteins, and they are the main MHC II antigen presenting cell in the brain [67]. Therefore, a single microglia can present antigen to both CD4 and CD8 T cells to activate them. Interestingly, microglia up-regulate both MHC I and II in AD patients, and increased MHC II is correlated with an increase in cognitive deficits [67, 91]. This suggests a negative role for CD4 T cell activation in cognitive decline. Indeed, activated T-helper 1 (T_{H1}) cells secrete IFNγ, TNFα, and GM-CSF, which in turn activate microglia further [72, 92]. This effect was seen with adoptive transfer of amyloid-reactive CD4 T cells into AD model mice, which was shown to increase microgliosis, accelerate memory impairment, and worsen amyloid pathology [92]. Activated CD4 T cells have been shown to be similarly harmful in MS and PD model mice [66, 67], demonstrating a feedback loop between microglial activation, CD4 T cell activation, and worsening neurodegeneration.

In contrast, some studies have found that T cells also help boost protective functions in glia. One study found that AD mice without T cells, B cells, or NK cells had increased microglial activation, decreased glial phagocytosis, and a two-fold increase in amyloid burden compared to immune-intact AD mice [93]. Another study of AD mice found that prolonged ablation of $Foxp3^+$ T_{regs}, which suppress other T cells, resulted in increased T cell infiltration, reduced gliosis, lowered plaque burden, and improved cognition compared to control AD mice [94]. These two studies suggest that communication between T cells and glia is critical in maintaining glial phagocytic function in AD.

CD8+ and γδ T cells affect synaptic function and cognition

Although many studies focus on $CD4^+$ T cells in AD, $CD8^+$ and γδ T cells are also capable of directly affecting glia and neurons, often resulting in a detrimental effect on cognition. A study of human AD patients found that increased numbers of $CD8^+CD45RA^+$ T cells (T_{EMRA}) in the brain negatively correlated with cognition [69]. In AD model mice, one study found that depletion of $CD8^+$ T cells resulted in increased expression of neuronal genes related to synaptic plasticity without affecting plaque load [70]. Another study found that depletion of T cells from tau model mice, where the majority of brain-infiltrating T cells are $CD8^+$, resulted in rescue of spatial memory deficits and a reduction in microgliosis without affecting tau pathology [90]. Experiments on 3xTg model mice, which develop both amyloid and tau pathology, revealed a buildup of IL-17-secreting immune cells in the brain and meninges, most of which were γδ T cells. Anti-IL-17 antibody treatment in these mice improved short-term memory without affecting amyloid or tau pathology [95], suggesting that activated γδ-17 cells have a harmful effect on cognition. Together, these four studies suggest that $CD8^+$ and γδ T cells either directly or indirectly affect neuronal health and synaptic function more than they affect pathology-clearing mechanisms of glia.

Although it is clear that certain T cell phenotypes can either improve or worsen AD symptoms, these conflicting interactions do not happen in isolation and their mechanisms remain understudied. It is therefore critical to investigate the factors that drive recruitment and activation of different T cell populations in AD, with an eye toward therapeutically influencing these systems for better patient outcomes.

CHAPTER 1

Investigating brain-infiltrating T cells in Alzheimer's Disease

Jaclyn Beck[#], Jessica Ramirez Sanchez[#], Sepideh Kiani Shabestari, Samuel E. Marsh, Laura L. McIntyre, Vanessa M. Scarfone, Pauline U-P Nguyen, Erika S. Varady, Jorge Silva, Christel Claes, Joia Capocchi, Jean Paul Chadarevian, Alina Lahian, Matthew Inlay, Craig M. Walsh, Hayk Davtyan, Mathew Blurton-Jones

[#] J Beck and JR Sanchez contributed equally to this study

Introduction

Alzheimer's Disease (AD) is the most common cause of age-related dementia and currently affects over 6 million people in the United States alone [1]. AD is a progressive and debilitating disease that gradually impairs memory and cognition, eventually robbing patients of the ability to perform basic daily functions [1]. AD neuropathology is primarily characterized by the accumulation of two hallmark protein aggregates; amyloid plaques and neurofibrillary tangles that are composed of insoluble beta-amyloid (Aβ) and hyperphosphorylated tau respectively [96]. These key pathologies are further accompanied by microgliosis and progressive neuronal and synaptic loss [97–99].

In the past decade significant advances have been made in our understanding of the role of innate immunity in the pathogenesis of Alzheimer's disease. Much of this progress has been inspired by Genome-wide association studies (GWAS) that have identified over 80 loci linked to AD risk, many of which are associated with changes in expression of microglial genes [8–10, 100]. These discoveries have in turn lead to development of exciting new tools and approaches including stem cell-based modeling of human microglial function and novel genetic and pharmacological approaches to examine the interactions between microglia, the brain's endogenous innate immune

cells, and Aβ and tau pathology [24, 101–105]. Collectively, these studies have greatly advanced our understanding of the role of innate immunity in AD. In contrast, only recently have a handful of groups begun to examine the potential role of adaptive immunity in this disease.

For many years, the brain was considered “immune privileged” implying that peripheral immune cells were largely excluded from the parenchyma in most neurological diseases, including AD (reviewed in [85]). However, recent studies have provided increasing evidence that peripherally-derived immune cells can indeed reach the brain and despite limited numbers, could mediate profound effects in various neurodegenerative diseases [69, 94, 105, 106]. Despite this progress, the frequency and precise subtypes of adaptive immune cells that reach the brain parenchyma in AD and AD mouse models remains unclear.

Initial histological studies found evidence of increased CD3+ T cells within AD brain tissue, but there remained skepticism as to whether those cells were recruited to the brain as a consequence of AD pathologies versus co-morbidities, such as stroke [107]. Subsequent studies of advanced AD patient brains revealed increased numbers of CD8+ T cells in the hippocampus that significantly correlated with tau pathology [71], suggesting a potential relationship between neurofibrillary tangles, neurodegeneration, and T cell recruitment. Additional studies in AD mouse models also began to provide evidence that various T cell populations including CD4, CD8, and T regulatory cells can infiltrate the brains of amyloid or tau-expressing transgenic mice and correlated with and in some cases influenced disease progression [89, 90, 94]. Most recently, studies of AD and control patient CSF revealed an enrichment of effector memory CD8+ T cells in AD subjects that were inversely associated with cognition. Examples of CD8+ T cells were also found adjacent to cerebral blood vessels, and TCR repertoire analysis revealed AD-associated increases in clonality [69].

To further investigate the role of adaptive immune cell infiltration in AD and the relationship between T cell recruitment and amyloid and tau pathologies, we utilized both immune-deficient and immune intact transgenic mouse models coupled with bone marrow transplantation, flow cytometry, and single cell RNA- and T cell receptor- (TCR) sequencing. Our experiments revealed a broad array of T cell subtypes that infiltrate the brain of transgenic AD mice and identified specific

subsets of CD8 T cells that are enriched in response to Aβ pathology or a combination of Aβ and tau pathologies. Analysis of AD GWAS variants found evidence that specific T cell subpopulations express relatively high levels of AD risk genes. In addition, TCR repertoire analysis revealed an amyloid-associated induction of CD8 T cell clonal expansion. Taken together, this study provides an important new resource that can be used to guide future investigations and further inform our collective understanding of AD immunology and the role of T cells in this disease.

Methods

Animals. All animal procedures were performed in strict accordance with National Institutes of Health and University of California guidelines. Sex- and age-matched littermates were used for all studies except single cell sequencing analysis which focused specifically on female mice from all four genotypes. All animals were group housed on a 12h/12h light/dark cycle with access to food and water ad libitum.

Immune-deficient mice. The Rag-5xfAD immune-deficient AD mouse model was created by backcrossing 5XFAD transgenic mice onto a Rag2/Il2rγ double knockout background as previously described [93]. Briefly, 5XFAD mice (MMRRC Strain: 034848-JAX), express two co-integrated and co-inherited transgenes coding for mutant human amyloid precursor protein (APP) and Presenilin-1 (PS1). The APP transgene includes three familial AD mutations (Swedish, Florida, London) and the PS1 transgene includes two mutations (M146L & L286V) [108]. Congenic C57Bl6 5XFAD mice were crossed with Rag2/Il2rγ double knockout mice (Taconic #4111) [109], followed by repeated littermate crosses from each generation, to create mice that are heterozygous for the APP/PS-1 transgenes and lack both copies of the Rag2 and Il2rγ genes (Il2rγ -/y in males). We also simultaneously generated strain matched immune-deficient wild-type mice for the AD transgenes hereafter referred to as Rag-WT. For bone marrow adoptive transfer experiments, WT-5XFAD mice were crossed with CAG-eGFP mice (JAX Stock#: 006567), which express “enhanced” GFP under the control of chicken beta-actin promoter and cytomegalovirus enhancer, hereafter referred to as GFP-5XFAD.

Immune-intact mice. PS19 transgenic mice (Strain #:008169; B6C3F1/J) and 5XFAD mice (Strain #034848, C57BL6 congenic) were purchased from the Jackson Laboratories. PS19 mice express mutant human microtubule-associated protein tau (MAPT) driven by the mouse prion protein promoter. Hemizygous PS19 and hemizygous 5XFAD mice were crossed to create a colony of mice that carried one of four genotypes; WT/WT, bigenic $PS19^{+/0}/5XFAD^{+/0}$, $PS19^{+/0/WT}$, or $WT/5XFAD^{+/0}$. The colony was subsequently expanded via additional crosses of PS19 and 5XFAD hemizygous F1 progeny. Strain-matched littermates from each of the four genotypes were used for all experiments.

Tissue Processing. Immune deficient (Rag-5x and Rag-WT) mice were sacrificed by carbon dioxide asphyxiation and intracardiac perfusion with 0.01M phosphate buffered saline (PBS). Immediately following perfusion, brains were isolated and cerebellum and olfactory bulbs removed and hemispheres separated along the midsagittal plane. Half brains were then dissociated using a glass homogenizer on ice and a 23% percoll density gradient centrifugation was used to remove myelin and debris prior to flow cytometry. The other half of each brain was drop fixed in 4% paraformaldehyde for 48 hours at 4°C and then transferred to 0.01M PBS and 0.02% NaN3 and stored at 4°C. Prior to sectioning, fixed hemibrains were cryoprotected in 30% sucrose for three days and then sectioned in the coronal plane on a freezing microtome (Leica) at 40µm thickness.

For immune intact mouse studies, WT, 5XFAD, PS19, and PS-5X mice were sacrificed at 6, 9, and 12 months of age by carbon dioxide asphyxiation and spleen, deep cervical lymph nodes, and blood were gently removed prior to intracardiac perfusion with 0.01M phosphate buffered saline (PBS). Hemibrains were processed and one side drop-fixed, cryoprotected, and sectioned as detialed above. The other hemibrain was immediately placed in complete RPMI medium, cut into fine pieces and placed in dissociation tubes along with Collagenase IV+ DNase1 in complete RPMI. Tissue was then placed into a gentleMACS Dissociator for 30 mins on the ABDK setting at 37°C and then filtered through 70µm strainers. Further removal of myelin and debris was conducted using 23% Percoll density gradient centrifugation. After isolation, cells were processed for flow cytometry as described below.

Flow Cytometry. Single cell suspensions isolated from the brain, spleen, deep cervical lymph nodes, and blood were immunophenotyped with fluorescent antibodies for the following cell surface markers for pan T cells: PE-conjugated CD3e (500A2; BD Biosciences; San Jose, CA), PerCP-eFluor710-conjugated CD3e (17A2, eBioscience). CD4 and CD8 T cells: PE-conjugated CD4 (GK1.5, BD Biosciences), Pacific Blue-conjugated CD4 (RM4-5, BioLegend; San Diego, CA) APC-conjugated CD8 (Ly-2, BD Biosciences), PE/Cy7- conjugated CD8 (53-6.7, eBioscience). Memory markers: BV421-conjugated CD44 (Biolegend), APC-conjugated CD62L (Biolegend). Hematopoietic lineage and monocyte markers: BUV496-conjugated CD45 (Biolegend), Alexa 700-conjugated CD11b (Biolegend). All cells examined by flow cytometry were first FC blocked with anti-CD16/32 (1:200; BD Biosciences). Cells were examined on a Fortessa flow cytometer (BD Biosciences) or BD FACSAria II (BD Biosciences) and analyzed with FlowJo v10.7 software (FlowJo; Ashland, OR). Flow cytometry gating schema are provided in Figure S.1.

Immunohistochemistry and confocal microscopy. Fluorescent immunohistochemical analysis followed previously established protocols [22] and the following primary antibodies: Anti-GFP Alexa 488 conjugated (Life Technologies); Anti-GFP (Millipore; Temecula, CA); Iba1 (Wako; Richmond, VA), CD3e (Clone 500A2; BD Biosciences), CD4 (Clone RM4-5; AbD Serotec & BioLegend), CD8 (Clone YTS105.18; AbD Serotec; Raleigh, NC). Sections were rinsed, permeabilized with 0.2% Tx100, and blocked in 5% goat serum for one hour and then incubated in primary antibodies overnight at 4°C. Following three rinses in PBS, sections were incubated with appropriate Alexa Fluor® conjugated secondary antibodies (Life Technologies) and/or biotinylated secondary antibodies followed by Alexa Fluor conjugated streptavidin and coverslipped using Fluoromount-G with or without DAPI (Southern Biotech; Birmingham, AL). Fibrillar amyloid was visualized using Amylo-Glo (Biosensis; Temecula, CA) diluted 1:100 in 0.01M PBS. Immunofluorescent sections were imaged using an Olympus FX1200 confocal microscope. To avoid non-specific bleed-through, each laser line was excited and detected independently. All images represent confocal maximum projection z-stacks. In some non-quantified images, brightness and contrast were slightly adjusted or channels were pseudocolored for clarity.

***In vitro* T cell stimulation.** T cells were isolated from deep cervical lymph nodes of 6-month-old female mice using a negative magnetic bead selection and co-cultured with whole brain homogenates at a 1:1 ratio. 100,000 brain T cells from either 5X mice or WT female mice were cultured with 100,000 brain cells from either 5X mice or WT female mice. T cells from both genotypes were also cultured alone as a negative control. 96-well plates were coated with IgG and 1µg/mL anti-CD28 and T cells in each well were activated by adding 1µg/mL anti-CD3 when cultured. T cells were stained with CFSE proliferation dye, co-cultured for five days, and then analyzed using a Fortessa Flow Cytometer and FlowJo software v10.7 (FlowJo; Ashland, OR).

Bone Marrow Adoptive Transfer. Adoptive transfer experiments were performed according to previously published protocols [93]. Briefly, age- and sex-matched immune-intact GFP-5XFAD mice served as donors for bone marrow adoptive transfer. Donor mice were euthanized by CO2 asphyxiation, femurs and tibias were removed, and whole bone marrow harvested by flushing the marrow contents with PBS. Marrow was then treated with Ammonium-Chloride-Potassium (ACK) buffer to lyse red blood cells, filtered through a 40µm nylon mesh, and cell numbers counted by hemocytometer and automated cell counter. Recipient mice were 2-month old Rag-5XFAD and Rag-WT mice. A total of 13 Rag-5X (5F & 8M) and 9 Rag-WT (6F & 3M) mice were injected with BM. Each recipient was anesthetized with isoflurane prior to receiving 550,000 live cells in 100µl or equivalent volume of PBS via retro-orbital injection. To confirm engraftment, mice were bled 3 weeks post transplantation and analyzed for the presence of GFP+ B, T, and NK cells by flow cytometry.

Statistical Analysis. Statistical analysis was performed using Graphpad Prism 6 software and R. Comparisons involving more than two groups utilized one way analysis of variance (ANOVA). Comparisons of two groups utilized two-tailed Student's t-test. All differences were considered significantly different when $p<0.05$.

10x Single Cell Sequencing of Gene Expression and TCRs. A second cohort of 9 month old female mice from each of the four genotypes was used for 10x single cell sequencing. Mouse brains were processed for cell isolation using the gentleMACS Dissociator as described above and cells were then stained with the following antibodies: APC-CD8, APC-Cy7-CD45, FITC-CD4,

PE-TCRg/d, BV421-CD11b, and PI (all with 1:200 dilution). CD4+, CD8+, and γδ+ T cells were then sorted on a BD FACSAria II and cells from multiple mice were pooled for each genotype into 2 samples each for WT and 5XFAD and 1 sample each of PS19 and PS-5X: n=10 WT#1, n=8 WT#2, n=4 5XFAD#1, n=3 5XFAD#2, n=4 PS19, n=4 PS-5X. A total of six 10x libraries were then generated from these samples. Single cell 5' gene expression libraries and single cell V(D)J enriched libraries were prepared according to the 10x Genomics Chromium Single Cell 5' Reagent Kits User Guide v2 (Dual Index) (CG000331 Rev C). The Chromium Single Cell Mouse T Cell Enrichment Kit only enriches for αβ TCRs, so 5' gene expression was obtained for all T cells but clonotype data was limited to αβ T cells. The 10x Genomics workflow was followed according to the manufacturer protocol and libraries were pooled at equimolar concentrations for sequencing on an Illumina NovaSeq 6000, targeting 50,000 reads per cell for gene expression and 5,000 reads per cell for TCR expression. Gene expression and V(D)J FASTQ files from each sample were aligned to the GRCm38 (mm10) mouse transcriptome with the 10x Genomics Cell Ranger 6.0.1 *multi* command, using references provided by 10x Genomics ("refdata-gex-mm10-2020-A" for gene expression and "refdata-cellranger-vdj-GRCm38-alts-ensembl-5.0.0" for V(D)J alignment). For cellranger multi, "expect-cells" was set to 10,000 and all other arguments were set to default. Results from all samples were combined using *cellranger aggr*, with "normalize" set to none.

Quality control and filtering of single cell gene expression. Analysis of single-cell count and clonotype data was conducted in R using the Seurat package (version 4.1.0) [110]. A Seurat object was created from the filtered count matrix, as output by *cellranger aggr*, using min_cells = 10 and min_features = 200. Cells that contained multiple distinct TCR-β chains, as identified by TCR sequencing, were considered doublets and removed from the data set. Cells which did not have a recognized TCR and did not express at least one count of *Cd3d*, *Cd3e*, or *Cd3g* were also removed from the data set. Remaining cells were further filtered to only examine cells that had more than 800 genes expressed, less than 5% mitochondrial gene expression, and between 10% and 55% of ribosomal gene expression. These parameters were determined by visual inspection of population distribution along these variables. To preserve the cluster of proliferating cells but remove possible doublets missed by TCR filtering, cells were given a "complexity" score, defined

as the total count of RNA in the cell divided by the number of genes. Cells with a complexity score greater than 4.75 or with more than 20,000 RNA counts were discarded as doublets. After filtering, the data set contained a total of 16,135 T cells distributed across samples as follows: WT-1 (680 cells), WT-2 (3335 cells), 5XFAD-1 (2326 cells), 5XFAD-2 (1940 cells), PS19 (2186 cells), and PS5X (5668 cells).

Assigning a "stress score" to cells. During preliminary analysis, we discovered a batch effect between the first sequencing run of samples (WT-1, 5XFAD-1, PS19, and PS-5X) and the second run (WT-2 and 5XFAD-2). Differential expression between batches showed many genes known to be upregulated in response to heat dissociation of immune cells during preparation for RNA sequencing, including heat shock proteins (*Hspa8*, *Hspa1a*) and other stress-related chaperones (*Dnajb1*, *Fkbp4*) [111–113]. Differential genes were also enriched for the Reactome pathway "cellular response to heat stress" [114, 115]. This effect was most likely attributable to differences in preparation time between the two batches. To account for these differences in stress pathways, we created a "stress score" for each cell based on expression of 16 genes (*Atm, Bag3, Dnajb1, Hsp90aa1, Hsp90ab1, Hspa1a, Hspa1b, Hspa4l, Hspa5, Hspa8, Hsph1, Mapkapk2, Nup205, Nup98, Rpa3, Sirt1*). These genes were selected by starting with the list of 83 mouse genes in the Reactome "cellular response to heat stress" pathway and filtering down to genes that were expressed in at least 5% of cells in the data set and which were in the top 4000 most variable genes (as determined by the Seurat function *FindVariableFeatures*). The Seurat *AddModuleScore* function was used to calculate the stress score for each cell. This score was used as a latent variable in downstream analysis.

Clustering and subpopulation analysis. For clustering analysis, the filtered data set was scaled using the Seurat integration pipeline. Briefly, the Seurat object was split into multiple objects, one per sample. Each sample was scaled separately using *SCTransform*, regressing out total RNA count and stress score. Samples were combined back into one Seurat object with *IntegrateData*, using 4,000 integration features. The integrated data was clustered using *FindNeighbors* and *FindClusters* using PCA dimensions 1-40 and a resolution of 0.1. We were also interested in

examining CD8+, CD4+, and γδ cells separately, so subpopulation analyses were performed as described below.

Although αβ T cells can express TCRγ genes at the RNA level [75, 116], for both CD8+ and CD4+ analysis, we chose to remove all cells that expressed any markers of γδ lineage (*Trdc, Tcrg-V1, Tcrg-V3, Tcrg-V4, Tcrg-V5, Tcrg-V6, Tcrg-V7, Tcrg-C1, Tcrg-C3, Tcrg-C4, Trdv1, Trdv2-1, Trdv2-2, Trdv3, Trdv4, Trdv5, Sox13,* and *Blk*). We noted, however, that *Trgv2* and *Tcrg-C2* were expressed in an unusually large number of cells that was inconsistent with our own flow cytometry data and with the literature [76–78], so we did not use those two genes as a γδ marker. For CD8+ analysis, we filtered the data set to retain only cells that expressed at least one count of *Cd8a* or *Cd8b1* and did not express *Cd4* or any γδ markers described above. This left 9,127 CD8+ αβ cells. These cells were re-integrated using *SCTransform* and *IntegrateData* as above. Data was clustered using PCA dimensions 1-40 and a resolution of 0.5.

For CD4+ analysis, we filtered the original data set to retain cells that expressed at least one count of *Cd4* and did not express *Cd8a*, *Cd8b1*, or any γδ markers described above. This left 2,441 CD4+ αβ cells. There were too few cells to use the integration pipeline, so *SCTransform* was run on all cells together, using 4000 variable features and regressing out total RNA count and stress score. The SCT assay was used to calculate PCA, and data was clustered using PCA dimensions 1-25 and a resolution of 0.3.

For γδ analysis, we used a more stringent list of markers to retain only cells that were highly likely to be true γδ cells. We filtered the original data set to contain only cells that expressed at least 1 count of any Tcrδ gene gene, as alpha rearrangement removes the delta locus [75], or γδ-specific transcription factor (*Trdc, Trdv1, Trdv2-1, Trdv2-2, Trdv3, Trdv4, Trdv5, Sox13*, or *Blk*). We then removed all CD8+ and CD4+ cells from this group, as most of these cells were *Trac*+*Trdc*- and had a recognized αβ TCR. This left 1,062 γδ cells. There were too few cells to use the integration pipeline, so *SCTransform* was run on all cells together, using 4000 variable features and regressing out total RNA count, stress score, and sample. The SCT assay was used to calculate PCA, and data was clustered using PCA dimensions 1-30 and a resolution of 0.2. The γδ-1 cluster was

further sub-clustered using *FindSubCluster* with a resolution of 0.2 to separate naive cells from effector cells.

Differential expression analysis. For all differential gene testing, Seurat's *FindAllMarkers* or *FindMarkers* functions were called on log-normalized counts using MAST [117] to test for significance and regressing out total RNA count and stress score as latent variables. All p-values were adjusted using Bonferroni correction. Genes were considered significantly different if adjusted p <= 0.01, log fold-change >= 0.25, and at least 10% of the cells in the cluster (or genotype) expressed the gene.

Differential composition analysis. To assess potential differences in population proportion between genotypes, given only one to two samples per genotype, we used a modified version of scDC (version 0.1.0) [118]. Briefly, the *scDC_NoClustering* method was used to resample cells from each sample 10,000 times. This method then counted the number of cells with each cluster identity in each resample. To account for the large differences in total cell count between samples, re-sampled population counts were normalized to be between 0 and the minimum total cell count among the six samples. We then fit a generalized linear model to the distribution of counts using the formula *glm(cellCount* $\sim$ *cellType*genotype, family = poisson(link=log))* where cellCount is the number of cells identified as a certain cell type (cluster) for a certain genotype. Statistics from each GLM were pooled into a single statistic as in [118] using the R package *mice's* pool function [119]. Significance of the pooled estimates was determined by the univariate Wald test. We found significant interactions between multiple clusters and genotypes, so we also conducted post-hoc pairwise comparisons. For each GLM, we ran the *multcomp* function *glht(fit, linfct=emm(pairwise genotype|cellTypes, adjust="tukey"))* [120], which generated pairwise comparisons between genotypes within each cluster. Estimates from each GLM for each comparison were pooled using mice's pool.scalar function, using the Benjamini-Hochberg correction for multiple comparisons. Population differences were considered significant if p <= 0.05.

Creation of an epitope database. To look for possible epitope matches for our sequenced clonotypes, we created a database of known TCR / epitope pairs by combining data from the

Immune Epitope Database (IEDB) [121] and VDJdb [122]. IEDB data was exported to a CSV file using the search function with the following parameters: Epitope: linear peptide, Epitope Source: (blank), Host: Any, Assay: T Cell only, Assay (Outcome): Positive only, MHC restriction: Any, Disease: Any. VDJdb data was exported to a CSV file using the search function with the following parameters: Species: Human, Monkey, Mouse, Gene (Chain): TRA, TRB, CDR3 Length: 5 to 30, Substitutions: 0, Insertions: 0, Deletions: 0, Class: MHC I, MHCII, Assay Type: all boxes selected, Sequencing: all boxes selected, Minimal confidence score: 0. All other fields not specified here were left blank or unselected. Both files were downloaded on January 23, 2022. For each database file, entries with TCR sequences less than 5 amino acids long were removed, and the remaining sequences had the initial "C" and ending "F" or "W" trimmed from the sequence. Slight differences in source organism naming between IEDB and VDJdb were corrected to be consistent between both sets of data, and duplicate entries were deleted. The remaining TRA sequence entries from both databases were combined into one file, and TRB entries were combined into a separate file.

Epitope matching. We used TCRMatch [123] to identify potential epitope matches for our clonotypes. Briefly, this program uses a BLOSUM62 matrix to score amino acid similarity between a query sequence and TCRs in the database. The scores are then normalized to between 0 and 1, with 1 being a perfect match. Prior to running the program, we split our list of clonotypes into TRA and TRB sequences and trimmed the initial "C" and ending "F" or "W" from each sequence. TCRMatch was run with a cutoff score of 0.9, and we compared our TRA sequences to the combined database's TRA sequences, and our TRBs were compared to the database's TRBs separately. After TCRMatch generated matches and scores, we conducted post-processing to map the separated TRA and TRB matches back to complete clonotypes. For each clonotype, if both the TRA and TRB matched the same epitope, their scores were averaged to create a final score for that epitope. If only one chain had a match to an epitope, that score was left as-is. The highest-scoring epitope among single-chain or paired matches for all epitopes was used to determine the most likely match to the clonotype. Any final matches with a score >= 0.97 were considered probable matches for that clonotype, resulting in 3,787 clonotypes that matched at

least one TCR/epitope pair. We allowed multiple final epitope matches if their scores were equal and that score was the highest score for the clonotype.

Code Availability. The code written to process 10x scSeq data is publicly available on GitHub: https://github.com/jaclynrbeck/TCellsAD2022.

Results

Cytotoxic CD8 T cells infiltrate the Brains of Immune Deficient Rag-5XFAD Mice following Bone Marrow Transplantation

In previous studies we generated immunodeficient AD mice by backcrossing 5XFAD mice onto a Rag2 and il2rγ double knockout background ($RAG2^{-/-}$,$IL2r\gamma^{-/-}$,$5XFAD^{+/0}$). The resulting mice, hereafter referred to as Rag-5XFAD, lack T, B, and NK cells and remarkably exhibited a greater than two-fold increase in beta-amyloid plaque pathology [93]. Conversely, when wildtype bone marrow was transplanted (BMT) into Rag-5XFAD mice amyloid levels were reduced. In the current study we sought to further determine whether these changes in amyloid load might be accompanied by infiltration of specific peripheral immune cells into the brain parenchyma. We therefore transplanted GFP-expressing bone marrow hematopoietic stem cells (HSCs) into 2-month old Rag-5XFAD mice and wild-type 'Rag-WT' immunodeficient controls ($RAG2^{-/-}$,$IL2r\gamma^{-/-}$,WT) (Figure 1.1A). Because Rag-5XFAD and Rag-WT mice lack an adaptive immune system, successful engraftment of donor-derived hematopoietic cells can be achieved without the need for preconditioning irradiation or chemoablation that can disrupt the blood brain barrier [93]. Four months after bone marrow transplantation (BMT), mice were sacrificed and brains examined by immunohistochemistry (IHC), revealing an increase in GFP+ donor cell infiltration within 5XFAD brains in comparison to Rag-WT mice (Figures 1.1B–C). Thus, amyloid accumulation or other neuropathological changes induced by plaque pathology, promote the recruitment of donor derived immune cells into the brain. Interestingly, GFP+ cells were observed throughout the brain of Rag-5XFAD mice including the hippocampus, cortex, and meninges

(Figures 1.1D–E), but also in greater numbers adjacent to the lateral ventricles (Figure 1.1F). To determine whether GFP+ cells might simply be localized within cerebral blood vessels, sections were counterstained with the blood vessel marker GLUT1, demonstrating that virtually all GFP+ cells were located within the brain parenchyma (Figure 1.1G).

As BMT into immune-deficient recipients repopulates various blood lineages, we began by examining CD45, a marker that labels all hematopoietic cells. As expected, all GFP+ cells within either Rag-5XFAD or RAG-WT recipient brains co-expressed CD45. Interestingly, CD45/GFP double-positive cells exhibited small circular morphologies that contrasted with a subset of CD45+/GFP- brain resident cells that, based on their morphology, likely represent microglia (Figure 1.1H). Further staining with the microglial/monocyte marker IBA-1 revealed no examples of GFP-expressing IBA-1 cells. Thus, donor-derived cells did not give rise to brain-infiltrating monocytes or macrophages in this chemoablation- and irradiation-free BMT paradigm. Given the ameboid morphology of GFP-expressing cells and prior reports demonstrating T cell infiltration into AD mouse models [70, 89], we next examined the pan T-cell marker CD3. IHC staining revealed that virtually all GFP+ cells detected in the AD brain co-expressed CD3+ (Figures 1.1J–L). Interestingly, T cells were sometimes observed adjacent to IBA-1+ microglia (Figures 1.1M–O) and Aβ plaques (Figure 1.1P) within Rag-5XFAD brains, suggesting that activated microglia may play a role in T cell recruitment and/or antigen presentation in the AD brain environment.

To further understand whether specific subtypes of T cells are recruited to the brains of Rag-5XFAD mice, we next performed flow cytometry. This analysis revealed a significant increase in GFP/CD3/CD8+ T cells (P=0.0390), but no significant changes in GFP+/CD3+/CD4+ T cell numbers (P=0.4363) in bone marrow transplanted Rag-5XFAD mice in comparison to Rag-WT BMT recipients (Figures 1.1Q–R). As bone marrow transplantation into immune-deficient recipients can induce homeostatic expansion it is possible that T cell infiltration might be amplified in this paradigm. Our findings in Rag-WT mice suggest this is unlikely to be the case. Nevertheless, we sought to either corroborate or refute our initial Rag-5XFAD findings by examining immune-intact 5XFAD mice. Both male and female 6-month old 5XFAD and wildtype littermates (n=6/genotype) were sacrificed via intracardiac perfusion of PBS and brains were

processed and stained for flow cytometry. This analysis revealed similar results to our Rag-5XFAD studies, demonstrating a significant increase in CD8+ T cells in 5XFAD brains versus wildtype littermates, but no significant changes in CD4+ cells (Figure 1.1S).

CD8+ T cells infiltrate the brains of immune intact PS-5X mice across multiple ages

Given the robust infiltration of CD8 T cells observed in bone marrow transplanted Rag-5XFAD mice and corroborating evidence of infiltration in immune intact 5XFAD mice, we next sought to determine whether accumulation of another hallmark AD pathology, neurofibrillary tangles, could similarly induce T cell infiltration. As human AD patients exhibit both amyloid plaques and tau-laden neurofibrillary tangles, we also examined the impact of combined amyloid and tau pathologies by crossing 5XFAD mice with the PS19 model of tau pathology to generate bigenic AD mice that develop both plaques and tangles. PS19 mice express a human MAPT transgene carrying the frontotemporal dementia (FTD)-linked P301S mutation and develop progressive tau hyperphosphorylation and tangle formation [124]. While the P301S tau mutation leads to FTD, not AD, these mice develop neurofibrillary tangle pathology that closely mimics that of AD patients and are therefore widely used to examine FTD- and AD-related aspects of tau pathology [124–126].

As amyloid and plaque pathologies can exhibit substantial age and sex-dependent differences we examined T cell infiltration by flow cytometry in both male and female mice across three ages: 6-, 9-, and 12-months of age. At 6-months of age, sex-specific analysis of female or male 5XFAD mice reveals a non-significant trend towards increased CD8 T cell infiltration in female mice ($p=0.0559$), but no differences in male 5XFAD mice (Figure 1.2A). In contrast, tau pathology alone has no effect on CD8 recruitment in female mice but leads to a significant increase in male PS19 mice ($P=0.0007$). These sex-dependent differences in CD8 T cell recruitment are consistent with prior reports that female 5XFAD mice exhibit increased plaque pathology at early ages, whereas PS19 male mice exhibit increased Tau pathology versus females [127, 128]. When amyloid and tau pathologies are combined in 6-month-old bigenic PS-5X mice, flow cytometry reveals a greater than 4-fold increase in CD8 T cell recruitment to the brain of both female and male PS-5X mice versus wild-type littermates (female $P=0.0005$, male $P=<0.0001$) (Figure 1.2A). Representative

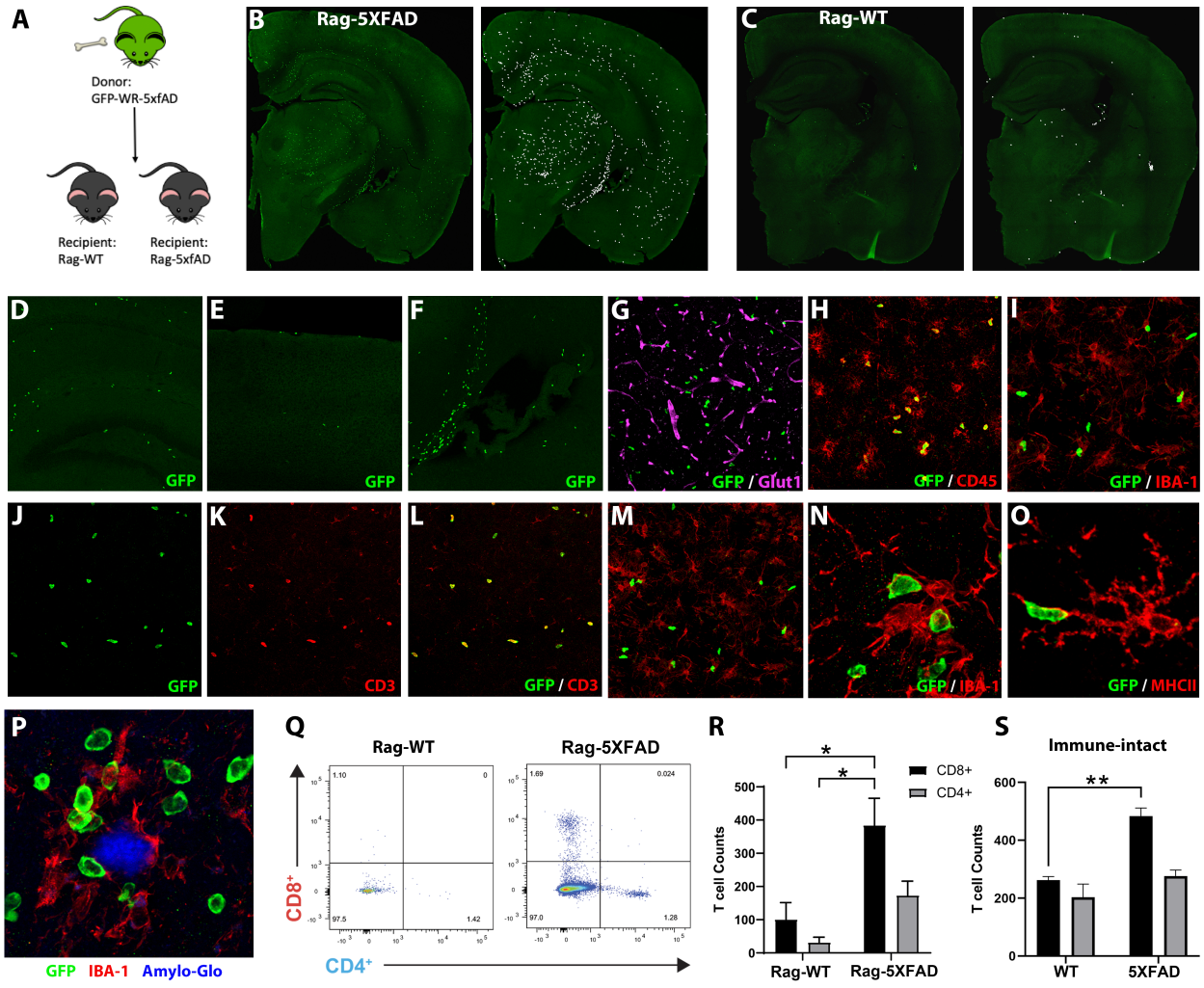

Figure 1.1: Cytotoxic T cells infiltrate Rag-5XfAD mice brains. (A) Adoptive transfers were conducted of GFP+ bone marrow cells into 2 mo Rag-WT and Rag-5xfAD via retro-orbital injections. (B) Increased numbers of GFP+ cells infiltrate the brain parenchyma in AD mice (B) but not WT mice (C). (D,E) IHC images of GFP+ cells in hippocampus, cortex, and meninges. (F) IHC image showing GFP+ cells in lateral ventricles. (G) IHC staining of GLUT1 blood vessel marker. (H) IHC staining of GFP+/CD45+ cells and GFP+/CD45+ microglia. (I) IHC staining of microglial/monocyte marker IBA-1 and GFP cells. IHC staining of GFP+ cells (J), CD3 T cell marker (K) and colocalization of GFP+/CD3+ cells (L). IHC staining of GFP+ cells, IBA-1+ (M) and MHCII+ (N) microglia, and Amylo-glo+ plaques (P). (Q,R) Flow cytometry analysis of CD8+ and CD4+ T cells in Rag-5xfAD and Rag-WT mice brains. (S) Flow cytometry analysis of CD8+ and CD4+ T cells in immune intact 5xfAD and WT mice brains. Statistical significance was determined if $p < 0.05$.

FACS plots of 6-month old wild-type and PS-5X female mice are shown in Figure 1.2A and gating strategies are provided in Figure S.1. Interestingly, the effects of amyloid, tau, and combined pathology appear to be restricted to CD8 T cells, as no significant differences in CD4 T cell recruitment are detected across any genotype.

By 9-months of age, increasing amyloid pathology in female mice is associated with a more than 3-fold increase in CD8 T cells recruitment to the brain (P=0.0023), but no significant difference in male 5XFAD mice (P=0.9694). Combined amyloid and tau pathology also continues to recruit significant numbers of CD8 T cells into the brains of both male and female 9-month old PS-5X mice (female P=<0.0001, male P=<0.0001) (Figure 1.2B). In contrast, CD4 T cell recruitment continues to show no significant differences. Similar results are observed at 12-months of age, except that the magnitude of CD8 T cell recruitment continues to expand in bigenic PS-5X mice with both sexes exhibiting a more than 4-fold increase in CD8 T cells in the brain in comparison to wild-type littermates (female P=0.0496, male P=0.0057) (Figure 1.2C). To further understand whether T cell recruitment is dependent on age, flow cytometry data was plotted across each of the three timepoints. Analysis by repeated-measures ANOVA revealed a significant effect of age on CD8 T cell recruitment in both female and male mice (Figure 1.2D). In contrast, no significant main effect of age was detected in CD4 T cell recruitment. To determine whether CD8 T cells can also be observed within the brain of PS-5X mice via immunohistochemical approaches we examined representative fixed coronal brain sections by confocal microscopy. This analysis revealed evidence of scattered CD8+ immunoreactive cells (red) adjacent to both amyloid plaques (blue) and tau immunoreactive neurons (white) within the hippocampus (Figure 1.2E) and multiple other brain regions. Taken together, our experiments confirm that either amyloid or tau pathology can induce the recruitment of CD8 T cells to the brain, although the magnitude of these effects appear to be sex dependent. Furthermore, we find that combined amyloid and tau pathologies lead to a substantial increase in CD8 T cell recruitment to the brain in PS-5X mice that is well beyond that observed in 5XFAD or PS19 mice alone, demonstrating that AD pathologies produce a synergistic effect on CD8 T cell recruitment to the brain.

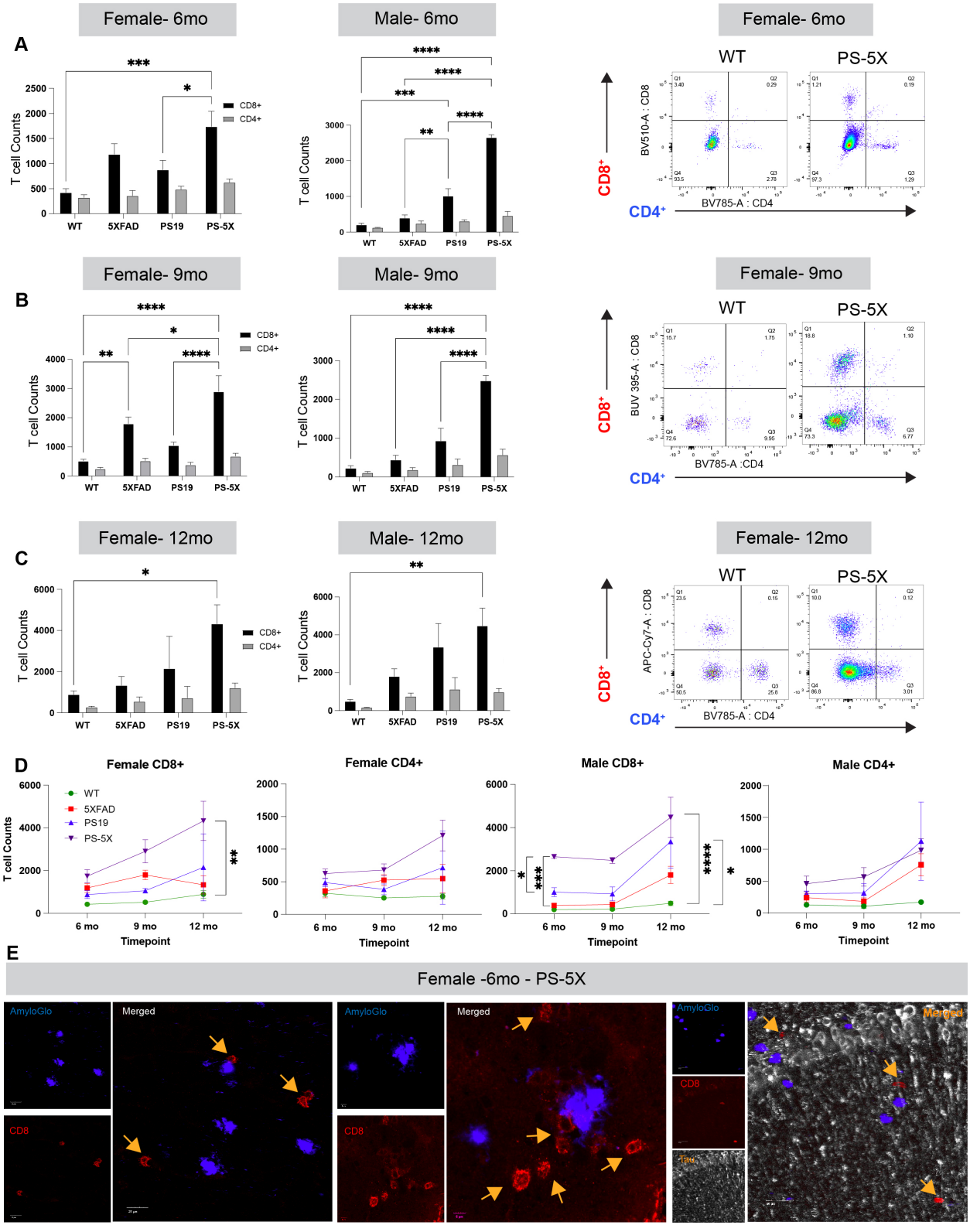

Figure 1.2: CD8+ cytotoxic T cells infiltrate the bigenic PS-5X mice model at 6, 9, and 12 months old. (Caption on next page.)

Figure 1.2: CD8+ cytotoxic T cells infiltrate the bigenic PS-5X mice model at 6, 9, and 12 months old. (A) Flow cytometry of live PI- CD45+ CD8+ and CD4+ T cell counts in female and male WT (no pathology), 5xFAD (plaque pathology), PS19 (tangle pathology), and PS-5X (tangle & plaque pathology) 6mo mice. Representative flow graphs of CD8+ and CD4+ T cells infiltrating 6mo female WT and PS-5X mice brains. (B) Flow cytometry of live PI- CD45+ CD8+ and CD4+ T cell counts in female and male WT, 5xFAD), PS19, and PS-5X 9mo mice. Representative flow graphs of CD8+ and CD4+ T cells infiltrating 9mo female WT and PS-5X mice brains. (C) Flow cytometry of live PI- CD45+ CD8+ and CD4+ T cell counts in female and male WT, 5xFAD, PS19, and PS-5X 12mo mice. Representative flow graphs of CD8+ and CD4+ T cells infiltrating 12mo female WT and PS-5X mice brains. (D) Flow cytometry analysis across the three timepoints for T cells counts of female CD8+ T cells, female CD4+ T cells, male CD8+ T cells, and male CD4+ T cells for each genotype. Statistical significance was determined if p value is <0.05.

Enrichment of Effector Memory CD8 T cells within the brains of AD transgenic mice

Recent reports have shown that effector memory CD8 T cells are enriched within the cerebral spinal fluid of AD patients and exhibit evidence of T cell receptor clonality [69]. We therefore hypothesized that increased CD8 T cells observed within AD transgenic mice might also exhibit an effector memory phenotype. Whereas human effector memory cells (TEMRA) can be examined via co-expression of CCR7 and CD45RA, these markers do not accurately distinguish murine effector memory cells. However, murine effector memory cells (TEM) can be measured via a combination of high expression of the effector marker CD44 and low expression of the central memory marker CD62L [81, 129]. Flow cytometry analysis using a panel of antibodies against CD45, CD3, CD8, CD4, CD44, and CD62L was performed to distinguish between naive (CD44-CD62+), effector (CD44-/CD62-), central memory (CD44+/CD62+), and effector memory (CD44+/CD62-) T cell subsets (Figure S.1C). These experiments revealed a significant enrichment of effector memory CD8 T cells in male PS-5X mice across all three ages and a similar increase in female PS-5X mice at both 9- and 12-months of age (Figures 1.3A–C). Interestingly, both male and female 5XFAD mice and PS19 mice also exhibited significant increases in TEM cells versus wild-type littermates at 9-months of age (Figure 1.3B). Thus, it appears that either amyloid pathology, tau pathology, or combined pathologies can induce a significant increase in effector memory CD8 T cell recruitment to the brain. Whereas effector and central memory T cell subsets show no significant differences across any age or genotype, the proportion of naive CD8 T cells is significantly reduced in male PS-5X mice at 6- and 9-months age and in female PS-5X mice at

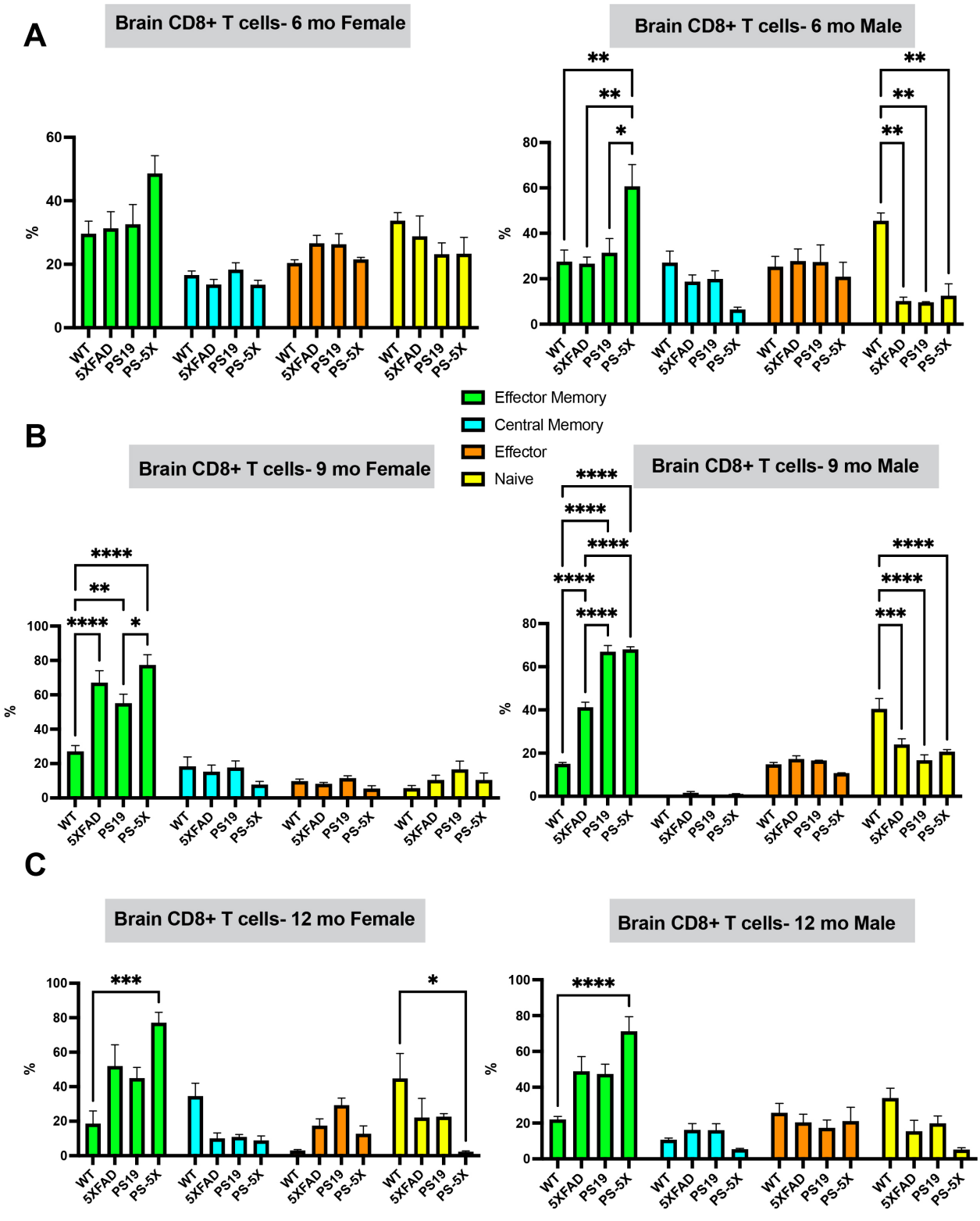

Figure 1.3: Effector memory CD8+ T cells infiltrate the brains of bigenic PS-5X mice. (Caption on next page.)

Figure 1.3: Effector memory CD8+ T cells infiltrate the brains of bigenic PS-5X mice. (A) 6mo female and male PS-5X, PS19, 5XFAD, and WT CD8+ T cells were analyzed via flow with memory markers CD44 and CD62L. Memory T cells were gated on as follows: central memory (CD44+,CD62L+), effector memory (CD44+, CD62L-), effector (CD44-, CD62L-), or naive (CD44-, CD62L+). (B) 9mo female and male PS-5X, PS19, 5XFAD, and WT CD8+ T cells were analyzed via flow with memory markers CD44 and CD62L. Memory T cells were gated on as follows: central memory (CD44+,CD62L+), effector memory (CD44+, CD62L-), effector (CD44-, CD62L-), or naive (CD44-, CD62L+). (C) 12mo female and male PS-5X, PS19, 5XFAD, and WT CD8+ T cells were analyzed via flow with memory markers CD44 and CD62L. Memory T cells were gated on as follows: central memory (CD44+,CD62L+), effector memory (CD44+, CD62L-), effector (CD44-, CD62L-), or naive (CD44-, CD62L+). Statistical significance was determined if $p < 0.05$.

12-months of age (Figures 1.3A–C). This analysis demonstrates that almost 80% of CD8 cells are effector memory T cells in 9 month old PS-5X female mice and almost 70% in 9 month old male PS-5X mice (Figure 1.3B). Thus, the majority of infiltrating CD8 T cells are antigen-experienced and were likely specifically recruited to brain tissue. Additionally, flow cytometry results showed that at 6 months of age CD4 T cells were mainly effector T cells, whereas by 9 and 12 months of age brain-infilatrating CD4 cells are mainly effector memory cells (Figures S.2A–C).

Cytotoxic T cells respond and proliferate in an Amyloid-enriched *in vitro* environment

To determine whether brain tissue from AD mice can elicit T cell proliferation, indicative of AD-specific memory T cell activation, we conducted *in vitro* co-culture studies (Figure 1.4A). T cells were isolated from deep cervical lymph nodes via negative magnetic bead sorting, then co-cultured with whole brain homogenates. T cells from either 5X or WT mice were cultured with brain cells from either 5X or WT mice. After 5 days of co-culture, the cells were analyzed by flow cytometry. Results showed that 5X-experienced T cells responded robustly to an amyloid enriched brain environment. CD8+ T cells from AD mice proliferated significantly when co-cultured with AD brain cells exhibiting a 2-fold increase compared to CD4+ T cells (Figure 1.4B), suggesting an AD-related antigen-specific response. In contrast, very little proliferation was observed when T cells isolated from wild type mice were cultured with AD homogenates or when T cells from AD mice were cultured with homogenates derived from wild type mice. Taken together these results

suggest that antigen-experienced CD8 T cells can proliferate in response to an Amyloid-enriched environment *in vitro*.

Single cell sequencing reveals a diverse array of T cell subtypes that infiltrate the brains of AD mice

To further investigate the role of T cells in the AD brain environment, we next profiled T cell gene expression and T cell receptors (TCRs) at the single-cell level using 10x Genomics' single cell immune profiling. We isolated and sequenced CD8+, CD4+, and γδ T cells from 9 month old female mice from each of the four different genotypes (WT, 5XFAD, PS-19, and PS-5X) (Figure 1.5A). Each sample contained a pool of T cells from multiple mice of the same genotype. Clustering of all samples based on gene expression revealed 7 distinct clusters, including cytotoxic cells, naive cells, and a population of γδ-17 cells (Figures 1.5B, S.3). Consistent with our flow cytometry data, CD8+ T cells made up the majority of the population of infiltrating cells. Additionally, there was a significant increase in the proportion of cytotoxic CD8+ T cells in the amyloid-model mice (5XFAD and PS-5X) compared to WT or PS19 (Figures 1.5D–E). This corresponded with a significant increase in the proportion of naive-like T cells in the WT and PS-19 samples. This suggests that amyloid pathology promotes the recruitment and expansion of cytotoxic T cells into the brain.

Differential gene expression between genotypes provided further evidence that amyloid pathology, but not tau pathology alone, alters T cell activation state. For example, both 5XFAD and PS-5X T cells show significantly increased expression of cytotoxic and effector genes including *Gzmk, Xcl1, Ccl4, Ctsw*, and *Cd69*, while down-regulating genes associated with naive T cells, including *Sell, Ccr7, Tcf7*, and *Lef1* (Figure 1.5F). The amyloid models also show increased expression of genes associated with tissue residency (*Cxcr6, Cxcr3, Itgae, Litaf*, and *Cd69*) and proliferative exhaustion (*Pdcd1, Ctla4, Lag3, Tigit*), revealing a higher level of T cell recruitment and clonal expansion in the 5XFAD and PS-5X brain. Interestingly, 5XFAD and PS-5X cells also show a significant up-regulation of interferon-stimulated genes (ISGs) including *Ifit3, Ifitm3, Irf7*, and *Bst2*, with PS-5X cells having the largest increase in expression. Examination of these gene profiles at the single-cell level reveals distinct sub-populations of exhausted cells and interferon-stimulated

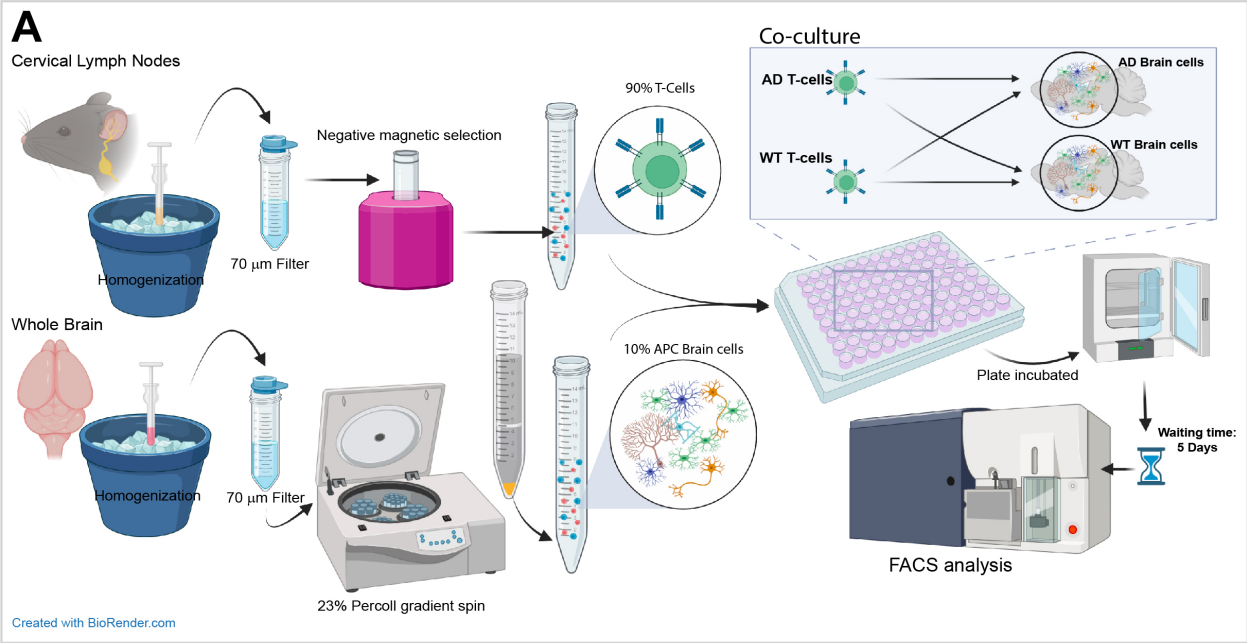

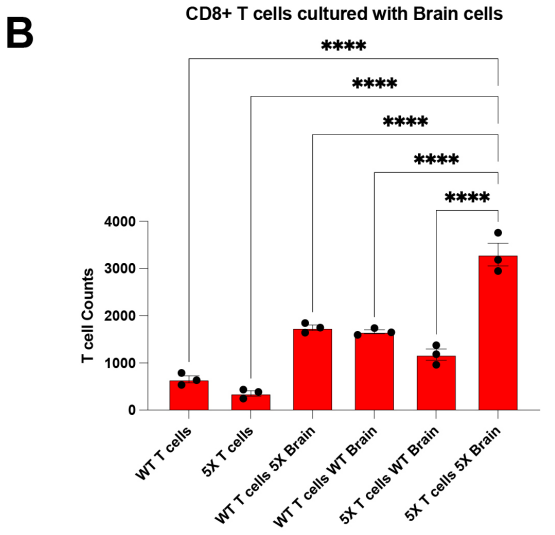

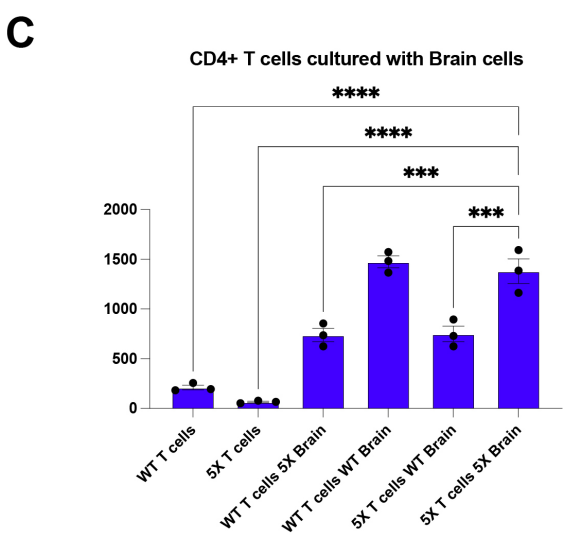

Figure 1.4: AD cytotoxic T cells proliferate significantly when co-cultured with AD brain cells *in vitro*. (A) Deep cervical lymph nodes were extracted from mice, homogenized, filtered, and then T cells were isolated using a negative magnetic bead selection. Whole brains were extracted from mice, homogenized, filtered, and then brain cells were isolated as a pellet using 23% percoll gradient. Isolated T cells and brain cells were co-cultured at a 1:1 ratio (100,000 cells each). T cells from 5X (amyloid plaque pathology) and WT (no pathology) 6mo mice were co-cultured with brain cells from 5X and WT 6mo mice. (B) Flow cytometry analysis of CD8+ and CD4+ T cells in different co-culture conditions. Statistical significance was determined if $p < 0.05$.

cells in the cytotoxic cluster (Figures 1.5G, S.3). Together with the differential expression results, this suggests that these two phenotypes may be over-represented in the 5XFAD and PS-5X mice and therefore increased in response to amyloid pathology.

We noted a disproportionate increase of "activated" CD8+ cells in one of our WT samples which is not reflected in the other WT sample or in samples from the other genotypes. Cells in this "activated" cluster are the only cells in the data set that express high levels of *Gzma, Cx3cr1, Zeb2, Klrg1*, and *S1pr5*, and they also express higher levels of *Ifng, Gzmb, Prf1, Klrk1, Ccl5*, and *Nkg7* than other clusters. This suggests that these are highly activated effector cells responding to an acute insult. Additionally, of the top 10 clonally expanded TCRs in this cluster, 8 belong to this single WT sample. Given the gene expression profile and the amount of clonal expansion in these WT cells, we believe the cells are likely to be from the same mouse and reflect an anomalous acute immune response, not present in the other mice. The effect of these cells is visible in population distribution statistics (Figures 1.5D–E) and differential gene expression between genotypes (Figure 1.5F), so we are cautious about making claims about this specific cluster or its genetic profile in relation to genotype differences.

T cells show high expression of multiple AD risk genes

Recent genome-wide association studies have implicated many immune-related genes in AD risk [8–10]. As microglia are the primary and most abundant immune cell within the brain many groups have sought to understand the impact of AD risk genes on microglia function. However, some of these AD risk genes are also expressed in adaptive immune cells. To better understand whether AD risk genes might influence the infiltration or function of T cells, we examined the expression levels of mouse homologues of AD risk genes identified from GWAS studies in our single cell sequencing data. Remarkably, we find that many of these AD risk genes are highly expressed in multiple T cells subtypes. 42 AD risk genes were significantly upregulated in at least one cluster, including 16 upregulated in the γδ-17 cluster alone (Figure 1.5H). Notably, the risk genes *Clnk* and *Hbegf* are almost exclusively expressed in γδ cells. These data suggest that mutations in AD risk

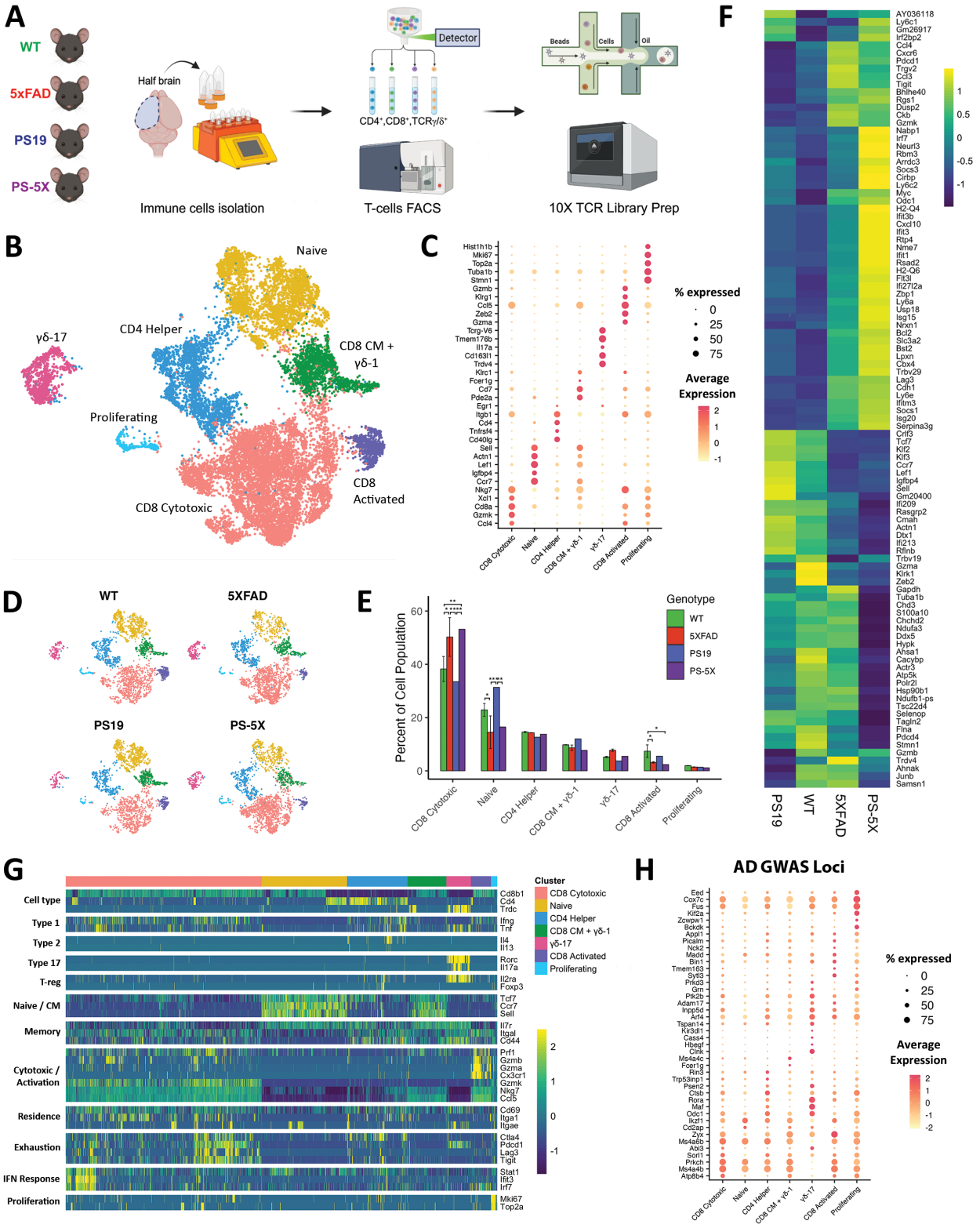

Figure 1.5: Single cell sequencing of infiltrating T cells reveals a variety of phenotypes. (Caption on next page.)

Figure 1.5: Single cell sequencing of infiltrating T cells reveals a variety of phenotypes. (A) Schematic of workflow to obtain single-cell sequencing data. T cells were isolated from half-brains, sorted based on the presence of CD8, CD4, or γδ TCR, and then sequenced for both general RNA and TCR-specific RNA using the 10X Genomics workflow. (B) Clustering of all samples together revealed grouping by common T cell phenotypes. The seven clusters were identified by characteristic markers as Naive (*Sell, Ccr7, Cd44*-), Central Memory (*Sell, Ccr7, Cd44*) + γδ type 1 (*Trdc, Nkg7, Il4-, Il17a*-), Activated (*Ccl5++, Cx3cr1, Klrk1*), Cytotoxic (*Gzmb, Gzmk, Nkg7*), CD4 Helper (*Cd4, Cd40lg, Cd44*), γδ type 17 (*Trdc, Blk, Il17a*), and Proliferating (*Mki67, Top2a*). (C) Dot plot of the top 5 most up-regulated genes in each cluster. Dot color represents average expression value in the cluster, and dot size represents the proportion of cells in the cluster that express each gene. (D) UMAP of cell clusters split by genotype. Cell populations were randomly downsampled for each genotype to match the smallest sample size, in order to reveal population differences. (E) Population analysis revealed significant differences in cluster proportions between genotypes. Error bars show maximum and minimum values for genotypes that have two samples. Significance markers: * = $p < 0.05$, ** = $p < 0.01$, *** = $p < 0.001$. (F) Heatmap of the top 100 most up- or down-regulated genes when comparing each genotype to WT cells. Mitochondrial and ribosomal genes, as well as genes related to heat stress, have been removed from the list. (G) Single-cell heatmap of scaled expression values for key genes used to identify T cell phenotypes. Cells are grouped by cluster. (H) List of GWAS-identified AD risk genes which are significantly changed in at least one of the 7 clusters when compared to all other cells, ignoring genotype.

genes not only alter microglia function but may also influence the function and/or infiltration of T cells. These findings also suggest that the specific role of γδ cells in AD bears further scrutiny.

T cells exhibit clonal expansion in response to amyloid pathology

Single-cell TCR sequencing further revealed evidence of significant clonal expansion of T cells in AD mice compared to wild-type controls. Clonally expanded TCRs were found to be enriched specifically in cytotoxic CD8 T cells (Figure 1.6A), with 7 of the top 10 expanded clonotypes in the data set belonging to cells from amyloid-model mice (5XFAD and PS-5X clonotypes). Conversely, at 9 months of age tau pathology alone fails to stimulate clonal expansion beyond WT levels (Figure 1.6B). Notably, the top PS-5X clonotype makes up 7.2% of all PS-5X cells in our data set, and the top 5XFAD clonotype makes up 7.5% of 5XFAD-1 cells. In contrast, the top clonotypes for WT and PS19 cells represent only 3.6% and 1.2% of those groups, respectively.

To examine whether any TCR clonotypes recognize known antigens, we used TCRMatch [123] to compare clonotype sequences from our data set to two databases of experimentally determined TCR/epitope pairs, the Immune Epitope Database (IEDB) [121] and VDJdb [122]. We found that

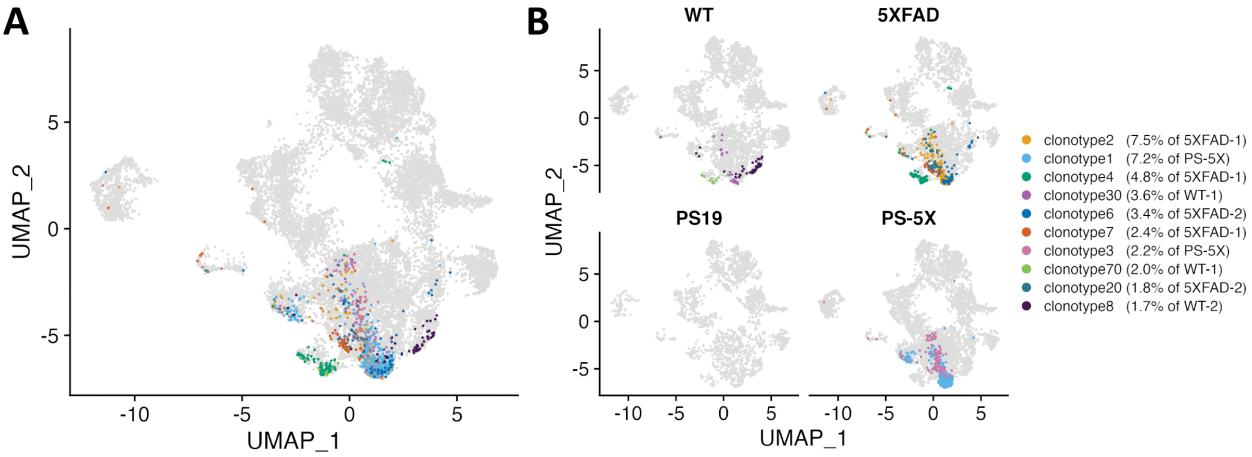

Figure 1.6: Locations of top 10 most-expanded clonotypes. (A) UMAP showing that the top 10 most clonally expanded clonotypes are primarily located in the CD8 cytotoxic cluster. (B) UMAPs split by genotype show large clonal expansion in the 5XFAD and PS-5X samples. Percentages are calculated as the number of cells with a given clonotype divided by the total number of the sample's cells with any identified clonotype.

out of 10,481 clonotypes, only 3,787 (36%) had high similarity in either the alpha chain or beta chain to a TCR/epitope pair in the databases, matching to epitopes of many common viruses like Influenza A and mouse cytomegalovirus. However, 59 of the top 100 expanded clonotypes had either no match or did not score above the threshold for a probable match, indicating a need for future studies to investigate and identify the antigens that are recognized by these clonally expanded TCRs.

Analysis of CD8 T cell gene expression reveals different activation states

To examine the CD8 T cells in more detail, we next subset our single cell data set to contain only cells that express *Cd8a* or *Cd8b1*, without expression of *Cd4* or γδ-specific markers, and re-clustered the cells. This revealed several more sub-populations of CD8 cytotoxic cells that appear to reflect different stages of T cell activation, including a unique cluster that expresses high levels of interferon response genes (ISGs) (Figures 1.7A, 1.7C, S.4A). This cluster appears to be primarily made up of PS-5X and 5XFAD cells. Although individual comparisons between genotypes for this cluster were not significant (Figures 1.7B, 1.7D), we did find significant interactions between the

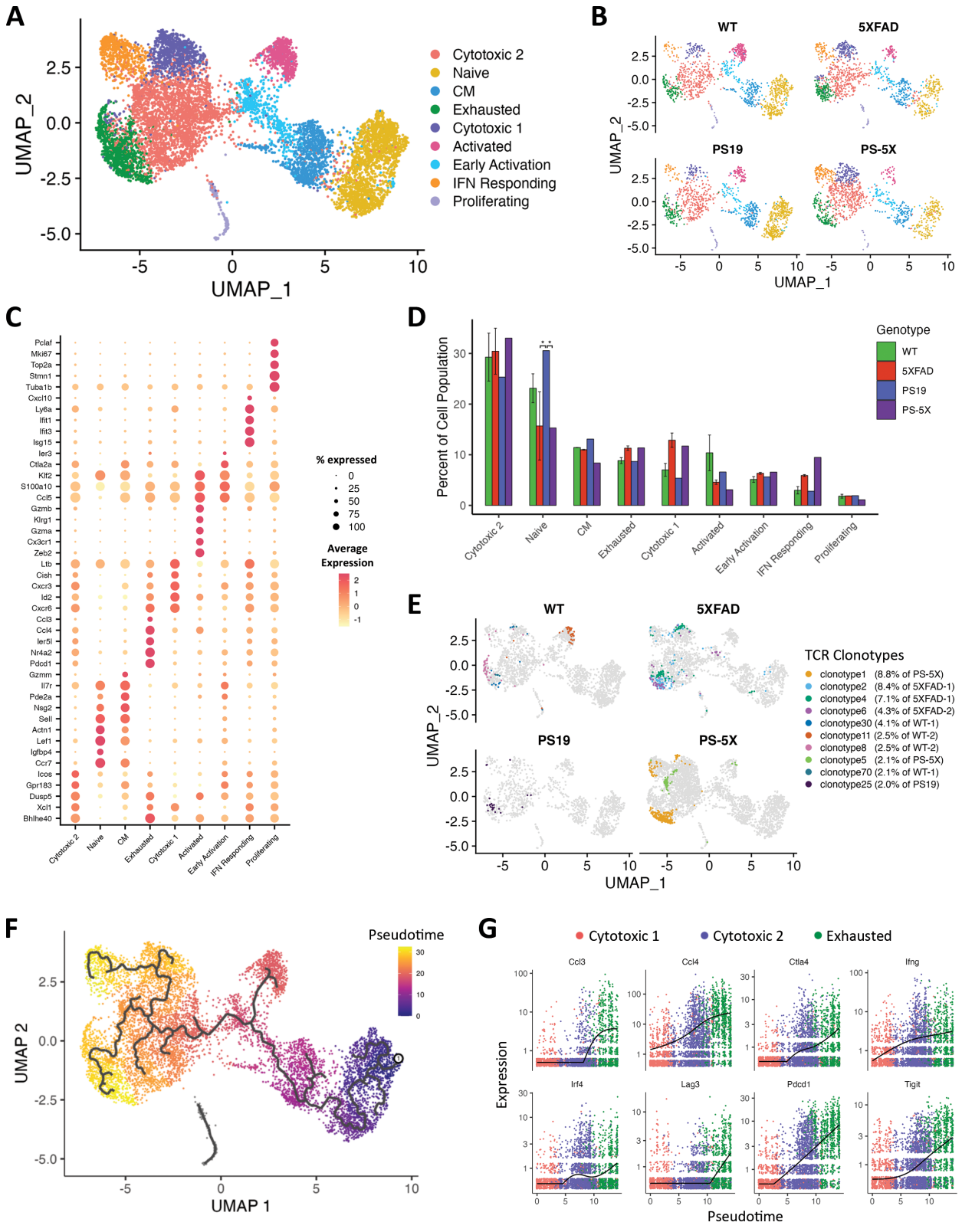

Figure 1.7: Analysis of C84+ T cell RNA and TCR expression. (Caption on next page)

Figure 1.7: Analysis of C84+ T cell RNA and TCR expression. (A) Clustering of CD8+ T cells after removal of CD4+ cells, γδ cells, and double-positive cells. The nine clusters were identified by characteristic markers as Cytotoxic 1 and 2 (*Gzmk, Fasl, Ifng*), Naive (*Sell, Ccr7, Cd44-*), Central Memory (*Sell, Ccr7, Cd44*), Exhausted (*Pdcd1, Tigit, Ctla4*), Activated (*Ccl5++, Cx3cr1, Klrg1*), Early Activation (*Ccl5++, Itga4++, Slamf6*), Interferon Responding (*Ifit3, Stat1, Irf7*), and Proliferating (*Mki67, Top2a*). (B) UMAP of clusters split by genotype. Cell populations were randomly downsampled for each genotype to match the smallest sample size, in order to reveal population differences. (C) Dot plot of the top 5 most up-regulated genes in each cluster. Dot color represents average expression value in the cluster, and dot size represents the proportion of cells in the cluster that express each gene. (D) Population analysis revealed significant differences in the Naive cluster between genotypes. Error bars show maximum and minimum values for genotypes that have two samples. (E) Locations of the top 10 clonally expanded clonotypes assigned to CD8+ cells. Percentages are calculated as the number of CD8+ cells with a given clonotype divided by the total number of the sample's CD8+ cells with any identified clonotype. (F) Pseudotime analysis reveals cell progression from the Naive cluster toward the Activated, IFN Responding, and Exhausted clusters. (G) Expression of several key proliferative exhaustion genes across pseudotime shows that the Cytotoxic 1, Cytotoxic 2, and Exhausted clusters are partially differentiated by stages of exhaustion.

IFN Responding cluster and the PS-5X genotype ($p < 0.001$), and between the IFN Responding cluster and the 5XFAD genotype ($p = 0.0011$). We also found that the main "body" of cytotoxic cells was split into three subclusters (Cytotoxic 1, Cytotoxic 2, and Exhausted) that were not acutely activated and had similar expression of hallmark cytotoxic genes (*Ifng, granzymes, Prf1*). Trajectory analysis and differential gene expression along pseudotime revealed that these three clusters appear to be stages of proliferative exhaustion, with cells in Cytotoxic 1 being the least exhausted and cells in the Exhausted cluster expressing the highest levels of exhaustion genes (Figures 1.7F–G). Lastly, analysis of clonotypes for CD8+ T cells revealed a similar pattern to that observed in Figure 1.4, with the largest clonal expansion detected in the PS-5X and 5XFAD samples (Figure 1.7E). Interestingly, the majority of the cells within these top clonotypes were located within the "Exhausted" cluster.

Subcluster analysis of CD4 and γδ T cells

We further performed subtype-specific analysis of CD4+ T cells and γδ T cells to identify smaller populations that were not evident in the combined full data set UMAP. The majority of CD4+ T helper cells appeared to exhibit a Th1 transcriptomic profile, as evidenced by high expression

of the Th1-specific markers (*Ifng, Tnf, Cxcr3*) and low or absent expression of *Il4* and *Il17a* (Figures S.4B, S.5A–D). Surprisingly, we also detected a population of CD4+ cells that expressed many cytotoxic genes and had a large amount of clonal expansion, primarily from one 5XFAD sample (Figures S.5E–F). Most $\gamma\delta$ cells in our data set were type 17 ($\gamma\delta$-17) T cells, which are analogous to Th17 cells and have been shown to primarily secrete IL-17 and IL-22. We also found a small group of type 1 $\gamma\delta$ cells ($\gamma\delta$-1), which were cytotoxic and exhibit similar gene expression profiles to innate natural killer (NK) cells (Figure S.6). For both CD4 and $\gamma\delta$ cells, there were not enough total cells to determine genotype-level differences in population distribution. As we only sequenced $\alpha\beta$ TCRs, we were unable to perform clonotype analysis of the $\gamma\delta$ cells.

CHAPTER 2

Validation of ERCC1 knockout as a model of premature aging

Jaclyn Beck, Jean Paul Chadarevian, Christina Tu, Sepideh Kiani Shabestari, Morgan Coburn, Joia Capocchi, Hayk Davtyan, Jonathan Hasselmann, Alyssa Bilheimer, Mathew Blurton-Jones

Introduction

Microglia are the brain's resident innate immune cells. They play a role in brain development and maintenance by pruning synapses, removing debris and dying cells, and clearing misfolded proteins [2–4, 12–15]. These functions are also necessary in protecting against neurodegenerative diseases, such as Alzheimer's disease (AD), where the buildup of misfolded proteins contributes to neuronal dysfunction and death. Recent genome-wide association studies (GWAS) have identified microglia as key players in the development and progression of AD. A majority of known late-onset AD risk genes, such as TREM2, MS4A6A, and CD33, are preferentially or exclusively expressed by microglia in the brain [2–4, 8, 9, 14]. The risk-increasing variants of these genes are typically associated with loss of functional and neuroprotective responses to Aβ, and/or increased activity of immune-dampening pathways [2, 3, 8], both of which imply that normal microglia function serves a protective role in the aging brain.

However, buildup of Aβ fibrils and oligomers and hyperphosphorylated tau promotes chronic inflammation, and persistently-activated microglia can convert from protective to detrimental states as AD progresses [24, 27, 28, 31, 32, 34]. Importantly, many features of AD-associated microglial dysfunction seem to be an exacerbation of age-related traits rather than a novel pattern of dysfunction [23, 40]. Much of the inflammation and dysfunction present in AD is also present in "healthy" aged brains. Both aging and AD-associated glia exhibit a decrease in lysosomal function coupled with an increase in immune signaling, including up-regulation of the complement

pathway, inflammasome activity, and phagocytic machinery, and a general increase in both pro- and anti-inflammatory cytokine production [12, 28, 40–42].

Analysis of RNA from human brain tissue revealed a general decline with age in genes related to microglia-neuron interaction (CX3CR1, P2RY12, P2RY13, CSF1R, TREM2, and TYROBP) and immune signaling through toll-like receptors (TLRs 1, 5, 6, 7, and 10) [62]. Single-cell RNA sequencing of human microglia from healthy aged donors further demonstrated that a large proportion of aged cells are characterized by high expression of SPP1, APOE, LPL, and LIPA [45], revealing a population of pro-inflammatory lipid-processing microglia. Many, but not all, of these changes are also reflected in studies of aged mice [42, 46–49].

Aging microglia exhibit a dysfunctional combination of both increased and decreased immune signaling, over-reactive but less effective responses to immune insults, and decreased communication and self-regulation [12, 56]. Taken together, these age-related changes show a shift away from homeostasis toward inflammation and neurotoxicity. These changes largely parallel those seen between AD and healthy brains, and it may be that small perturbations to an already stressed system are enough to drive the brain toward neurodegeneration. Therefore, it is critical to understand the interplay between healthy and dysfunctional microglial aging if we are to understand how AD and other neurodegenerative diseases develop.

However, it is extremely difficult to study glial aging in humans. Biological samples are only available from biopsies or post-mortem tissue, making *in vivo* functional or longitudinal studies impossible in living humans. Studies in mice provide a useful substitute, however caution is necessary when applying findings to humans. Studies have revealed large differences between mouse and human microglia, including differing responses to cytokines, low transcriptomic overlap in aging and disease, and lack of homology in key microglial genes [43, 59].

Given these differences and lack of studies comparing young and aged human tissue, very little is known about many aspects of microglial aging in humans, including proliferative ability, cytokine and chemokine production, immune function, and, importantly, interaction with neurodegenerative conditions [59]. This disparity highlights the need for more studies of human microglia and

better models of human aging, which may in turn shed light on the processes driving AD-related dysfunction.

One potential solution is to use human induced pluripotent stem cells (iPSCs) and subject them to differing environments to explore aging-related mechanisms. However, iPSC reprogramming essentially "rejuvenates" cells to an embryonic-like state. The reprogramming process results in lengthened telomeres, increased mitochondrial fitness, and decreased levels of senescence markers $p16^{INK4A}$ and SA-β-Gal [130, 131]. Any existing damage to DNA is also repaired, and genome-wide tri-methylation (H3K9me3) is increased to levels found in younger cells [132]. These changes have a profound effect on cell health and behavior, and this youthful phenotype persists beyond differentiation to somatic cells. iPSC-derived neurons exhibit a fetal rather than adult phenotype regardless of donor age or disease state [133, 134], and xenotransplanted iPSC-derived microglia retain a fetal or infant-like profile even in adult mice [22]. These issues make it challenging to study age-related neurodegeneration in iPSCs, despite the many benefits that iPSCs offer. This necessitates finding methods of retaining or re-introducing an aged phenotype into iPSCs to improve iPSC-driven study of neurodegeneration.

Our study sought to create and validate a model of aging in iPSC-derived microglia by genetic knockout of ERCC1 (excision repair cross-complementation protein 1). This protein is a necessary component of nucleotide excision repair, which recognizes and repairs single-strand DNA damage. Patients with severe loss-of-function mutations in ERCC1 develop rapid aging diseases like Cockayne Syndrome (CS) or Cerebro-Oculo-Facio-Skeletal Syndrome (COFS), which include dementia and neurodegeneration as a key symptom [135, 136].

Mouse studies have shown that ERCC1 knockdown ($ERCC1^{\Delta/-}$) results in microglia that show signs of age-related dysfunction in young mice [47, 137], but a similar approach has not been explored in human cells. Therefore, our study examines whether ERCC1 KO in human iPSC-derived microglia (iMGLs) will produce an aged phenotype both *in vitro* and when xenotransplanted into chimeric mice, which provide an *in vivo* environment for the further maturation of human microglia [22]. To examine the effects of ERCC1 deletion, we used several assays to quantify proliferation and phagocytic function of $ERCC1^{KO}$ iMGLs *in vitro*, bulk RNA

sequencing to analyze transcriptomic changes at baseline and after exposure to Aβ *in vitro*, and single-cell RNA sequencing of xenotransplanted microglia (xMGs) to determine if ERCC1^{KO} microglia exhibit an aged-like phenotype.

Methods

Cell Lines

Human iPSC control line

For all studies, we used a human iPSC line provided by the University of California Alzheimer's Disease Research Center (UCI-ADRC). The iPSC line (designated "ADRC5") was generated from subject fibroblasts under approved IRB and hSCRO protocols and provided by the Institute for Memory Impairments and Neurological Disorders. The ADRC5 line is from a female donor and does not harbor any FAD-causing mutations, nor any LOAD-associated high- or medium-risk alleles like APOE4 or TREM2 R47H.

Creation of ERCC1^{KO} iPSCs using CRISPR

Homozygous deletion of ERCC1 was achieved on the ADRC5 iPSC line using CRISPR/Cas9, which introduced a frame shift resulting in a premature stop codon in exon 2 on both alleles for the gene ERCC1. 2×10^5 induced pluripotent stem cells were isolated following Accutase enzymatic digestion for 3 min at 37°C. Cells were resuspended in 100 µL nucleofection buffer from Human Stem Cell Nucleofector Kit 2 (Lonza). The suspension was combined with 50 µg of RNP complex formed by incubating Alt-R S.p. HiFi Cas9 Nuclease V3 (IDTDNA) with fused crRNA:tracrRNA (5' CTCTGTGTAGATCGGAATAA; IDTDNA) duplex for 15 min at 23°C. The suspension was transferred to the Amaxa Nucleofector cuvette and transfected using program B-016. Cells were plated in TeSR™-E8™ (STEMCELL Technologies) media with 0.25 µM Thiazovivin (STEMCELL Technologies) overnight to recover. Cells were digested the following

day with Accutase and single-cell plated to 96-well plates in TeSR™-E8™ media with 0.25 μM Thiazovivin and CloneR (STEMCELL Technologies) supplement for clonal isolation and expansion. Genomic DNA was extracted using Extracta DNA prep for PCR (Quantabio) from a sample of each clone upon passage and amplified for sequencing using Taq PCR Master Mix (ThermoFisher Scientific) and the following primers: ERCC1_F 5'AGATGTCCTCTGCTCACCCC and ERCC1_R 5'GGAGTCATCCCTAGAACAGCG. PCR product from promising clones was transformed using TOPO TA Cloning Kit for Subcloning, with One Shot TOP10 (ThermoFisher Scientific) for allele-specific sequencing. Stable clones were further analyzed by array CGH (Cell Line Genetics) and found to be karyotypically normal before proceeding with experiments.

Cell Culture

iPSC maintenance

iPSCs were grown in 6-well plates coated with 1 mg/mL Matrigel (Corning), and media was replaced daily with 1.5 to 2.5 mL of fresh media (TeSR-E8, STEMCELL Technologies). When colonies reached sufficient size, 6-8 days after seeding, cells were either frozen for storage in liquid nitrogen using BamBanker Cell Freezing Medium (Wako) or passaged using ReLeSR (STEMCELL Technologies) into fresh wells. Passaging was typically done at a ratio of 1:6 (one confluent well split into six new wells) using TeSR-E8 media supplemented with 5 μM thiazovivin (STEMCELL Technologies). 24 hours after passaging, media was changed to TeSR-E8 without thiazovivin, and daily feedings continued as above.

iHPC differentiation

Frozen iPSCs were thawed into Matrigel-coated 6-well plates with TeSR-E8 and 5 μM thiazovivin. Cells were grown to confluence and passaged an additional two times prior to differentiation to allow for cell cycle recovery after freezing. Upon reaching confluence after the last passage, iPSCs were passaged into fresh Matrigel-coated wells and differentiated to $CD43^{+}$ iHPCs according to

[138]. Briefly, iPSCs were passaged to new wells at a concentration of approximately 80 colony aggregates per well, in TeSR-E8 with 5 µM thiazovivin. The next day ("Day 0" of differentiation), TeSR-E8 medium was removed and replaced with 2 mL/well of Medium A from the STEMdiff Hematopoietic Kit (STEMCELL Technologies). On Day 2 of differentiation, 50% of the media was replaced with fresh Medium A. On Day 3 (or day 4, if colonies had not yet taken on the flattened morphology shown in [138]), Medium A was removed and replaced with 2 mL/well Medium B. On days 5, 7, and 9, 1 mL/well fresh Medium B was added to existing media. Non-adherent cells (iHPCs) were collected on days 10 and 12. Conditioned media was returned to wells on day 10 to allow for collection on day 12. The collected iHPCs were either frozen in BamBanker Cell Freezing Medium or passaged into fresh wells for iMGL differentiation.

iMGL differentiation

iMGL differentiation was carried out as in [138]. Fresh or thawed iHPCs were added to Matrigel-coated 6-well plates at 10^5 cells per well, in 2 mL/well basal iMGL medium. iMGL medium consisted of DMEM/F12, 2X insulin-transferrin-selenite, 2X B27, 0.5X N2, 1X GlutaMAX, 1X non-essential amino acids (NEAA), 400 µM monothioglycerol, and 5 µg/mL human insulin. Immediately before feeding, media was supplemented with 100 ng/mL IL-34, 50 ng/mL TGFβ1, and 25 ng/mL M-CSF. iMGLs were fed every other day up through day 24 by adding 1 mL/well basal media plus cytokines to existing media. On days 12 and 25, partial media changes were performed as follows: All but 1 mL of conditioned media from each well was collected and centrifuged at 300xG for 5 minutes. Collected media was aspirated and the cell pellet was resuspended in 1 mL/well fresh media plus cytokines. 1 mL/well of resuspended cells were added back to wells. On day 25, the fresh media included the three cytokines listed above plus 100 ng/mL CD200 and 100 ng/mL CX3CL1. On day 27, 1 mL/well of maturation media (iMGL media containing all 5 cytokines) was added to the existing media. Cells were ready for experimentation on day 28 but could be kept in culture for up to one week if fed every other day with maturation media.

For some studies, a shorter 2-week differentiation protocol was used. On day 12 of differentiation, media was partially changed as in the 4-week protocol, but the fresh media was maturation media

as in day 25 of the 4-week protocol. On day 14, 1 mL/well of maturation media was added, and cells were ready for experimentation on day 15.

In Vitro Assays

Western blot

Levels of ERCC1 and DNA damage were quantified using Western blot. Primary antibodies used for Western blot include ERCC1 (Cell Signaling Technology, Abcam), GAPDH, Lamin B1, p16INK4A (Abcam), XPF, and XPA (Cell Signaling Technology).

To obtain whole-cell lysates, cells were lysed in 1X RIPA buffer with added 1X Halt Protease Inhibitor Cocktail and 1X Halt Phosphatase Inhibitor Cocktail (ThermoFisher Scientific). Lysates were stored at -80°C until analysis. All lysate concentrations were quantified using the Pierce BCA Protein Assay Kit (ThermoFisher Scientific) prior to use in Western blots.

Phagocytosis assays

Phagocytosis was measured kinetically using the Incucyte Live Imaging System (Sartorius). iMGLs were plated at $6x10^4$ cells per well in 96-well plates coated with fibronectin. 100 µL iMGL media with 1:1000 NucLight Rapid Red Reagent (Sartorius) was added to each well and plates were incubated at 37°C for 1 hour or overnight to allow the iMGLs to adhere. 20 µL of iMGL media mixed with phagocytosis substrate was then added to each treatment well, and 20 µL of unaltered iMGL media was added to each control well. Plates were placed inside the IncuCyte, imaged every 15 minutes to 4 hours at 10X magnification, and analyzed using the provided Incucyte software. If experiments continued beyond 48 hours, cells were fed by adding an additional 50 µL fresh iMGL media every 2 days.

Final concentrations for substrates were as follows: 2 µg/mL and 5 µg/mL fibril $A\beta_{42}$, and 25 µg/mL and 50 µg/mL pHrodo-tagged synaptosomes.

Preparation of fibril $A\beta_{42}$

1 mg of fluorescent monomeric $A\beta_{42}$ (AnaSpec) was dissolved in 100 µL 1% NaOH to a concentration of 1 mg/mL. The mixture was further diluted to 100 µg/mL with nuclease-free water, and incubated at 37°C for 7 days to create fibrils.

Proliferation and differentiation

3 wells each of WT and ERCC1^{KO} cells were counted manually every 4 days during iMGL differentiation beginning on day 2. Wells were scraped with a cell scraper to collect both adherent and non-adherent cells, and cells were centrifuged at 300xG for 5 minutes. Conditioned media was placed into fresh Matrigel-coated plates, and the cell pellet was resuspended in 1 mL fresh media. 10 µL cells were added to 10 µL of Trypan Blue and counted in the TC20 Automated Cell Counter (Bio-Rad). Fresh media was added to resuspended cells to total 1 mL/well, and 1 mL/well of cell mixture was added to wells with conditioned media.

RNA extraction and sequencing of *in vitro* cells

To perform bulk RNA sequencing of iMGLs, mature WT and ERCC1^{KO} iMGLs were collected from 6-well plates with approximately 1x10^6 cells per sample, and 4-5 samples per group. RNA was extracted using the RNeasy Mini Kit (Qiagen), including the optional DNase digestion steps. RNA pellets were re-suspended in RNAse-free water, quantified with NanoDrop, and frozen at -80°C. Samples were sequenced using the Illumina HiSeq 4000 System. One group of 4 WT and 4 KO samples was exposed to 1 µg/mL fibril $A\beta_{42}$ for 24 hours prior to lysis.

Mouse Studies

Mice

We used three mouse strains for transplant experiments. For the pilot 2-month transplant study, we used hCSF1-WT and hCSF1-PS5x mice. The hCSF1-WT model lacks T cells, B cells, and NK cells, and contains humanized CSF1 to promote human hematopoietic cell survival and deletions in Rag2 and Il2rγ to enable xenotransplantation ($Rag2^{-/-}$; $Il2r\gamma^{-/y}$; $CSF1^{h}$, The Jackson Laboratory #017708). hCSF1-PS5x mice were generated by backcrossing 5XFAD mice (MMRRC Strain #034848-JAX) and PS19 mice (Jax #008169) onto the hCSF1 background as detailed in [139].

For the 4-month transplant study we used MITRG mice, which also lack T cells, B cells, and NK cells, and contain several humanized proteins to promote microglial growth ($Rag2^{-/-}$; $Il2r\gamma^{-/y}$; $CSF1^{h}$; IL-3/$CSF2^{h}$; TPO^{h}, The Jackson Laboratory).

Xenotransplantation

Xenotransplants of iHPCs were conducted using our established and validated protocol [22]. Briefly, iPSCs were differentiated to iHPCs as in [138]. For the 2-month pilot study, iHPCs were transplanted into female postnatal day 3 (P3) hCSF1-WT or hCSF1-PS5x pups. For the 4-month study, iHPCs were transplanted into female postnatal day 2 (P2) MITRG pups. Prior to transplant, pups were placed on ice for 2-3 minutes to induce hypothermic anesthesia. After confirming anesthesia, pups were injected with 1 µL of iHPCs (62.5K cells/µL in sterile DPBS) at each of 8 injection sites (4 locations at 2 depths). After injection, mice were returned to their home cages and weaned at P21.

Brain tissue and xMG collection

Animals were euthanized and brain tissue collected as in [22]. Briefly, mice were administered Euthasol, and after verification of loss of consciousness, intracardially perfused with ice cold 1X

DPBS. Half brains from each mouse were reserved for single-cell RNA sequencing. The other half of each brain was drop fixed in 4% (w/v) PFA for 48 hours, and then cryoprotected in 30% (w/v) sucrose. Preserved brains were sliced into 30 µm thick coronal sections on a sliding microtome, and collected in PBS with 0.05% sodium azide.

Immunohistochemistry

Tissue sections were blocked for 1 h in 1X PBS, 0.2% Triton X-100, and 10% goat or donkey serum. After blocking, tissue was placed in 1X PBS, 1% goat or donkey serum with primary antibodies, and left overnight on a shaker at 4°C. Sections were incubated in fluorescent secondary antibodies for 1 h at room temperature, washed, and mounted on microscope slides. Tissue was imaged using the Olympus FluoView Confocal Microscope. Images were analyzed using Imaris, ImageJ, and a modified version of 3DMorph [140] (see below). Primary antibodies included Iba-1, human Ku80, and HLA-DR.

Morphological analysis

Morphological analysis on stained brain slices was done using a modified version of 3DMorph [140]. Some key changes we have implemented include additional thresholding to find cell nuclei prior to cell segmentation, nucleus-based segmentation rather than size-based segmentation, and alteration of segmentation algorithm to use geodesic distance rather than Euclidean distance. A full list of modifications and code can be accessed on GitHub at `https://github.com/jaclynrbeck/3DMorph`.

10x single cell RNA sequencing of xMGs

Single-cell RNA sequencing was carried out on xMGs from 4-month-old female MITRG mice. Extraction was performed as in [141]. Briefly, anesthetized mice were intracardially perfused with 1X DPBS, half brains were dissected, and the cerebellum was removed. Brains were manually

homogenized using a 7mL Dounce homogenizer and then run through a pre-soaked 70 µm filter. The sample was pelleted by centrifugation, resuspended in 30% Percoll overlaid with 2 mL of 1X DPBS, and centrifuged again. The myelin band and supernatant were discarded and cell pellets were resuspended in 80 µL MACS buffer (0.5% BSA in 1X DPBS) + 20 µL Mouse Cell Removal beads (Miltenyi) and incubated at 4°C for 15 min. Magnetically labelled mouse cells were separated using LS columns and the MidiMACs separator (Miltenyi) while the unlabeled human cells were collected in the flow through. Human cells were then pelleted by centrifugation and dead cells were magnetically removed using the Dead Cell Removal kit, Annexin V (Stem Cell Technologies) according to manufacturer protocol. Live cells were centrifuged, resuspended in 50–100 µL of MACS buffer, and concentrations were determined by counting on a hemocytometer. Final cell concentrations were then adjusted to 900-1,000 cells/µL per sample.

Libraries were prepared from 3 WT and 3 KO samples, according to the 10x Genomics Chromium Single Cell 3' Reagent Kits User Guide (v3.1 Chemistry) except that sample volumes containing 25,000 cells were loaded onto the 10X Genomics flow cell in order to capture around 10,000 total cells. The 10x Genomics workflow was then followed according to the user guide and libraries were sequenced on an Illumina NovaSeq 6000 targeting 50,000 reads per cell. FASTQ files from each sample were aligned to the human GRCh38 transcriptome using the CellRanger 6.0.1 *count* command, using the "refdata-gex-GRCh38-2020-A" pre-built reference provided by 10x Genomics. The *count* command was run with "expect-cells" set to 10,000, "include-introns", and all other arguments set to default. Results from all samples were combined using the CellRanger *aggr* command, with "normalize" set to none.

Samples were extracted and sequenced in two separate batches, with Batch 1 containing 2 WT and 2 KO samples and Batch 2 containing 1 WT and 1 KO sample.

Data Analysis

Statistical methods

An unpaired, two-tailed student's T test was used to determine statistical significance in Western blot and IHC data. For Incucyte assays, 2-way ANOVAs with post-hoc pairwise comparisons were conducted to examine interactions between iMGL genotype and time.

Analysis of Bulk RNA sequencing data

Bulk FASTQ files were preprocessed using BBDuk [142] to filter out ribosomal RNA and PhiX reads, trim Illumina adapters, and to quality trim any base pairs below a PHRED score of 10. FASTQC [143] was then performed to verify the quality of the sequencing files and all files were determined to be of sufficient quality for downstream processing. Reads were then pseudoaligned to the human GRCh38.p12 transcriptome (Ensembl release 94) [144, 145] using Kallisto [146]. Transcripts were summarized to the gene level in R using *tximport* [147], and differential gene expression (DGE) analysis was performed using *DESeq2* [148] after removing genes with summed counts < 10. An FDR cutoff of 0.05 was used to determine significance for DGE analysis.

DGE sets were analyzed for comparisons between *in vitro* WT and ERCC1^{KO} iMGLs, with or without exposure to Aβ. Gene Set Enrichment Analysis (GSEA) [149] was performed using pre-ranked analysis to analyze pathways that are enriched in these DGE sets. Results were ranked by $\text{sign}(\text{fold change}) * \text{-log}_{10}(\text{adjusted p value})$ for analysis. Results were compared to MSigDB's Gene Ontology database (c5.all.v7.1.symbols.gmt) and REACTOME database (c2.cp.reactome.v7.1.symbols.gmt). DGEs were also compared to existing human microglia bulk RNA sets and analyses across a range of ages [43, 150].

Analysis of single cell RNA sequencing data

Single-cell analysis was conducted in R using the Seurat package (version 4.1.0) [151]. A Seurat object was created from the filtered count matrix of all samples, as output by CellRanger *aggr*, using min_cells = 10 and min_features = 200. The data set was filtered to retain only cells that had at least 1,200 genes expressed, less than 5% mitochondrial gene expression, and between 1.2% and 20% ribosomal gene expression. Batch 1 (containing 2 WT and 2 KO samples) had higher overall counts for every sample, so Batch 1 samples were additionally thresholded to retain cells with at least 2,000 expressed genes. To remove potential doublets, cells were given a "complexity" score, defined as the total count of RNA in the cell divided by the number of genes. Cells with a complexity score greater than 4.0 were removed. These parameters were determined by visual inspection of cell distribution along these variables.

As there were clear batch differences between samples, LIGER was used to integrate the samples for clustering and display. The LIGER functions *optimizeALS* and *quantile_norm* were run with k=40, and the resulting dimensional reduction was added back to the Seurat object. The Seurat functions *RunUMAP*, *FindNeighbors*, and *FindClusters* were run using the LIGER reduction with dimensions 1-40 and a cluster resolution of 0.1. At this point, three small clusters were removed due to high expression of hemoglobin genes (HBA1, HBB, HBD) or high expression of monocyte genes (RNASE1, SELEOP, CD163) in combination with low expression of microglial marker genes (CX3CR1, P2RY12, P2RY13). This left a total of 36,437 cells distributed across samples as follows: WT-1 (4,189 cells), WT-2 (4,838 cells), WT-3 (9,550 cells), KO-1 (3,061 cells), KO-2 (6,560 cells), KO-3 (8,269 cells).

For all differential gene testing, Seurat's *FindAllMarkers* or *FindMarkers* functions were called on log-normalized counts using MAST to test for significance and regressing out total RNA count, percent mitochondrial genes, and percent ribosomal genes as latent variables. All p-values were adjusted using Bonferroni correction. Genes were considered significantly different if adjusted p <= 0.01, log fold-change >= 0.25, and at least 10% of the cells in the cluster (or genotype) expressed the gene.

Gene Ontology analysis was performed using PANTHER, using differentially expressed genes as input. GO terms with an enrichment FDR ≤ 0.05 were considered significant. Single cell gene set enrichment analysis (GSEA) was performed using the R package *fgsea* (version 1.16.0) [149, 152]. The list of differentially expressed genes (DEGs) between ERCC1^{KO} and WT cells was input using the average log-2-fold change as the rank. DEGs were compared to the Reactome pathway gene set [114], which was retrieved using the R package *msigdbr* (version 7.4.1) [153]. Reactome terms with a p value ≤ 0.05 were considered significant.

Results

Creation of ERCC1 genetic knockout iPSCs

To create a model of premature aging in iPSCs, CRISPR gene editing was used to knock out the ERCC1 gene on a healthy patient cell line referred to as "ADRC5". Patient studies show that COFS and CS only manifest in patients homozygous for disease-causing ERCC1 mutations which result in almost no expression of ERCC1 [135, 136], so we created a homozygous knockout of the ERCC1 gene by introducing a premature stop codon in exon 2 of both alleles (Figure 2.1A). The unaltered wild-type line (ADRC5-WT) was used as an isogenic control.

Although Sanger sequencing revealed homozygous incorporation of premature stop codons within exon 2, Western blots of ERCC1 expression levels surprisingly revealed that the ERCC1^{KO} line still has some expression of ERCC1 (Figures 2.1B–C). Exon 2 is contained in every known splice variant of ERCC1, however it is possible that this cell line was able to up-regulate an unknown variant to maintain some ERCC1 function. The ERCC1^{KO} line exhibited reduced growth rates, suggesting that *in vitro* selective pressure may have promoted the induction of a novel splicing variant to provide some degree of ERCC1 activity and iPSC survival. However, we have also been unable to rule out other explanations such as antibody non-specificity or antibody detection of truncated non-functional ERCC1 protein. Regardless of the reason, the significant decrease

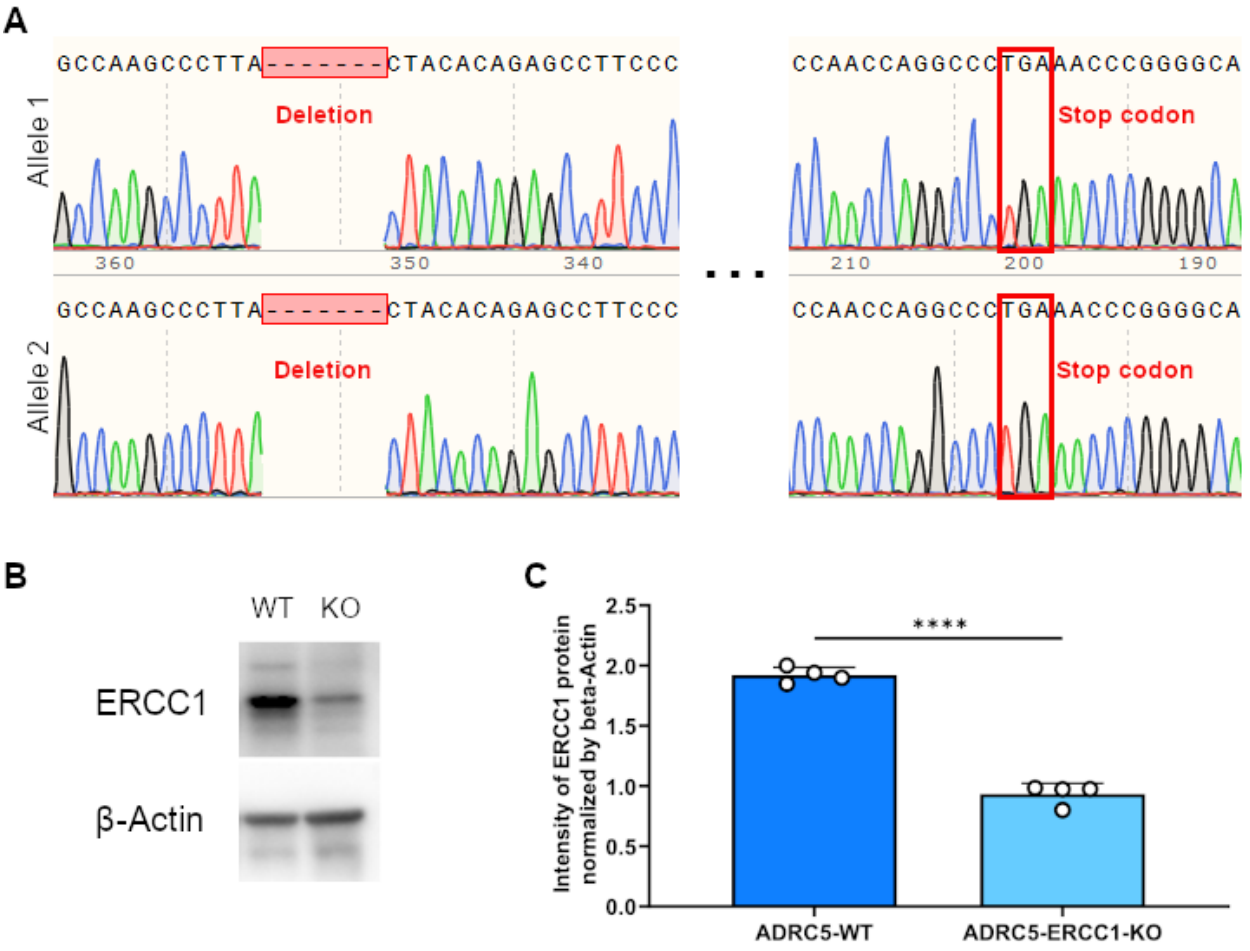

Figure 2.1: Verification of ERCC1 knockout in the ADRC5 iPSC line. (A) Chromatogram of ADRC5 clone shows homozygous deletion in exon 2 of the ERCC1 gene, leading to premature stop codons approximately 150 base pairs downstream. (B) Example lanes from a Western blot of ADRC5-WT and ADRC5-ERCC1-KO iPSCs. (C) Western blot data shows a large decrease but not complete knockout of ERCC1 expression in ERCC1^{KO} iPSCs. n = 4 WT, 4 KO samples.

in ERCC1 protein expression in ERCC1^{KO} cells was enough to cause noticeable differences in microglial function in the experiments detailed below.

DNA damage and iMGL differentiation are affected by ERCC1 KO

After verification of ERCC1 protein reduction, we next assessed levels of DNA damage with Western blots of WT and KO iMGLs. We examined γH2AX, a marker for double-stranded breaks, p16INK4A, a marker of cell senescence, XPF, which forms a dimer with ERCC1, XPG, which

cuts DNA on the opposite side of the damage as ERCC1-XPF, and XPA, which recognizes DNA damage in the NER pathway. As expected, levels of XPF were decreased in ERCC1^{KO} cells (Figure 2.2B). There was no significant difference in the expression of p16INK4a, XPG, or XPA (Figures 2.2C–E). Unexpectedly, the level of γH2AX was significantly lower in ERCC1^{KO} cells (Figure 2.2F), and this particular result has been replicated in multiple experiments.

This unusual result could have a number of potential explanations. For example, DNA damage, especially double-strand breaks, can prevent cells from proliferating [154, 155]. Positive selection pressure on iPSCs and iHPCs would therefore select for ERCC1^{KO} cells with the least DNA damage. ERCC1 also creates DSBs to facilitate ICL repair [156, 157], and loss of ERCC1 would result in decreased creation of DSBs from this source of damage. It is important to note that these blots were normalized with Lamin B1, which is known to decrease with lowered levels of ERCC1 [158, 159], and the normalized values for ERCC1^{KO} cells may have been slightly altered by this effect.

To examine proliferation and survival, WT and KO cells were counted after HPC differentiation and periodically during the iMGL differentiation cycle. While cells from both lines grow comparably at the iPSC stage, ERCC1 KO has a clear detrimental effect on differentiation from iPSCs to iHPCs (Figure 2.2G) and from iHPCs to iMGLs (Figures 2.2H–I). Live imaging experiments using Caspase 3/7 as a marker for apoptosis revealed that mature ERCC1^{KO} iMGLs do not have a significantly increased rate of death compared to WT iMGLs. This makes it likely that the effect on differentiation is due to decreased proliferation or a lowered ability to differentiate, rather than increased cell death.

ERCC1 KO significantly impacts microglial phagocytosis *in vitro*

We conducted several live imaging experiments on iMGLs in an Incucyte Live Cell Analysis System to examine the impact of ERCC1 KO on microglial-specific functions like phagocytosis. iMGLs were given either pHrodo-tagged synaptosomes or fluorescent fibril Aβ_{42}, both of which only

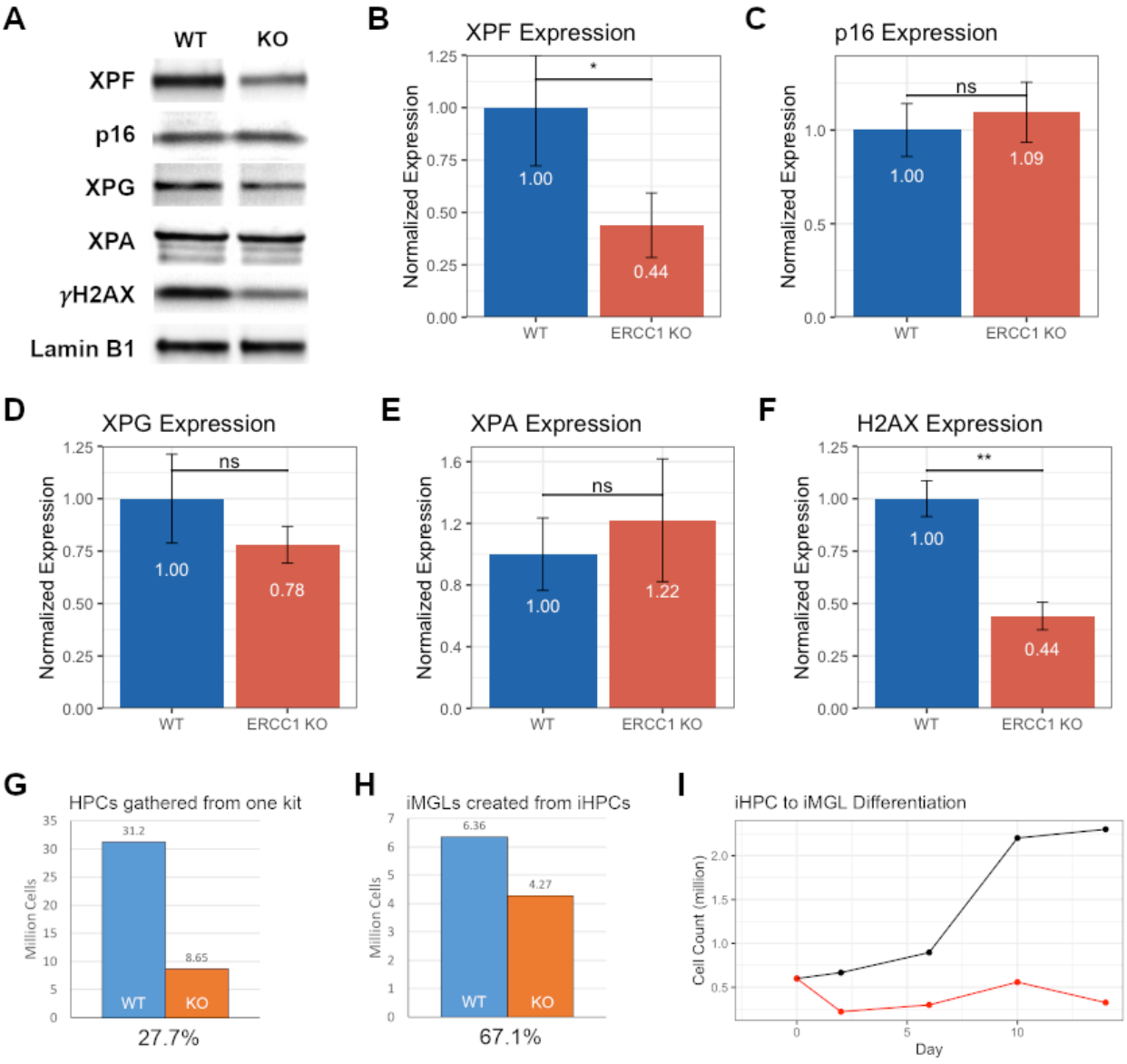

Figure 2.2: Analysis of DNA damage markers and differentiation. A) Example lanes from a Western blot, normalized to Lamin B1. B) XPF expression is decreased in ERCC1^{KO} iMGLs. C-E) No significant difference was found in p16, a marker of senescence, or XPG and XPA, markers of DNA damage. F) γH2AX expression was surprisingly lowered in ERCC1^{KO} iMGLs. n = 3 WT, 3 KO samples. G) Cell count of WT and ERCC1^{KO} HPCs gathered from using one StemDiff Hematopoietic Differentiation Kit each on iPSCs from each genotype. H) Cell count of iMGLs created from a 12-day differentiation of HPCs. Each genotype started differentiation with 1.2 million HPCs. I) Manual count every 4 days of iMGLs during differentiation. Each genotype started with 600,000 HPCs.

fluoresce brightly when in an acidic environment like a cell lysosome (Figure 2.3A). We found that ERCC1 KO had a significant effect on phagocytosis of both substrates.

ERCC1^{KO} cells had significantly reduced uptake of synaptosomes in a dose-dependent manner. We found that after 18 hours, nearly 100% of WT cells contained synaptosomes, regardless of dose, but only 60-70% of the KO cells had detectable fluorescence from synaptosome uptake (Figure 2.3B). Additionally, among the cells that had detectable internal fluorescence, the average level of fluorescence inside of each cell was much higher in WT cells than in KO cells, independent of dose (Figure 2.3C). Assuming brightness is correlated with internal concentration of synaptosomes, this suggests that KO cells did not ingest as many synaptosomes as WT cells. These two measures indicate that ERCC1 KO decreases a cell's ability to recognize or ingest synaptosomes. This result would be consistent with a more aged phenotype, as a major function of young microglia is synaptic pruning and this function is down-regulated after puberty [160].

In contrast, ERCC1 KO seemed to slightly increase Aβ phagocytosis. We found that initially, more ERCC1^{KO} cells than WT cells had detectable levels of Aβ inside them, independent of dose, but that this gap narrowed over the course of 24 hours (Figure 2.3D). This suggests an initial increased activation in KO cells that normalizes to WT levels over time. Curiously, we found no difference in the amount of Aβ ingested between WT and KO cells with detectable fluorescence (Figure 2.3E). From this data it appears that ERCC1 KO does not unilaterally decrease phagocytic function but rather affects cells in a substrate-dependent manner.

ERCC1 KO changes expression of over 400 genes *in vitro*

Bulk RNA sequencing of *in vitro* WT and KO iMGLs revealed 443 significantly differentially expressed genes with a log fold change $\geq$ 1 or $\leq$ -1 (Figure 2.4A), one of which was ERCC1. 1482 genes were changed in total, including those with a log fold change $<$ 1. Of those genes, 67 genes were known to change with aging according to [43] (Figures 2.4B–C). Oddly, many of the aging-related genes were changed in the opposite direction as expected. We hypothesize that this may be due to changes induced by the *in vitro* environment. Specifically, iMGLs are

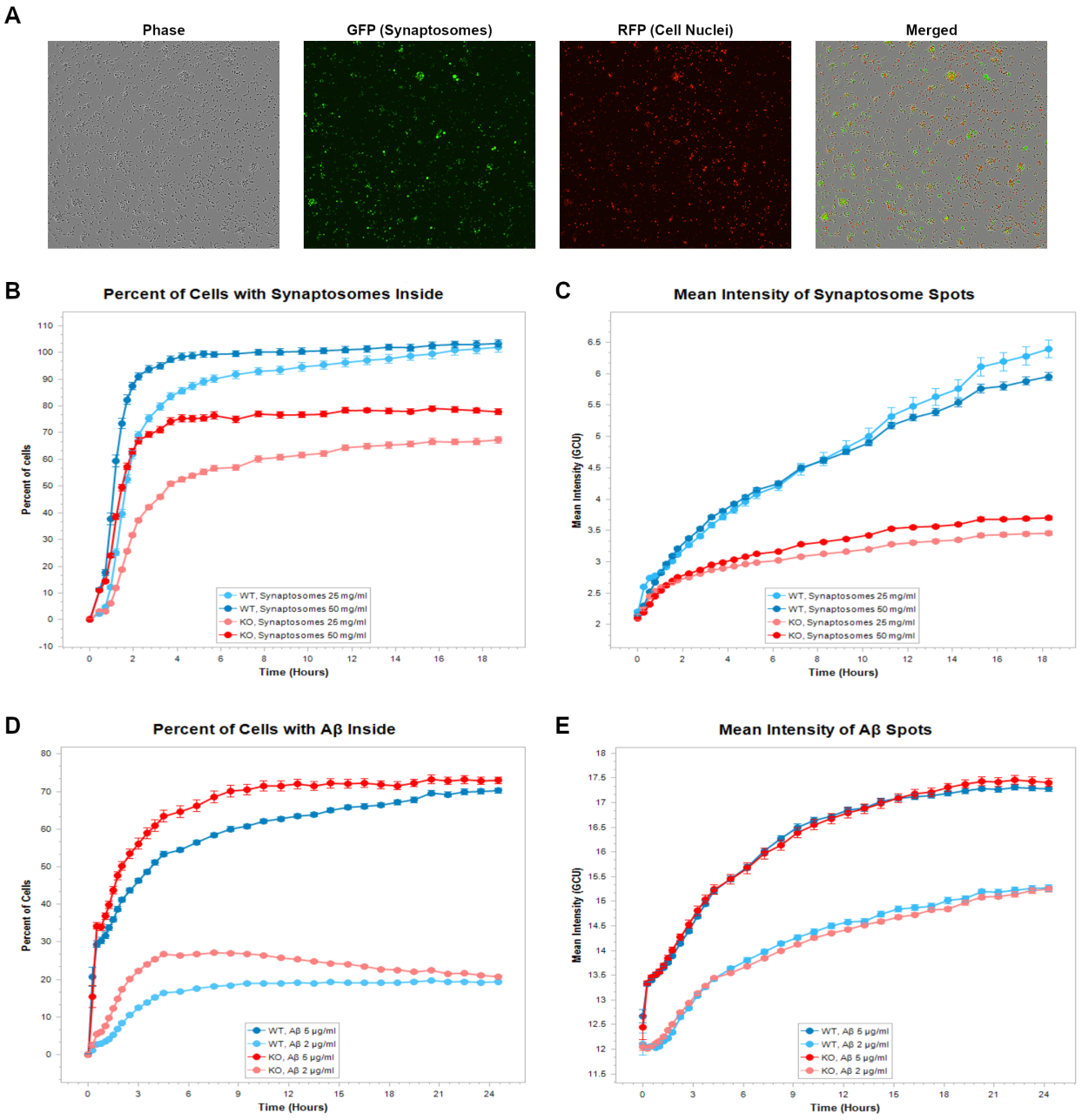

Figure 2.3: ERCC1 deletion affects microglial phagocytosis of synaptosomes and Aβ. A) Example images from the Incucyte Live Imaging System, containing iMGLs, pHrodo-tagged synaptosomes, and nuclear marker NucLight Rapid Red Reagent. B) Percentage of each cell population with detectable synaptosome fluorescence. C) Mean intensity of each each detectable synaptosome cluster. D) Percentage of each cell population with detectable Aβ fluorescence. E) Mean intensity of each detectable Aβ cluster.

grown by themselves with no neurons or other glia for interaction. iMGL media also contains homeostasis-inducing cytokines including TGFβ and CD200, which may be preventing some of the expected priming, activation, and dysfunction we would expect from aging cells. Significant changes in gene expression between *in vivo* and *in vitro* microglia have been documented [161], which demonstrates the necessity of using *in vivo* models. Another potential explanation is the type of comparisons carried out in [43], where the youngest patient in the study was 34 years old. Therefore, gene changes from that data set reflect changes with aging from adulthood onward, while we expect our data to be more similar to a comparison between older adult microglia and fetal microglia.

Some gene changes hint at mechanisms that may drive the alteration of differentiation and phagocytosis seen in (Figure 2.3). ERCC1^{KO} cells significantly up-regulate MSR1, a receptor for Aβ, which could explain the increased initial response to Aβin phagocytosis assays. Conversely, they down-regulate C2, a necessary component of the synapse engulfment pathway [160], which would result in lower synaptosome phagocytosis. This finding is also consistent with a study finding downregulation of C2 with age in human microglia [43].

To assess which functions and pathways were most affected by these gene changes, we performed Gene Set Enrichment Analysis (GSEA) on this data (Figure 2.4D). Only one GO term (Cell Adhesion) is up-regulated, while 34 are down-regulated. The majority of down-regulated GO terms involve immune response, indicating a general decrease in immune function in ERCC1^{KO} cells.

ERCC1 KO changes genetic response to Aβ

Bulk RNA sequencing was also performed on iMGLs that had been exposed to fibril Aβ_{42} for 24 hours. As seen by the clustering in (Figure 2.5A), Aβ exposure has a stronger effect than genotype on gene expression. However, when analyzing only the Aβ-exposed groups, nearly 2500 genes are changed between ERCC1^{KO} and WT iMGLs (Figure 2.5B). MSR1, a receptor for Aβ, is up-regulated in ERCC1^{KO} cells, while other immune-response genes including CD14, LGALS3,

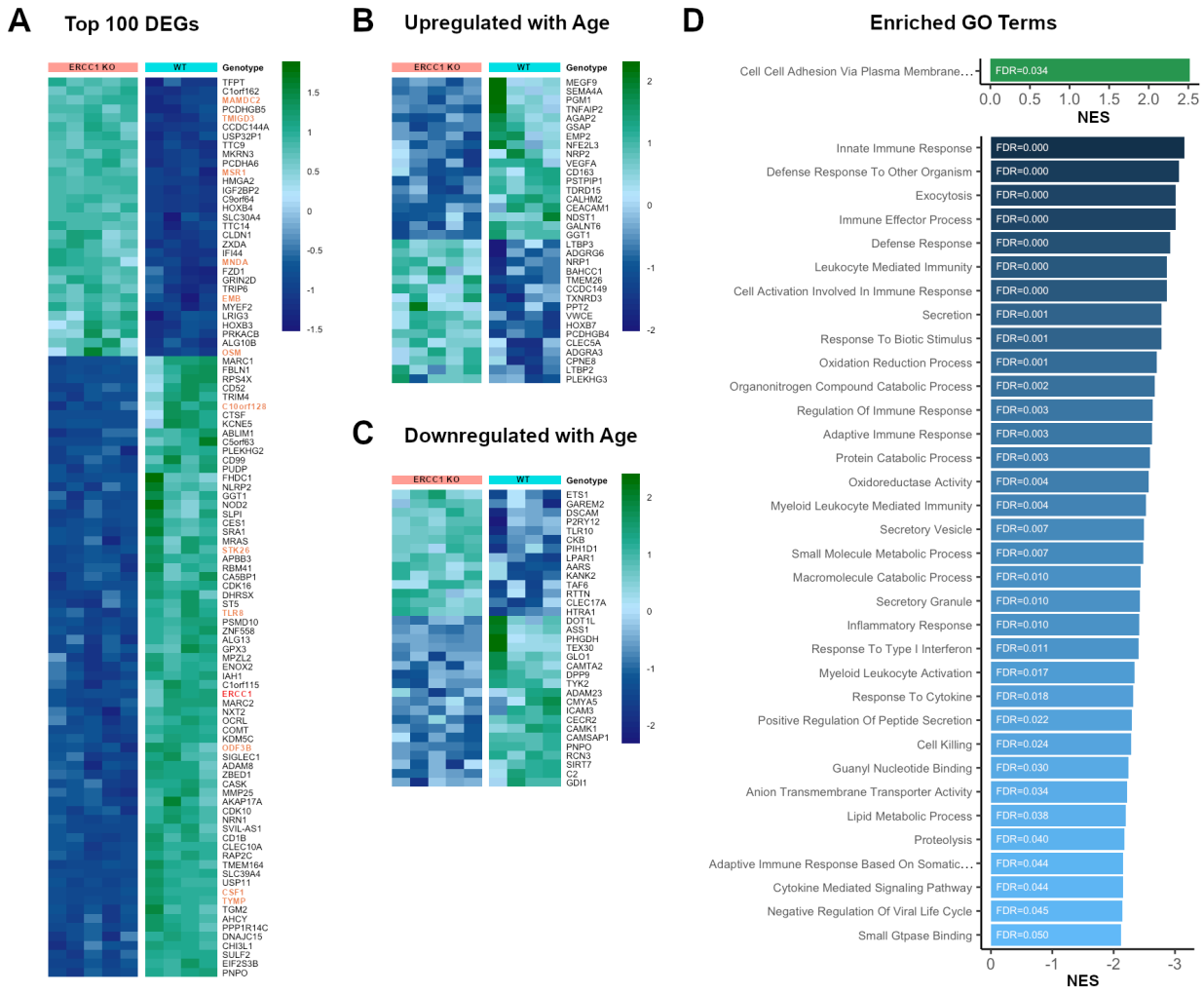

Figure 2.4: Differential gene expression between WT and ERCC1^{KO} iMGLs. A) Top 100 differentially-expressed genes (DEGs). Microglia "signature" genes [161] are highlighted. B) Significantly-changed genes known to increase with aging according to [43]. C) Significantly-changed genes known to decrease with aging according to [43]. D) Gene Ontology (GO) terms that are enriched in the set of DEGs.

and IL1A are down-regulated. Surprisingly, TREM2, another Aβ receptor, is down-regulated in ERCC1^{KO} iMGLs exposed to Aβ, which could indicate some dysfunctional signaling.

We also conducted GSEA on the set of genes changed between ERCC1^{KO} and WT iMGLs when exposed to Aβ. 161 GO terms were significantly enriched in this gene set (FDR $\leq$ 0.05) (Figure 2.6). Interestingly, exposure to Aβ causes ERCC1^{KO} cells to up-regulate several DNA repair mechanisms, including double-strand break repair. In addition to a general decrease in immune response, ERCC1^{KO} iMGLs also down-regulate GO terms related to protein processing

and clearance, including "Macromolecule Catabolic Process," "Proteolysis," and "Regulation of Protein Catabolic Process." However, in contrast to the "primed" phenotype of aged and Ercc1$^{\Delta/-}$ microglia in [47, 137], ERCC1^{KO} cells exposed to Aβ appear to down-regulate both cytokine production and cytokine response (Figure 2.3D).

Transplanted ERCC1^{KO} iHPCs successfully differentiate into microglia

Our lab has developed a reliable protocol for transplanting iHPCs into chimeric mice, where the iHPCs proliferate, differentiate to microglia, and spread throughout the brain [22]. Although mice with body-wide Ercc1-mutations have good survival until 4-6 months of age [47, 137, 162], it was unknown whether ERCC1^{KO} iHPCs could be successfully transplanted into chimeric mice and whether they would survive as microglia.

We conducted a preliminary 2-month-long transplantation study with WT and ERCC1^{KO} iHPCs. Cells were transplanted into female hCSF1-WT and hCSF1-PS5x mouse pups on postnatal day 3, and the transplanted mice were sacrificed at 2 months of age. Two PS5x mice were used due to a limited number of WT pups, however at 2 months these mice should not have developed enough amyloid pathology to significantly affect the microglia for the purposes of this study. Transplants were done as follows:

iHPC Genotype	Number of Mice Transplanted
ERCC1^{KO}	4 WT / 0 AD
WT	2 WT / 2 AD

Mouse brain tissue was stained with antibodies against Iba-1, human Ku80, and HLA-DR and we imaged the dentate gyrus (DG, gray matter) and the fimbria fornyx (fi, white matter) of each mouse. Overall brain engraftment for both WT and ERCC1^{KO} cells was poor, possibly due to performing transplants on P3 instead of P1 or P2, however both cell lines presented with a high number of human microglia in the DG and fi (Figures 2.7A–B). Analysis of these images show that there was no significant difference between WT and ERCC1^{KO} xMGs in count or morphology (Figure 2.7C).

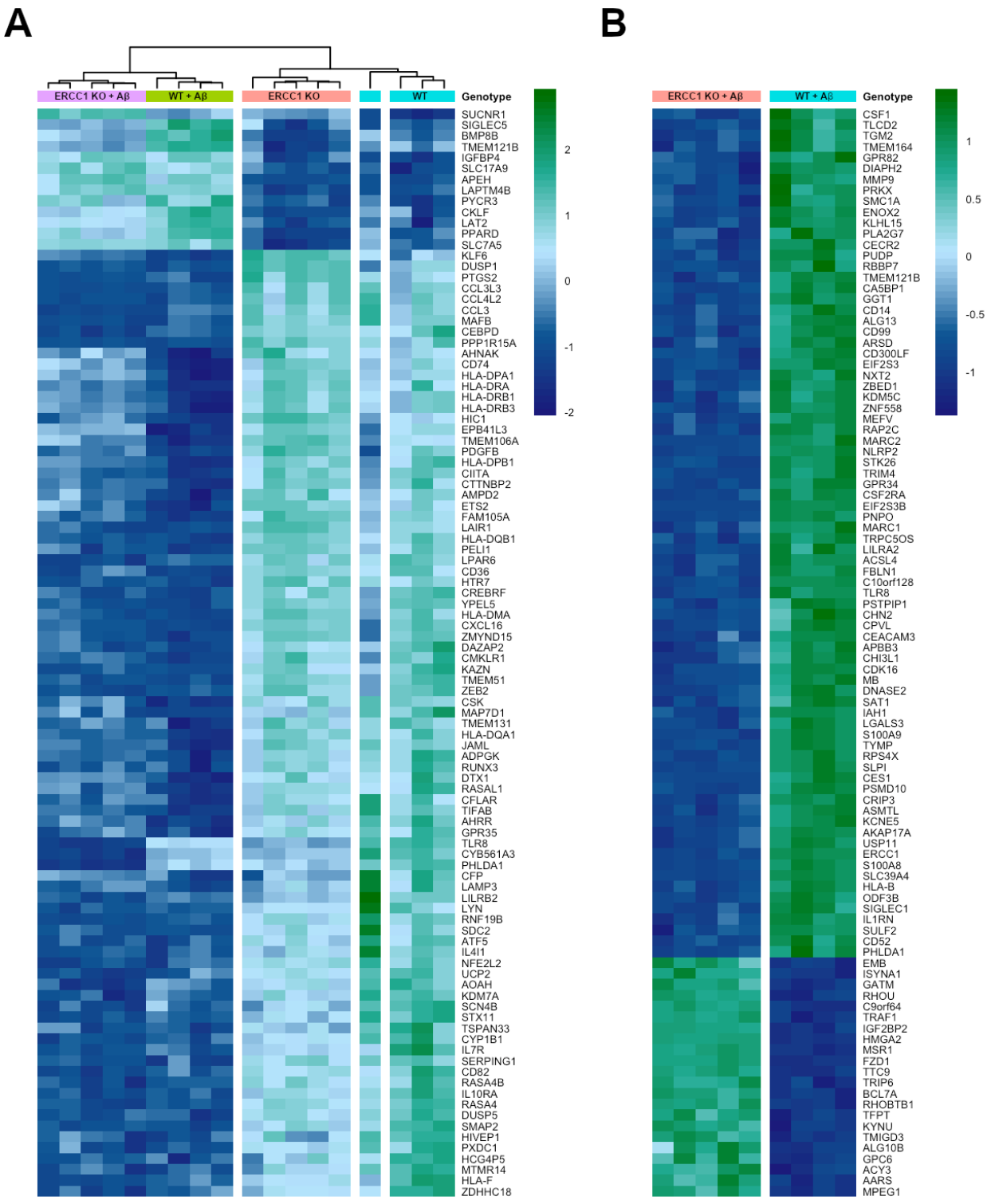

Figure 2.5: Differential gene expression upon exposure to fibril Aβ. A) Comparison of exposed and non-exposed iMGLs reveals that Aβ exposure has a stronger effect on gene expression than genotype. B) Top 100 differentially expressed genes between ERCC1^{KO} and WT iMGLs after 24 hours of Aβ exposure.

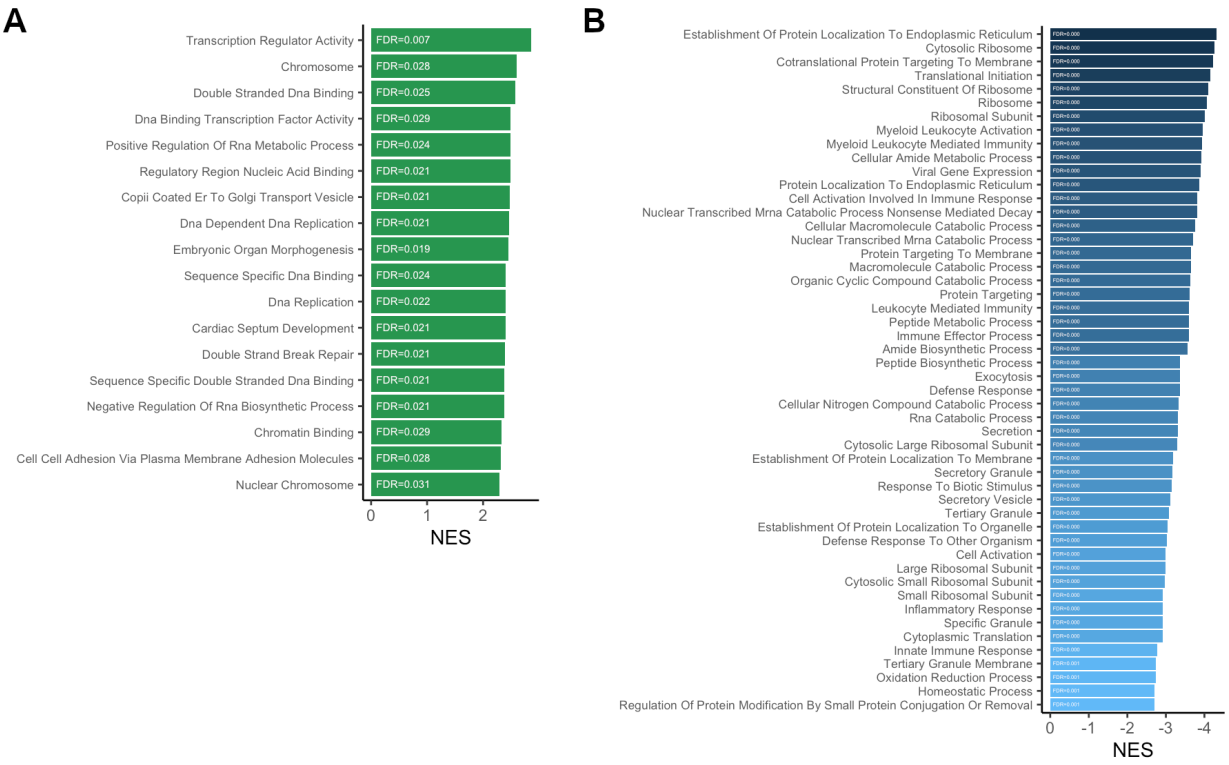

Figure 2.6: GSEA for differential gene expression after Aβ exposure. A) Enriched GO terms that are up-regulated in ERCC1^{KO} iMGLs after exposure to Aβ. B) Enriched GO terms that are down-regulated in ERCC1^{KO} iMGLs after exposure to Aβ. Only the top 50 down-regulated GO terms are shown.

This transplant study showed that the ERCC1^{KO} iPSC line is capable of proliferating and differentiating in the mouse brain to roughly the same extent as the WT iPSC line, and can survive at least two months in the murine brain without apparent detrimental effects.

Transplanted ERCC1^{KO} microglia display signs of immune dysfunction

To examine whether ERCC1^{KO} microglia exhibit signs of premature aging *in vivo*, we transplanted WT and ERCC1^{KO} iHPCs into female WT-MITRG pups and sacrificed the mice when they were 4 months old. We then performed single-cell RNA sequencing on purified xMGs from the mice. Dimensional reduction and clustering of all samples shows a large population of homeostatic microglia, which express HEXB, P2RY12, and CX3CR1, and multiple smaller specialized clusters (Figure 2.8A). These include disease-associated microglia (DAM), characterized by high

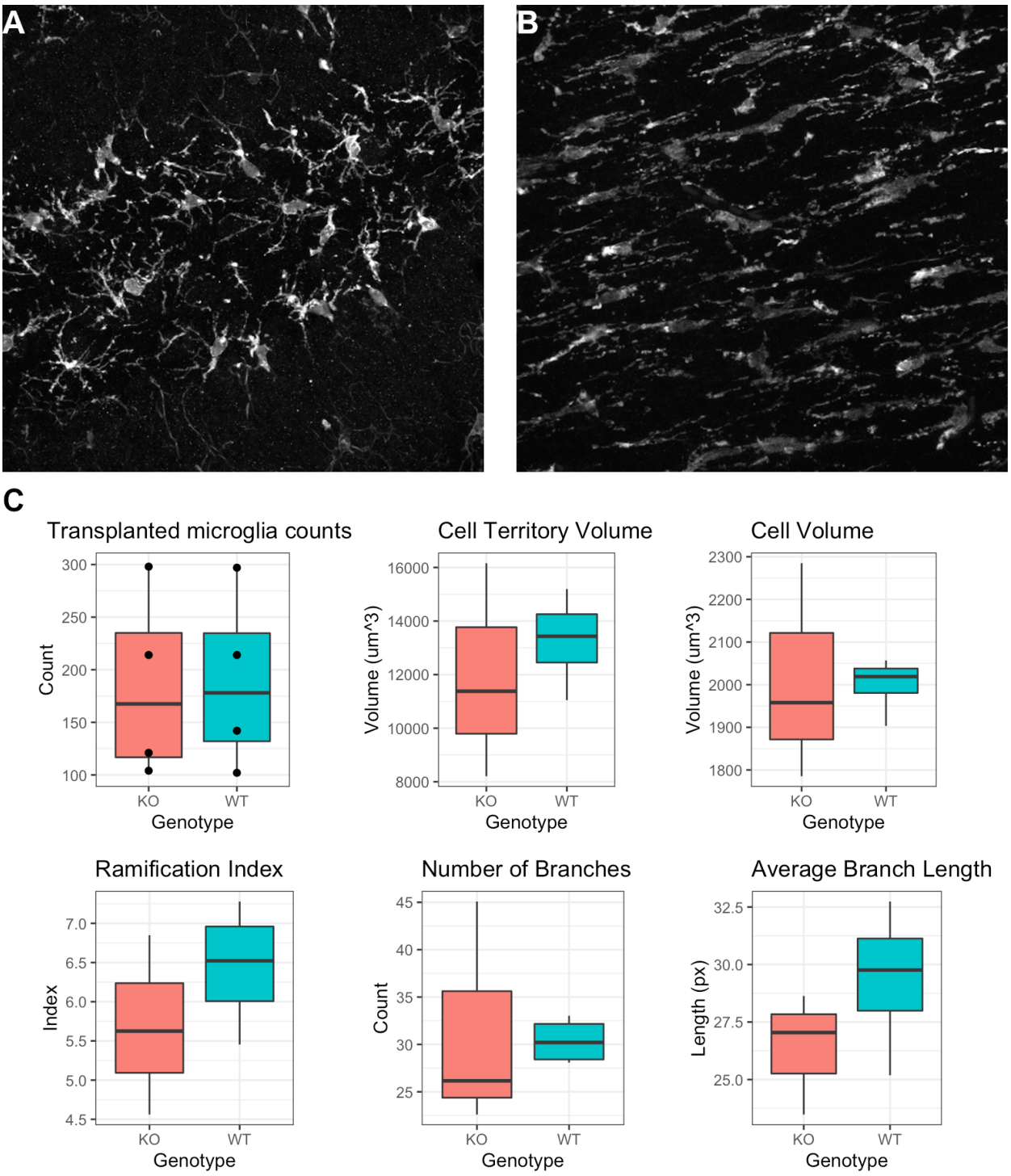

Figure 2.7: Xenotransplanted ERCC1^{KO} microglia survive in the murine brain. A-B) Iba+ ERCC1^{KO} microglia in the Dentate Gyrus (A) and Fimbria Fornix (B) of a 2 month old mouse. C) No significant difference was seen between WT and ERCC1^{KO} microglia along multiple measures.

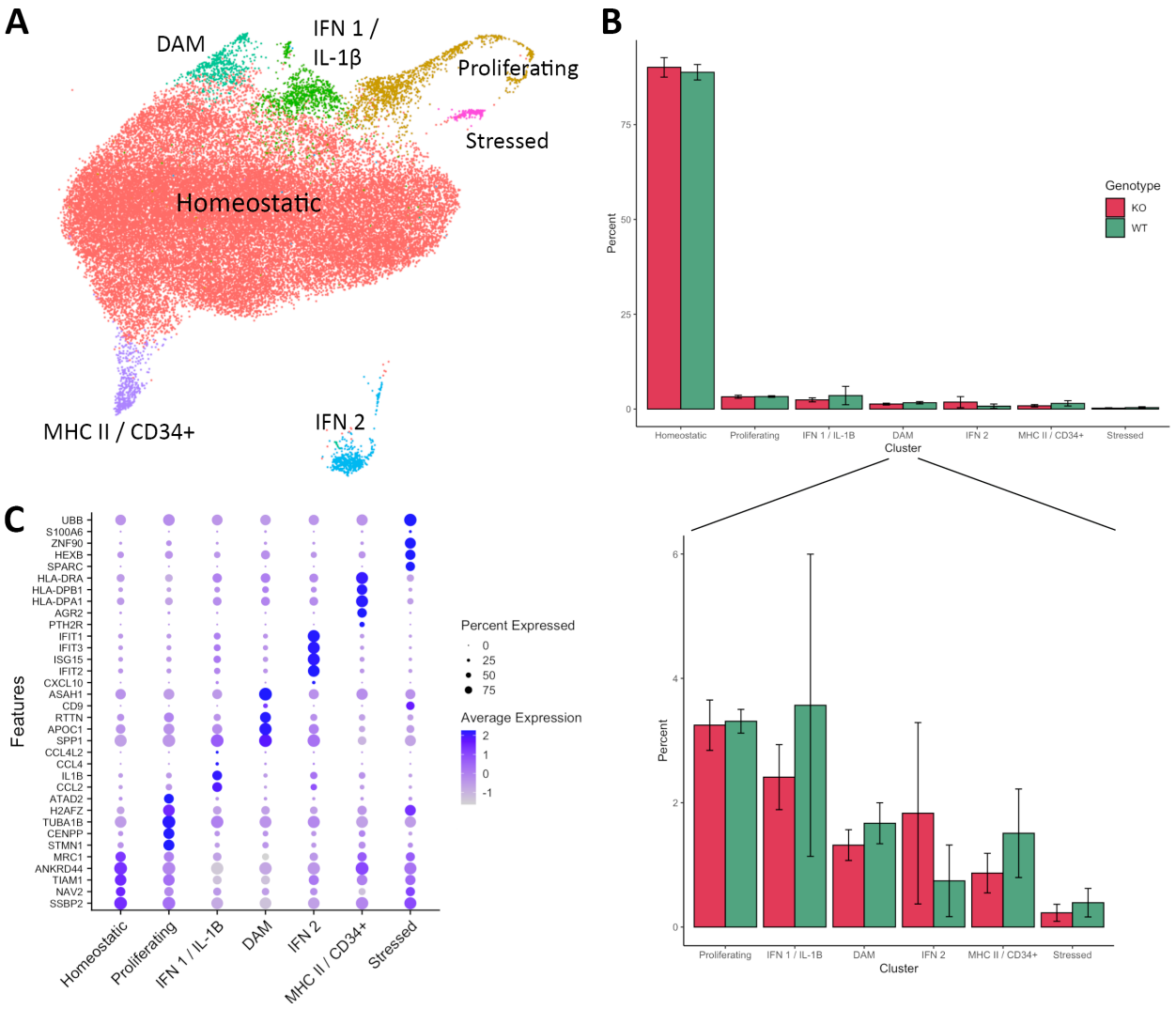

Figure 2.8: Single-cell RNA sequencing reveals a largely homeostatic population. A) UMAP of combined WT and KO cells reveals clusters based on different microglial functionality. B) No significant difference in population distribution was seen between WT and ERCC1^{KO} microglia. C) The top 5 most up-regulated genes in each cluster. Sample n = 3 WT, 3 KO.

expression of multiple DAM markers including TREM2, APOE, and ITGAX/Cd11c, two clusters that express high levels of interferon response genes (ISGs), and a cluster with high expression of CD34 and MHC II genes (Figure 2.8C). Surprisingly, we saw no significant differences in population composition between WT and KO samples (Figure 2.8B), suggesting that in the absence of any major immune challenge, the ERCC1^{KO} cells remain largely homeostatic.

Differential gene expression (DGE) analysis between WT and KO xMGs revealed 1,080 significantly changed genes, many related to essential immune functions (Figure 2.9A). ERCC1^{KO}

cells have increased expression of genes related to interferon signaling (BST2, STAT1, MX1, IRF7) and several genes that have been shown to be enriched in DAMs (CLEC7A, ITGAX, AXL, SPP1, APOE). However, these cells also exhibit decreased expression of some other activation genes including TSPO, CD68, and LPL, and downregulated expression of complement-related genes (C1QA, C1QB, C1QC, C2) and several HLA genes. Consistent with the observed lack of changes in the DAM cluster, these data suggest that the precise "activation state" of ERCC1^{KO} cells is more nuanced than a typical amyloid-responsive DAM phenotype.

Gene set enrichment analysis (GSEA) of differential genes further revealed an increased enrichment of Reactome pathways related to interferon signaling and cytokine signaling in ERCC1^{KO} microglia, despite their largely homeostatic phenotype. In contrast, ERCC1^{KO} microglia exhibit decreased enrichment for pathways related to response to reactive oxygen species, autophagy, complement signaling, and antigen presentation (Figure 2.9B). Combined, this suggests a dysregulation of important immune functions as well as a decreased ability to deal with stress in ERCC1^{KO} cells.

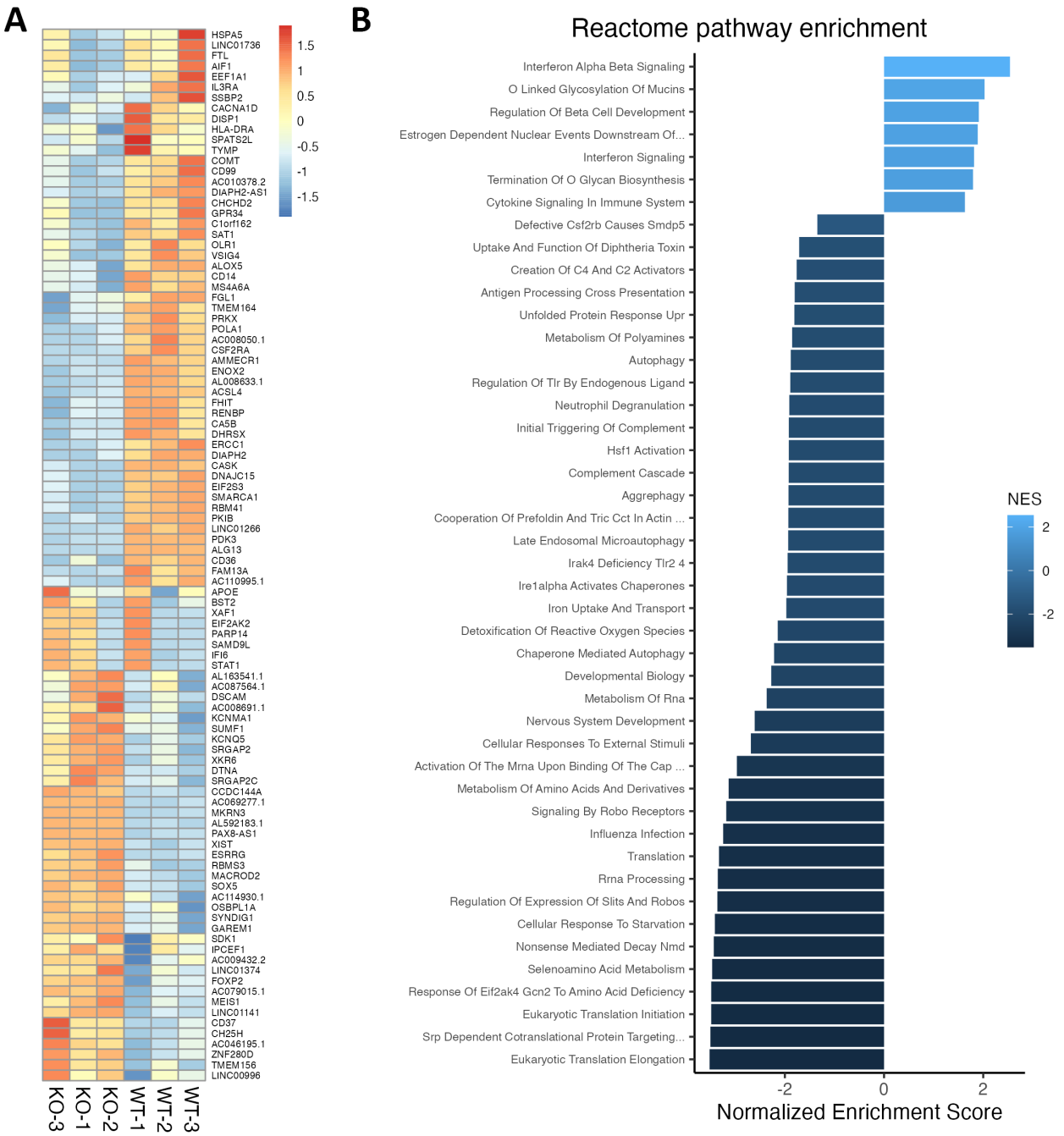

Figure 2.9: Differential gene expression analysis of WT and KO cells. A) The top 100 up- or down-regulated genes between KO and WT samples. B) Reactome pathways that are positively or negatively enriched in ERCC1 KO cells.

DISCUSSION

Despite years of research and considerable progress, Alzheimer's disease continues to represent a major emotional and financial burden to patients, caregivers, and society as a whole. Current therapies are largely palliative, and once-promising approaches heralded as "disease-modifying" continue to fail in late-stage clinical trials [163]. It therefore remains critically important to improve our understanding of the cell types and mechanisms that underlie this devastating disease. Within the last decade, a great deal of progress has been made in our collective understanding regarding the role of microglia and innate immunity in AD. Yet innate and adaptive immunity rarely work in isolation. Instead, complex signaling between innate brain-resident microglia and T cells that routinely survey and sometimes infiltrate the CNS are likely important in the development and progression of AD and other neurodegenerative disorders.

T cells infiltrate the brain in AD and respond to amyloid pathology

To further advance our understanding of the potential role of adaptive immunity in AD, we coupled traditional immunological methods, including flow cytometry and bone marrow transplantation paradigms, with modern approaches such as single cell RNA sequencing and TCR repertoire analysis. Using these complementary methods, we have found that memory CD8+ T cells infiltrate the brains of AD mice *in vivo* and proliferate in response to an AD-like environment *in vitro*. We first explored the role of the adaptive immune system in AD by using bone marrow transplantation into the Rag-5XFAD immune-deficient AD mouse model. These initial experiments demonstrated that a significant amount of memory cytotoxic T cells respond to AD brain-derived signals and infiltrate the brain. Our immunohistochemical analysis further revealed that transplanted T cells can be observed adjacent to and even surrounded by microglial processes, confirming that direct interaction and even antigen presentation by microglia which can express both MHCI and MHCII molecules likely occurs within the brain of AD mice [67, 91].

To further understand which aspects of AD pathology enhance the recruitment of T cells to the brain, we utilized three different immune-intact AD mouse models: 5XFAD mice which develop amyloid plaques, PS19 mice which develop tau tangles, and PS-5X biogenic mice that develop both hallmark AD pathologies. We examined mice across multiple ages finding that memory CD8+ T cells are significantly elevated in both male and female bigenic PS-5X mouse brains at 6-, 9-, and 12-months of age.

Using co-culture experiments we further demonstrated that 5X brain samples elicit robust proliferation of T cells derived from 5X deep cervical lymph nodes. In contrast, co-culture of 5X T cells with WT brain tissue samples or co-culture of WT T cells with either WT or 5X tissue samples has little effect on T cell proliferation. These experiments further confirm that amyloid-associated pathology induces memory CD8 activation in response to AD mouse brain samples. While these *in vitro* findings are exciting, they also point to the need to pursue additional experiments to determine whether cytotoxic T cell responses are triggered specifically by amyloid pathology itself or in response to some other downstream pathological component such as neuronal apoptosis.

To examine infiltrating T cells at the single cell level, we conducted single cell sequencing of RNA and T cell receptors (TCRs). Our RNA-seq analysis of infiltrating T cells revealed that the majority of sequenced cells expressed markers of memory T cells and were antigen-experienced. Many of these cells also expressed markers of tissue residency, suggesting that they had ceased circulating and instead remained within the brain. The largest population of brain-infiltrating cells were CD8+ cytotoxic T cells, with smaller populations of CD4 helper and $\gamma\delta$ cells also detected. Corroborating our flow cytometry and co-culture experiments, we detected a significant increase in the proportion of antigen-experienced CD8+ cytotoxic T cells in the 5XFAD and PS-5X mice, but not PS19 or WT mice, suggesting amyloid-driven recruitment of CD8 T cells to the brain.

Differential gene expression analysis between genotypes revealed a significant increase in interferon-stimulated genes (ISGs), including *Irf7, Ifit3*, and *Bst2*, in cytotoxic CD8 T cells from both 5XFAD and PS-5X mice. Clustering analysis also revealed a distinct sub-population of cells that express high levels of these genes, composed primarily of PS-5X and 5XFAD cells. This suggests that amyloid induces pro-inflammatory interferon-driven signaling between cytotoxic T

cells and other cell types. However, it is unclear whether this heightened interferon signaling arises primarily from T cells or from other cell types such as degenerating neurons or other brain resident cells. Type I interferon responses from plaque-associated microglia have been shown to enhance inflammation and drive synaptic loss in AD mice [164]. However, the role and impact of interferon-responsive T cells remains unclear. Future studies will likely be needed to determine whether IFN-responsive T cells similarly drive synaptic degeneration and/or enhance the microglial proinflammatory response.

Our single-cell analysis additionally revealed 42 GWAS-identified AD risk genes that were significantly upregulated in at least one cluster of T cells, demonstrating that microglia are not the only immune cell population within the brain of AD mice that may be affected by these AD risk alleles. Surprisingly, the γδ-17 cluster alone accounted for 16 of these genes, including genes like *Clnk* that are almost exclusively expressed in this cluster. Both neurons and glia directly respond to IL-17 [165], and IL-17-secreting γδ cells in the brain have been shown to negatively affect cognition in an AD mouse model [95] and to elicit harmful effects in other neurological diseases [78, 166]. Unlike αβ TCRs, γδ TCRs are not restricted to MHC I or II binding for antigen recognition, and antigen targets of γδ-17 cells are mostly unknown [77, 167]. Our data shows that this population of cells warrants further investigation, including exploration of potential AD-related antigens that might be recognized by γδ cells, and examination of interactions between these cells and neurons and glia in the AD brain as well as the impact of γδ cells on AD neuropathologies.

Finally, the 10X single cell sequencing platform used in this study enabled concurrent sequencing of T cell receptors (both alpha and beta chains) and RNA from each cell, allowing us to correlate clonal expansion with T cell function. We identified several clonally-expanded TCRs within CD8 cytotoxic cells from 5XFAD and PS-5X mice. Furthermore, we compared these TCRs to databases of known TCR/epitope pairs, and many of these clonal TCRs show little-to-no similarity with known mouse TCR sequences, suggesting they are responsive to novel, as of yet unidentified antigens. While the prevalence of these novel clones in 5XFAD and PS-5X mice suggests they may recognize amyloid-related epitopes, it is also quite possible that these TCRs bind to other neoepitopes that are exposed in response to AD neuropathologies. Fortunately, novel approaches

have recently been developed to utilize paired alpha and beta TCR sequences to specifically identify candidate antigens [168]. Thus, future studies can utilize the current dataset to pursue this goal.

Taken together this study has shown that cytotoxic T cells infiltrate the brains of AD model mice and adopt an effector memory phenotype indicative of an antigen-experienced and proliferative response. Single cell sequencing coupled with TCR repertoire analysis further demonstrates that these phenotypes are induced by amyloid-related processes and that AD risk genes expression is enriched within these infiltrating T cell populations. Based on these findings, future studies should determine the impact of specific T cell subpopulations and AD risk gene expression on AD pathologies, synaptic loss, and neurodegeneration.

Validating ERCC1 KO as a model of aging in iPSCs

To investigate the uniquely human aspect of aging microglia, we endeavored to induce an aged phenotype in iPSC-derived microglia through genetic knockout of ERCC1. We created an iPSC line with homozygous knockout of ERCC1, although these cells appear to still have some remaining expression of ERCC1 protein (Figure 2.1B) and RNA (Figure 2.9A). However, ERCC1 expression is reduced enough in the ERCC1^{KO} line to significantly affect microglial proliferation and immune function.

We found a large reduction in yield of ERCC1^{KO} cells during differentiation from iPSC to iMGL. Live imaging studies found no evidence of an increased rate of apoptosis in ERCC1^{KO} cells, and we found that xenotransplanted ERCC1^{KO} microglia were able to engraft and survive in the murine brain for at least 4 months. This suggests that lower yield is likely to be caused by a deficit of either proliferation or the ability to differentiate, rather than increased cell death.

To examine whether ERCC1 KO induced age-related changes in phagocytosis, we quantified microglial uptake of synaptosomes and fibril Aβ_{42} *in vitro*. We found that ERCC1^{KO} iMGLs have reduced phagocytosis of synaptosomes *in vitro* but are more quickly activated by Aβ. Reduced

synaptosome ingestion is consistent with known age-related changes in microglial pruning. Microglia prune synapses during early brain development, but this function decreases after puberty [160, 169]. Studies of microglial aging also show that C2, a necessary protein in synapse phagocytosis, is down-regulated with aging [43, 150]. We found that C2 is significantly decreased in ERCC1^{KO} microglia in both our *in vitro* bulk RNA and our xMG single-cell RNA sequencing data, suggesting that ERCC1^{KO} iMGLs display alterations in synaptosome phagocytosis that are consistent with aging.

Conclusions about age-related amyloid phagocytosis are more conflicted. Some studies in mice have shown that phagocytosis of Aβ is reduced in aged microglia [26, 42], while others show increased expression of phagocytic receptors for Aβ, such as MSR1 and MRC1, with age in mice [46, 47], or no significant change of major Aβ receptors in humans [43, 150]. Both MSR1 and MRC1 are up-regulated in ERCC1^{KO} microglia *in vitro*, which may explain the increased initial response to Aβ seen in live imaging experiments (Figure 2.3D). However, neither of these genes are significantly changed in ERCC1^{KO} xMGs in WT mice, and without exposure to Aβ *in vivo* it is unclear whether these cells will have an increased or decreased response.

When we compared differentially expressed genes between WT and ERCC1^{KO} microglia with other human and mouse microglial aging data sets [43, 47, 150], we found that many genes in our data set overlapped the reference sets but with the opposite direction of change (Figure 2.9B). However, there are several confounding issues when comparing our data to these reference sets. Age-related transcriptomic changes in human microglia and mouse microglia do not have high overlap [43], so differences between our data and mouse data are to be expected. Both human data sets obtained microglia from post-mortem tissue with varying post-mortem intervals before collection, and samples were from a few specific brain regions in the cortex and midbrain. In contrast, our xMGs were extracted from entire half-brains and therefore include microglia from all brain regions and from both gray and white matter. Brain region has a significant effect on microglial transcriptome [49], so we might expect to see some differences between our cells and the human aging data sets because of this.

Despite these differences, we did find signs of immune dysregulation and senescence in xMG single cell RNA sequencing. ERCC1^{KO} xMGs up-regulate many genes related to interferon signaling despite lack of immune challenge, similar to findings in microglia from aged mice [46, 47, 49]. These cells also up-regulate multiple markers of activation (APOE, ITGAX, AXL) while down-regulating others (TSPO, CD68, multiple HLA genes), suggesting possible immune dysfunction. ERCC1^{KO} xMGs also up-regulate several genes relating to cell cycle arrest, including TP53 (p53) and RB1, and in combination with dysfunctional activation and up-regulation of pro-inflammatory TNF and anti-inflammatory TGFβ1, this suggests that ERCC1^{KO} cells have a more senescent phenotype.

While ERCC1^{KO} microglia show multiple genetic and behavioral changes associated with aging, further exploration is necessary to determine if this model sufficiently creates an aged phenotype. We do not have data on what a "real" aged xMG transcriptome would look like, so xenotransplanted WT and KO cells should be examined from both young mice and very aged mice to provide a direct comparison between ERCC1^{KO} cells and aged xMGs under our experimental conditions. Additionally, xenotransplanted mice were raised in a fairly sterile and controlled environment, so they have not been subjected to the many serious immune challenges a human might encounter in their lifetime. As a consequence, we found that the majority of ERCC1^{KO} cells from these mice were homeostatic, similar to WT cells (Figure 2.8). Future experiments should examine whether delivering an immune insult, such as injection of LPS or buildup of Aβ pathology, will result in chronic activation or priming of ERCC1^{KO} cells consistent with aged microglial responses.

REFERENCES

1. Alzheimer's Association. 2022 Alzheimer's disease facts and figures. *Alzheimer's and Dementia* **18,** 700–789. https://onlinelibrary.wiley.com/doi/10.1002/alz.12638 (Apr. 2022).
2. Sarlus, H. & Heneka, M. T. Microglia in Alzheimer's disease. *Journal of Clinical Investigation* **127,** 3240–3249. https://www.jci.org/articles/view/90606 (Sept. 2017).
3. Zuroff, L., Daley, D., Black, K. L. & Koronyo-Hamaoui, M. *Clearance of cerebral Aβ in Alzheimer's disease: reassessing the role of microglia and monocytes* (Springer International Publishing, 2017).
4. Hansen, D. V., Hanson, J. E. & Sheng, M. Microglia in Alzheimer's disease. *Journal of Cell Biology,* 1–14 (2017).
5. Jack, C. R. *et al.* Hypothetical Pathological Cascade in Alheimer's Disease. *Lancet Neurology* **9,** 1–20 (2010).
6. Streit, W. J., Khoshbouei, H. & Bechmann, I. Dystrophic microglia in late-onset Alzheimer's disease. *Glia,* 1–10 (2020).
7. Gatz, M. *et al.* Role of genes and environments for explaining Alzheimer disease. *Archives of General Psychiatry* **63,** 168–174 (2006).
8. Sims, R. *et al.* Rare coding variants in PLCG2, ABI3, and TREM2 implicate microglial-mediated innate immunity in Alzheimer's disease. *Nature Genetics* **49,** 1373–1384 (2017).
9. Kunkle, B. W. *et al.* Genetic meta-analysis of diagnosed Alzheimer's disease identifies new risk loci and implicates Aβ, tau, immunity and lipid processing. *Nature Genetics* **51,** 414–430. http://www.nature.com/articles/s41588-019-0358-2 (2019).
10. Bellenguez, C. New insights into the genetic etiology of Alzheimer's disease and related dementias. *Nature Genetics* **54,** 33 (2022).
11. Mostafavi, S. *et al.* A molecular network of the aging human brain provides insights into the pathology and cognitive decline of Alzheimer's disease. *Nature Neuroscience* **21,** 811–819. http://dx.doi.org/10.1038/s41593-018-0154-9 (2018).
12. Mosher, K. I. & Wyss-Coray, T. Microglial dysfunction in brain aging and Alzheimer's disease. *Biochemical Pharmacology* **88,** 594–604. http://dx.doi.org/10.1016/j.bcp.2014.01.008 (2014).
13. Harry, G. J. Microglia during development and aging. *Pharmacology and Therapeutics* **139,** 313–326. http://dx.doi.org/10.1016/j.pharmthera.2013.04.013 (2013).
14. Derecki, N. C., Katzmarski, N., Kipnis, J. & Meyer-Luehmann, M. Microglia as a critical player in both developmental and late-life CNS pathologies. *Acta Neuropathologica* **128,** 333–345 (2014).
15. Nimmerjahn, A., Kirchhoff, F. & Helmchen, F. Resting microglial cells are highly dynamic surveillants of brain parenchyma in vivo. *Neuroforum* **11,** 95–96 (2005).
16. Michell-Robinson, M. A. *et al.* Roles of microglia in brain development, tissue maintenance and repair. *Brain* **138,** 1138–1159 (2015).

17. Prinz, M. & Priller, J. Microglia and brain macrophages in the molecular age: From origin to neuropsychiatric disease. *Nature Reviews Neuroscience* **15,** 300–312 (2014).

18. Hamelin, L. *et al.* Early and protective microglial activation in Alzheimer's disease: A prospective study using 18F-DPA-714 PET imaging. *Brain* **139,** 1252–1264 (2016).

19. Fan, Z., Brooks, D. J., Okello, A. & Edison, P. An early and late peak in microglial activation in Alzheimer's disease trajectory. *Brain* **140,** 792–803 (2017).

20. Condello, C., Yuan, P., Schain, A. & Grutzendler, J. Microglia constitute a barrier that prevents neurotoxic protofibrillar Aβ42 hotspots around plaques. *Nature Communications* **6,** 6176. http://www.nature.com/articles/ncomms7176 (May 2015).

21. Keren-Shaul, H. *et al.* A Unique Microglia Type Associated with Restricting Development of Alzheimer's Disease. *Cell* **169,** 1276–1290.e17. http://dx.doi.org/10.1016/j.cell.2017.05.018 (June 2017).

22. Hasselmann, J. *et al.* Development of a Chimeric Model to Study and Manipulate Human Microglia In Vivo. *Neuron* **103,** 1016–1033.e10. https://doi.org/10.1016/j.neuron.2019.07.002 (2019).

23. Srinivasan, K. *et al.* Alzheimer's Patient Microglia Exhibit Enhanced Aging and Unique Transcriptional Activation. *Cell Reports* **31,** 107843. https://doi.org/10.1016/j.celrep.2020.107843 (2020).

24. Spangenberg, E. E. *et al.* Eliminating microglia in Alzheimer's mice prevents neuronal loss without modulating amyloid-β pathology. *Brain* **139,** 1265–1281 (2016).

25. A Grathwohl, S. *et al.* Formation and maintenance of Alzheimer's disease β-amyloid plaques in the absence of microglia. *Nature Neuroscience* **12,** 1361–1363. http://www.nature.com/articles/nn.2432 (Nov. 2009).

26. Floden, A. M. & Combs, C. K. Microglia Demonstrate Age-Dependent Interaction with Beta-amyloid Fibrils. *Journal of Alzheimer's Disease* **25,** 279–293 (July 2011).

27. Krabbe, G. *et al.* Functional Impairment of Microglia Coincides with Beta-Amyloid Deposition in Mice with Alzheimer-Like Pathology. *PLoS ONE* **8** (2013).

28. Hickman, S. E., Allison, E. K. & El Khoury, J. Microglial Dysfunction and Defective β-Amyloid Clearance Pathways in Aging Alzheimer's Disease Mice. *Journal of Neuroscience* **28,** 8354–8360. http://www.jneurosci.org/cgi/doi/10.1523/JNEUROSCI.0616-08.2008 (Aug. 2008).

29. Frackowiak, J. *et al.* Ultrastructure of the microglia that phagocytose amyloid and the microglia that produce β-amyloid fibrils. *Acta Neuropathologica* **84,** 225–233 (1992).

30. Wisniewski, H., Wegiel, J., Wang, K., Kujawa, M. & Lach, B. Ultrastructural Studies of the Cells Forming Amyloid Fibers in Classical Plaques. *Canadian Journal of Neurological Sciences / Journal Canadien des Sciences Neurologiques* **16,** 535–542. https://www.cambridge.org/core/product/identifier/S0317167100029887/type/journal_article (Nov. 1989).

31. Baik, S. H., Kang, S., Son, S. M. & Mook-Jung, I. Microglia contributes to plaque growth by cell death due to uptake of amyloid β in the brain of Alzheimer's disease mouse model. *Glia* **64,** 2274–2290 (2016).

32. Spangenberg, E. *et al.* Sustained microglial depletion with CSF1R inhibitor impairs parenchymal plaque development in an Alzheimer's disease model. *Nature Communications* **10,** 1–21 (2019).

33. Kiani Shabestari, S. *et al.* Absence of microglia promotes diverse pathologies and early lethality in Alzheimer's disease mice. *Cell Reports* **39,** 110961. https://linkinghub.elsevier.com/retrieve/pii/S2211124722007434 (2022) (June 2022).

34. Asai, H. *et al.* Depletion of microglia and inhibition of exosome synthesis halt tau propagation. *Nature Neuroscience* **18,** 1584–1593 (2015).

35. Streit, W. J., Braak, H., Xue, Q. S. & Bechmann, I. Dystrophic (senescent) rather than activated microglial cells are associated with tau pathology and likely precede neurodegeneration in Alzheimer's disease. *Acta Neuropathologica* **118,** 475–485 (2009).

36. Ising, C. *et al.* NLRP3 inflammasome activation drives tau pathology. *Nature* **575.** http://www.ncbi.nlm.nih.gov/pubmed/31748742 (2019).

37. Kitazawa, M., Oddo, S., Yamasaki, T. R., Green, K. N. & LaFerla, F. M. Lipopolysaccharide-induced inflammation exacerbates tau pathology by a cyclin-dependent kinase 5-mediated pathway in a transgenic model of Alzheimer's disease. *Journal of Neuroscience* **25,** 8843–8853 (2005).

38. Liddelow, S. A. *et al.* Neurotoxic reactive astrocytes are induced by activated microglia. *Nature* **541,** 481–487 (2017).

39. Pampuscenko, K. *et al.* Extracellular tau induces microglial phagocytosis of living neurons in cell cultures. *Journal of neurochemistry,* e14940. http://www.ncbi.nlm.nih.gov/pubmed/31834946 (2019).

40. Cribbs, D. H. *et al.* Extensive innate immune gene activation accompanies brain aging, increasing vulnerability to cognitive decline and neurodegeneration: A microarray study. *Journal of Neuroinflammation* **9,** 1–18 (2012).

41. Lu, T. *et al.* Gene regulation and DNA damage in the ageing human brain. *Nature* **429,** 883–891 (2004).

42. Njie, e. M. G. *et al.* Ex vivo cultures of microglia from young and aged rodent brain reveal age-related changes in microglial function. *Neurobiology of Aging* **33,** 195.e1–195.e12 (2012).

43. Galatro, T. F. *et al.* Transcriptomic analysis of purified human cortical microglia reveals age-associated changes. *Nature Neuroscience* **20,** 1162–1171 (2017).

44. Olah, M. *et al.* A transcriptomic atlas of aged human microglia. *Nature Communications* **9,** 1–8 (2018).

45. Sankowski, R. *et al.* Mapping microglia states in the human brain through the integration of high-dimensional techniques. *Nature Neuroscience* **22.** http://www.nature.com/articles/s41593-019-0532-y (2019).

46. Hickman, S. E. *et al.* The microglial sensome revealed by direct RNA sequencing. *Nature Neuroscience* **16,** 1896–1905. http://dx.doi.org/10.1038/nn.3554 (Dec. 2013).

47. Holtman, I. R. *et al.* Induction of a common microglia gene expression signature by aging and neurodegenerative conditions: a co-expression meta-analysis. *Acta neuropathologica communications* **3,** 31 (2015).

48. Sierra, A., Gottfried-Blackmore, A. C., McEwen, B. S. & Bulloch, K. Microglia derived from aging mice exhibit an altered inflammatory profile. *Glia* **55,** 412–424. http://doi.wiley.com/10.1002/glia.20468 (Mar. 2007).

49. Grabert, K. *et al.* Microglial brain region-dependent diversity and selective regional sensitivities to aging. *Nature Neuroscience* **19,** 504–516. http://www.nature.com/articles/nn.4222 (Mar. 2016).

50. Damani, M. R. *et al.* Age-related alterations in the dynamic behavior of microglia. *Aging Cell* **10,** 263–276 (2011).

51. Tremblay, M. È., Zettel, M. L., Ison, J. R., Allen, P. D. & Majewska, A. K. Effects of aging and sensory loss on glial cells in mouse visual and auditory cortices. *Glia* **60,** 541–558 (2012).

52. Lopes, K. O., Sparks, D. L. & Streit, W. J. Microglial dystrophy in the aged and Alzheimer's disease brain is associated with ferritin immunoreactivity. *Glia* **56,** 1048–1060 (2008).

53. Streit, W. J. *et al.* Microglial activation occurs late during preclinical Alzheimer's disease. *Glia* **66,** 2550–2562 (2018).

54. Angelova, D. & Brown, D. Model Senescent Microglia Induce Disease Related Changes in α-Synuclein Expression and Activity. *Biomolecules* **8,** 67. http://www.mdpi.com/2218-273X/8/3/67 (2018).

55. Hefendehl, J. K. *et al.* Homeostatic and injury-induced microglia behavior in the aging brain. *Aging Cell* **13,** 60–69 (2014).

56. Norden, D. M. & Godbout, J. P. Review: Microglia of the aged brain: primed to be activated and resistant to regulation. *Neuropathology and Applied Neurobiology* **39,** 19–34. http://doi.wiley.com/10.1111/j.1365-2990.2012.01306.x (Feb. 2013).

57. Safaiyan, S. *et al.* Age-related myelin degradation burdens the clearance function of microglia during aging. *Nature Neuroscience* **19,** 995–998 (2016).

58. Bisht, K. *et al.* Dark microglia: A new phenotype predominantly associated with pathological states. *Glia* **64,** 826–839 (2016).

59. Smith, A. M. & Dragunow, M. The human side of microglia. *Trends in Neurosciences* **37,** 125–135. http://dx.doi.org/10.1016/j.tins.2013.12.001 (2014).

60. Yin, Z. *et al.* Immune hyperreactivity of Aβ plaque-associated microglia in Alzheimer's disease. *Neurobiology of Aging* **55,** 115–122. http://dx.doi.org/10.1016/j.neurobiolaging.2017.03.021 (2017).

61. Mathys, H. *et al.* Single-cell transcriptomic analysis of Alzheimer's disease. *Nature* **570,** 332–337. http://dx.doi.org/10.1038/s41586-019-1195-2 (2019).

62. Wehrspaun, C. C., Haerty, W. & Ponting, C. P. Microglia recapitulate a hematopoietic master regulator network in the aging human frontal cortex. *Neurobiology of Aging* **36,** 2443.e9–2443.e20. http://dx.doi.org/10.1016/j.neurobiolaging.2015.04.008 (2015).

63. Friedman, B. A. *et al.* Diverse Brain Myeloid Expression Profiles Reveal Distinct Microglial Activation States and Aspects of Alzheimer's Disease Not Evident in Mouse Models. *Cell Reports* **22,** 832–847. https://doi.org/10.1016/j.celrep.2017.12.066 (2018).

64. Baik, S. H. *et al.* A Breakdown in Metabolic Reprogramming Causes Microglia Dysfunction in Alzheimer's Disease. *Cell Metabolism* **30,** 493–507.e6. https://doi.org/10.1016/j.cmet.2019.06.005 (2019).

65. Chen, W. *et al.* Increased tauopathy drives microglia-mediated clearance of beta-amyloid. *Acta Neuropathologica Communications* **4,** 63. http://actaneurocomms.biomedcentral.com/articles/10.1186/s40478-016-0336-1 (2016).

66. Hemmer, B., Kerschensteiner, M. & Korn, T. Role of the innate and adaptive immune responses in the course of multiple sclerosis. *The Lancet Neurology* **14,** 406–419. https://linkinghub.elsevier.com/retrieve/pii/S1474442214703059 (2022) (Apr. 2015).

67. Schetters, S. T. T., Gomez-Nicola, D., Garcia-Vallejo, J. J. & Van Kooyk, Y. Neuroinflammation: Microglia and T Cells Get Ready to Tango. *Frontiers in Immunology* **8,** 1905. http://journal.frontiersin.org/article/10.3389/fimmu.2017.01905/full (2022) (Jan. 2018).

68. Konjevic Sabolek, M. *et al.* Communication of CD8$^+$ T cells with mononuclear phagocytes in multiple sclerosis. *Annals of Clinical and Translational Neurology* **6,** 1151–1164. https://onlinelibrary.wiley.com/doi/10.1002/acn3.783 (2022) (July 2019).

69. Gate, D. *et al.* Clonally expanded CD8 T cells patrol the cerebrospinal fluid in Alzheimer's disease. *Nature* **577,** 399–404. http://www.nature.com/articles/s41586-019-1895-7 (Jan. 2020).

70. Unger, M. S. *et al.* CD8+ T-cells infiltrate Alzheimer's disease brains and regulate neuronal- and synapse-related gene expression in APP-PS1 transgenic mice. *Brain, Behavior, and Immunity* **89,** 67–86 (2020).

71. Merlini, M., Kirabali, T., Kulic, L., Nitsch, R. M. & Ferretti, M. T. Extravascular CD3+ T Cells in Brains of Alzheimer Disease Patients Correlate with Tau but Not with Amyloid Pathology: An Immunohistochemical Study. *Neurodegenerative Diseases* **18,** 49–56 (2018).

72. Stojić-Vukanić, Z. *et al.* CD8+ T Cell-Mediated Mechanisms Contribute to the Progression of Neurocognitive Impairment in Both Multiple Sclerosis and Alzheimer's Disease? *Frontiers in Immunology* **11,** 1–11 (2020).

73. Germain, R. N. T-cell development and the CD4–CD8 lineage decision. *Nature Reviews Immunology* **2,** 309–322. http://www.nature.com/articles/nri798 (2022) (May 2002).

74. Starr, T. K., Jameson, S. C. & Hogquist, K. A. Positive and Negative Selection of T Cells. *Annual Review of Immunology* **21,** 139–176. https://www.annualreviews.org/doi/10.1146/annurev.immunol.21.120601.141107 (2022) (Apr. 2003).

75. Dudley, E. C., Girardi, M., Owen, M. J. & Hayday, A. C. $\alpha\ \beta$ and $\gamma\ \delta$ T cells can share a late common precursor. *Current Biology* **5,** 659–669 (1995).

76. Carding, S. R. & Egan, P. J. $\gamma\delta$ T cells: Functional plasticity and heterogeneity. *Nature Reviews Immunology* **2,** 336–345 (2002).

77. Chien, Y. H., Meyer, C. & Bonneville, M. $\gamma\delta$ T cells: First line of defense and beyond. *Annual Review of Immunology* **32,** 121–155 (2014).

78. Wo, J. *et al.* The Role of Gamma-Delta T Cells in Diseases of the Central Nervous System. *Frontiers in Immunology* **11,** 1–10 (2020).

79. Samji, T. & Khanna, K. M. Understanding memory CD8 + T cells. *Immunology Letters* **185,** 32–39. https://linkinghub.elsevier.com/retrieve/pii/S0165247816302723 (May 2017).

80. Golubovskaya, V. & Wu, L. Different subsets of T cells, memory, effector functions, and CAR-T immunotherapy. *Cancers* **8** (2016).

81. Reiser, J. & Banerjee, A. Effector, Memory, and Dysfunctional CD8+ T Cell Fates in the Antitumor Immune Response. *Journal of Immunology Research* **2016** (2016).

82. Martin, M. D. & Badovinac, V. P. Defining memory CD8 T cell. *Frontiers in Immunology* **9,** 1–10 (2018).

83. Shechter, R., London, A. & Schwartz, M. Orchestrated leukocyte recruitment to immune-privileged sites: absolute barriers versus educational gates. *Nature Reviews Immunology* **13,** 206–218. http://www.nature.com/articles/nri3391 (2022) (Mar. 2013).

84. Natale, G. *et al.* Glymphatic System as a Gateway to Connect Neurodegeneration From Periphery to CNS. *Frontiers in Neuroscience* **15,** 639140. https://www.frontiersin.org/articles/10.3389/fnins.2021.639140/full (2022) (Feb. 2021).

85. Schwartz, M. & Kipnis, J. A conceptual revolution in the relationships between the brain and immunity. *Brain, Behavior, and Immunity* **25,** 817–819. https://linkinghub.elsevier.com/retrieve/pii/S088915911000588X (2022) (July 2011).

86. Smolders, J. *et al.* Tissue-resident memory T cells populate the human brain. *Nature Communications* **9,** 4593. http://www.nature.com/articles/s41467-018-07053-9 (2022) (Dec. 2018).

87. Togo, T. *et al.* Occurrence of T cells in the brain of Alzheimer's disease and other neurological diseases. *Journal of Neuroimmunology* **124,** 83–92. https://linkinghub.elsevier.com/retrieve/pii/S0165572801004969 (2022) (Mar. 2002).

88. Aliseychik, M. *et al.* Dissection of the Human T-Cell Receptor γ Gene Repertoire in the Brain and Peripheral Blood Identifies Age- and Alzheimer's Disease-Associated Clonotype Profiles. *Frontiers in Immunology* **11** (2020).

89. Ferretti, M. T. *et al.* T-cell brain infiltration and immature antigen-presenting cells in transgenic models of Alzheimer's disease-like cerebral amyloidosis. *Brain, Behavior, and Immunity* **54,** 211–225. http://dx.doi.org/10.1016/j.bbi.2016.02.009 (2016).

90. Laurent, C. *et al.* Hippocampal T cell infiltration promotes neuroinflammation and cognitive decline in a mouse model of tauopathy. *Brain* **140,** 184–200 (2017).

91. Parachikova, A. *et al.* Inflammatory changes parallel the early stages of Alzheimer disease. *Neurobiology of Aging* **28,** 1821–1833. https://linkinghub.elsevier.com/retrieve/pii/S0197458006003113 (2022) (Dec. 2007).

92. Machhi, J. *et al.* CD4+ effector T cells accelerate Alzheimer's disease in mice. *Journal of Neuroinflammation* **18,** 1–23. https://doi.org/10.1186/s12974-021-02308-7 (2021).

93. Marsh, S. E. *et al.* The adaptive immune system restrains Alzheimer's disease pathogenesis by modulating microglial function. *Proceedings of the National Academy of Sciences* **113,** E1316–E1325. http://www.pnas.org/lookup/doi/10.1073/pnas.1525466113 (2016).

94. Baruch, K. *et al.* Breaking immune tolerance by targeting Foxp3+ regulatory T cells mitigates Alzheimer's disease pathology. *Nature Communications* **6,** 7967. http://www.nature.com/articles/ncomms8967 (2022) (Nov. 2015).

95. Brigas, H. C. *et al.* IL-17 triggers the onset of cognitive and synaptic deficits in early stages of Alzheimer's disease. *Cell Reports* **36** (2021).

96. Selkoe, D. J. Alzheimer's Disease: Genes, Proteins, and Therapy. *Physiological Reviews* **81,** 741–766. https://www.physiology.org/doi/10.1152/physrev.2001.81.2.741 (2022) (Apr. 2001).

97. Terry, R. D. *et al.* Physical Basis of Cognitive Alterations in Alzheimer's Disease: Synapse Loss is the Major Correlate of Cognitive Impairment. *Annals of Neurology* **30,** 572–580. https://onlinelibrary.wiley.com/doi/10.1002/ana.410300410 (2022) (Oct. 1991).

98. Masliah, E. *et al.* Altered expression of synaptic proteins occurs early during progression of Alzheimer's disease. *Neurology* **56,** 127–129. https://www.neurology.org/lookup/doi/10.1212/WNL.56.1.127 (2022) (Jan. 2001).

99. McGeer, P. L., Itagaki, S., Tago, H. & McGeer, E. G. Reactive microglia in patients with senile dementia of the Alzheimer type are positive for the histocompatibility glycoprotein HLA-DR. *Neuroscience Letters* **79,** 195–200. https://linkinghub.elsevier.com/retrieve/pii/0304394087906963 (2022) (Aug. 1987).

100. Lambert, J.-C. *et al.* Meta-analysis of 74,046 individuals identifies 11 new susceptibility loci for Alzheimer's disease. *Nature Genetics* **45,** 1452–1458. http://www.nature.com/articles/ng.2802 (2022) (Dec. 2013).

101. Heneka, M. T. *et al.* Neuroinflammation in Alzheimer's disease. *The Lancet Neurology* **14,** 388–405. https://linkinghub.elsevier.com/retrieve/pii/S1474442215700165 (2022) (Apr. 2015).

102. Jay, T. R. *et al.* TREM2 deficiency eliminates TREM2+ inflammatory macrophages and ameliorates pathology in Alzheimer's disease mouse models. *Journal of Experimental Medicine* **212,** 287–295. https://rupress.org/jem/article/212/3/287/41763/TREM2-deficiency-eliminates-TREM2-inflammatory (2022) (Mar. 2015).

103. Wes, P. D., Sayed, F. A., Bard, F. & Gan, L. Targeting microglia for the treatment of Alzheimer's Disease: Targeting Microglia in Alzheimer's Disease. *Glia* **64,** 1710–1732. https://onlinelibrary.wiley.com/doi/10.1002/glia.22988 (2022) (Oct. 2016).

104. Shi, Y. & Holtzman, D. M. Interplay between innate immunity and Alzheimer disease: APOE and TREM2 in the spotlight. *Nature Reviews Immunology* **18,** 759–772. http://www.nature.com/articles/s41577-018-0051-1 (2022) (Dec. 2018).

105. Silvin, A. *et al.* Dual ontogeny of disease-associated microglia and disease inflammatory macrophages in aging and neurodegeneration. *Immunity* **55,** 1448–1465.e6. https://linkinghub.elsevier.com/retrieve/pii/S1074761322003375 (2022) (Aug. 2022).

106. Gate, D. *et al.* CD4 $^{+}$ T cells contribute to neurodegeneration in Lewy body dementia. *Science* **374,** 868–874. https://www.science.org/doi/10.1126/science.abf7266 (2022) (Nov. 2021).

107. Itagaki, S., McGeer, P. & Akiyama, H. Presence of T-cytotoxic suppressor and leucocyte common antigen positive cells in Alzheimer's disease brain tissue. *Neuroscience Letters* **91,** 259–264. https://linkinghub.elsevier.com/retrieve/pii/0304394088906908 (2022) (Sept. 1988).

108. Oakley, H. *et al.* Intraneuronal beta-Amyloid Aggregates, Neurodegeneration, and Neuron Loss in Transgenic Mice with Five Familial Alzheimer's Disease Mutations: Potential Factors in Amyloid Plaque Formation. *Journal of Neuroscience* **26,** 10129–10140. https://www.jneurosci.org/lookup/doi/10.1523/JNEUROSCI.1202-06.2006 (2022) (Oct. 2006).

109. Cao, X. *et al.* Defective lymphoid development in mice lacking expression of the common cytokine receptor γ chain. *Immunity* **2,** 223–238. https://linkinghub.elsevier.com/retrieve/pii/1074761395900470 (2022) (Mar. 1995).

110. Hao, Y. *et al.* Integrated analysis of multimodal single-cell data. *Cell* **184,** 3573–3587.e29. https://linkinghub.elsevier.com/retrieve/pii/S0092867421005833 (2022) (June 2021).

111. O'Flanagan, C. H. *et al.* Dissociation of solid tumor tissues with cold active protease for single-cell RNA-seq minimizes conserved collagenase-associated stress responses. *Genome Biology* **20,** 210. https://genomebiology.biomedcentral.com/articles/10.1186/s13059-019-1830-0 (2022) (Dec. 2019).

112. Denisenko, E. *et al.* Systematic assessment of tissue dissociation and storage biases in single-cell and single-nucleus RNA-seq workflows. *Genome Biology* **21,** 130. https://genomebiology.biomedcentral.com/articles/10.1186/s13059-020-02048-6 (2022) (Dec. 2020).

113. Marsh, S. E. *et al.* Dissection of artifactual and confounding glial signatures by single-cell sequencing of mouse and human brain. *Nature Neuroscience* **25,** 306–316. https://www.nature.com/articles/s41593-022-01022-8 (2022) (Mar. 2022).

114. Gillespie, M. *et al.* The reactome pathway knowledgebase 2022. *Nucleic Acids Research* **50,** D687–D692. https://academic.oup.com/nar/article/50/D1/D687/6426058 (2022) (Jan. 2022).

115. "Cellular response to heat stress". *Reactome* **79.** https://reactome.org/content/detail/R-MMU-3371556 (Apr. 2022).

116. Pizzolato, G. *et al.* Single-cell RNA sequencing unveils the shared and the distinct cytotoxic hallmarks of human TCRVδ1 and TCRVδ2 $\gamma\delta$ T lymphocytes. *Proceedings of the National Academy of Sciences of the United States of America* **116,** 11906–11915 (2019).

117. Finak, G. *et al.* MAST: a flexible statistical framework for assessing transcriptional changes and characterizing heterogeneity in single-cell RNA sequencing data. *Genome Biology* **16,** 278. https://genomebiology.biomedcentral.com/articles/10.1186/s13059-015-0844-5 (2022) (Dec. 2015).

118. Cao, Y. *et al.* scDC: single cell differential composition analysis. *BMC Bioinformatics* **20,** 721. https://bmcbioinformatics.biomedcentral.com/articles/10.1186/s12859-019-3211-9 (2022) (Dec. 2019).

119. van Buuren, S. & Groothuis-Oudshoorn, K. mice: Multivariate Imputation by Chained Equations in R. *Journal of Statistical Software* **45.** http://www.jstatsoft.org/v45/i03/ (2022) (2011).

120. Hothorn, T., Bretz, F. & Westfall, P. Simultaneous Inference in General Parametric Models. *Biometrical Journal* **50,** 346–363. https://onlinelibrary.wiley.com/doi/10.1002/bimj.200810425 (2022) (June 2008).

121. Vita, R. *et al.* The Immune Epitope Database (IEDB): 2018 update. *Nucleic Acids Research* **47,** D339–D343. https://academic.oup.com/nar/article/47/D1/D339/5144151 (2022) (Jan. 2019).

122. Bagaev, D. V. *et al.* VDJdb in 2019: Database extension, new analysis infrastructure and a T-cell receptor motif compendium. *Nucleic Acids Research* **48,** D1057–D1062 (2020).

123. Chronister, W. D. *et al.* TCRMatch: Predicting T-Cell Receptor Specificity Based on Sequence Similarity to Previously Characterized Receptors. *Frontiers in Immunology* **12,** 1–10 (2021).

124. Yoshiyama, Y. *et al.* Synapse Loss and Microglial Activation Precede Tangles in a P301S Tauopathy Mouse Model. *Neuron* **53,** 337–351. https://linkinghub.elsevier.com/retrieve/pii/S089662730700030X (2022) (Feb. 2007).

125. Gratuze, M. *et al.* Impact of TREM2R47H variant on tau pathology–induced gliosis and neurodegeneration. *Journal of Clinical Investigation* **130,** 4954–4968. https://www.jci.org/articles/view/138179 (2022) (Aug. 2020).

126. Sayed, F. A. *et al.* Differential effects of partial and complete loss of TREM2 on microglial injury response and tauopathy. *Proceedings of the National Academy of Sciences* **115,** 10172–10177. https://pnas.org/doi/full/10.1073/pnas.1811411115 (2022) (Oct. 2018).

127. Sil, A. *et al.* Sex Differences in Behavior and Molecular Pathology in the 5XFAD Model. *Journal of Alzheimer's Disease* **85** (ed Wirths, O.) 755–778. https://www.medra.org/servlet/aliasResolver?alias=iospress&doi=10.3233/JAD-210523 (2022) (Jan. 2022).

128. Li, X. *et al.* Sex differences between APPswePS1dE9 mice in A-beta accumulation and pancreatic islet function during the development of Alzheimer's disease. *Laboratory Animals* **50,** 275–285. http://journals.sagepub.com/doi/10.1177/0023677215615269 (2022) (Aug. 2016).

129. Bachmann, M. F., Wolint, P., Schwarz, K., Jäger, P. & Oxenius, A. Functional Properties and Lineage Relationship of CD8 $^{+}$ T Cell Subsets Identified by Expression of IL-7 Receptor α and CD62L. *The Journal of Immunology* **175,** 4686–4696. http://www.jimmunol.org/lookup/doi/10.4049/jimmunol.175.7.4686 (2022) (Oct. 2005).

130. Tang, Y., Liu, M.-L., Zang, T. & Zhang, C.-L. Direct Reprogramming Rather than iPSC-Based Reprogramming Maintains Aging Hallmarks in Human Motor Neurons. *Frontiers in Molecular Neuroscience* **10,** 1–13. http://journal.frontiersin.org/article/10.3389/fnmol.2017.00359/full (2017).

131. Lapasset, L. *et al.* Rejuvenating senescent and centenarian human cells by reprogramming through the pluripotent state. *Genes & Development* **25,** 2248–2253 (Nov. 2011).

132. Miller, J. D. *et al.* Human iPSC-based modeling of late-onset disease via progerin-induced aging. *Cell Stem Cell* **13,** 691–705. http://dx.doi.org/10.1016/j.stem.2013.11.006 (2013).

133. Klimmt, J., Dannert, A. & Paquet, D. Neurodegeneration in a dish: advancing human stem-cell-based models of Alzheimer's disease. *Current Opinion in Neurobiology* **61,** 96–104. https://doi.org/10.1016/j.conb.2020.01.008 (2020).

134. Ziff, O. J. & Patani, R. Harnessing cellular aging in human stem cell models of amyotrophic lateral sclerosis. *Aging Cell* **18** (2019).

135. Jaspers, N. G. *et al.* First reported patient with human ERCC1 deficiency has cerebro-oculo-facio- skeletal syndrome with a mild defect in nucleotide excision repair and severe developmental failure. *American Journal of Human Genetics* **80,** 457–466 (2007).

136. Kashiyama, K. *et al.* Malfunction of nuclease ERCC1-XPF results in diverse clinical manifestations and causes Cockayne syndrome, xeroderma pigmentosum, and Fanconi anemia. *American Journal of Human Genetics* **92,** 807–819. http://dx.doi.org/10.1016/j.ajhg.2013.04.007 (2013).

137. Raj, D. D. *et al.* Priming of microglia in a DNA-repair deficient model of accelerated aging. *Neurobiology of Aging* **35,** 2147–2160. http://dx.doi.org/10.1016/j.neurobiolaging.2014.03.025 (2014).

138. McQuade, A. *et al.* Development and validation of a simplified method to generate human microglia from pluripotent stem cells. *Molecular Neurodegeneration* **13,** 67. https://molecularneurodegeneration.biomedcentral.com/articles/10.1186/s13024-018-0297-x (Dec. 2018).

139. Coburn, M. *et al.* Human microglia differentially respond to beta-amyloid, tau and combined Alzheimer's Disease Pathologies in vivo. *EMBO (In Review)* (2022).

140. York, E. M., Ledue, J. M., Bernier, L. P. & Macvicar, B. A. 3Dmorph Automatic Analysis of Microglial Morphology in Three Dimensions From Ex Vivo and in Vivo Imaging. *eNeuro* **5,** 1–12 (2018).

141. Claes, C. *et al.* Plaque-associated human microglia accumulate lipid droplets in a chimeric model of Alzheimer's disease. *Molecular Neurodegeneration* **16,** 50. https://molecularneurodegeneration.biomedcentral.com/articles/10.1186/s13024-021-00473-0 (2022) (Dec. 2021).

142. Bushnell, B. BBMap. sourceforge.net/projects/bbmap (2018).

143. Andrews, S. FastQC: a quality control tool for high throughput sequence data. https://www.bioinformatics.babraham.ac.uk/projects/fastqc/ (2014).

144. Schneider, V. A. *et al.* Evaluation of GRCh38 and de novo haploid genome assemblies demonstrates the enduring quality of the reference assembly. *Genome Research* **27,** 849–864 (2017).

145. Zerbino, D. R. *et al.* Ensembl 2018. *Nucleic Acids Research* **46,** D754–D761 (2018).

146. Bray, N. L., Pimentel, H., Melsted, P. & Pachter, L. Near-optimal probabilistic RNA-seq quantification. *Nature Biotechnology* **34,** 525–527 (2016).

147. Soneson, C., Love, M. I. & Robinson, M. D. Differential analyses for RNA-seq: Transcript-level estimates improve gene-level inferences [version 2; referees: 2 approved]. *F1000Research* **4,** 1–22 (2016).

148. Love, M. I., Huber, W. & Anders, S. Moderated estimation of fold change and dispersion for RNA-seq data with DESeq2. *Genome Biology* **15,** 1–21 (2014).

149. Subramanian, A. *et al.* Gene set enrichment analysis: A knowledge-based approach for interpreting genome-wide expression profiles. *Proceedings of the National Academy of Sciences of the United States of America* **102,** 15545–15550 (2005).

150. Lopes, K. d. P. *et al.* Genetic analysis of the human microglial transcriptome across brain regions, aging and disease pathologies. *Nature Genetics* **54,** 4–17 (2022).

151. Butler, A., Hoffman, P., Smibert, P., Papalexi, E. & Satija, R. Integrating single-cell transcriptomic data across different conditions, technologies, and species. *Nature Biotechnology* **36,** 411–420 (2018).

152. Korotkevich, G. *et al. Fast gene set enrichment analysis* preprint (Bioinformatics, June 2016). http://biorxiv.org/lookup/doi/10.1101/060012 (2022).

153. Dolgalev, I. msigdbr: MSigDB Gene Sets for Multiple Organisms in a Tidy Data Format. https://CRAN.R-project.org/package=msigdbr (2021).

154. Goukassian, D. *et al.* Mechanisms and implications of the age-associated decrease in DNA repair capacity. *The FASEB journal : official publication of the Federation of American Societies for Experimental Biology* **14,** 1325–1334 (2000).

155. Rodier, F. *et al.* Persistent DNA damage signalling triggers senescence-associated inflammatory cytokine secretion. *Nature Cell Biology* **11,** 973–979 (2009).

156. Manandhar, M., Boulware, K. S. & Wood, R. D. The ERCC1 and ERCC4 (XPF) genes and gene products. *Gene* **569,** 153–161. http://dx.doi.org/10.1016/j.gene.2015.06.026 (2015).

157. Ahmad, A. *et al.* ERCC1-XPF Endonuclease Facilitates DNA Double-Strand Break Repair. *Molecular and Cellular Biology* **28,** 5082–5092 (2008).

158. Freund, A., Laberge, R. M., Demaria, M. & Campisi, J. Lamin B1 loss is a senescence-associated biomarker. *Molecular Biology of the Cell* **23,** 2066–2075 (2012).

159. López-Otín, C., Blasco, M. A., Partridge, L., Serrano, M. & Kroemer, G. The hallmarks of aging. *Cell* **153,** 1194 (2013).

160. Schafer, D. P. *et al.* Microglia Sculpt Postnatal Neural Circuits in an Activity and Complement-Dependent Manner. *Neuron* **74,** 691–705. http://dx.doi.org/10.1016/j.neuron.2012.03.026 (2012).

161. Gosselin, D. *et al.* An environment-dependent transcriptional network specifies human microglia identity. *Science* **356,** 1248–1259 (2017).

162. De Waard, M. C. *et al.* Age-related motor neuron degeneration in DNA repair-deficient Ercc1 mice. *Acta Neuropathologica* **120,** 461–475 (2010).

163. Golde, T. E. Disease-Modifying Therapies for Alzheimer's Disease: More Questions than Answers. *Neurotherapeutics* **19,** 209–227. https://link.springer.com/10.1007/s13311-022-01201-2 (2022) (Jan. 2022).

164. Roy, E. R. *et al.* Type I interferon response drives neuroinflammation and synapse loss in Alzheimer disease. *Journal of Clinical Investigation* **130,** 1912–1930 (2020).

165. Moynes, D. M., Vanner, S. J. & Lomax, A. E. Participation of interleukin 17A in neuroimmune interactions. *Brain, Behavior, and Immunity* **41,** 1–9. http://dx.doi.org/10.1016/j.bbi.2014.03.004 (2014).

166. Chen, J., Liu, X. & Zhong, Y. Interleukin-17A: The Key Cytokine in Neurodegenerative Diseases. *Frontiers in Aging Neuroscience* **12,** 1–13 (2020).

167. Constantinides, M. G. & Belkaid, Y. Early-life imprinting of unconventional T cells and tissue homeostasis. *Science* **374** (2021).

168. Li, G. *et al.* T cell antigen discovery via trogocytosis. *Nature Methods* **16,** 183–190. http://www.nature.com/articles/s41592-018-0305-7 (2022) (Feb. 2019).

169. Gabandé-Rodríguez, E., Keane, L. & Capasso, M. Microglial phagocytosis in aging and Alzheimer's disease. *Journal of Neuroscience Research,* 1–15 (2019).

APPENDIX A: Supplemental Figures

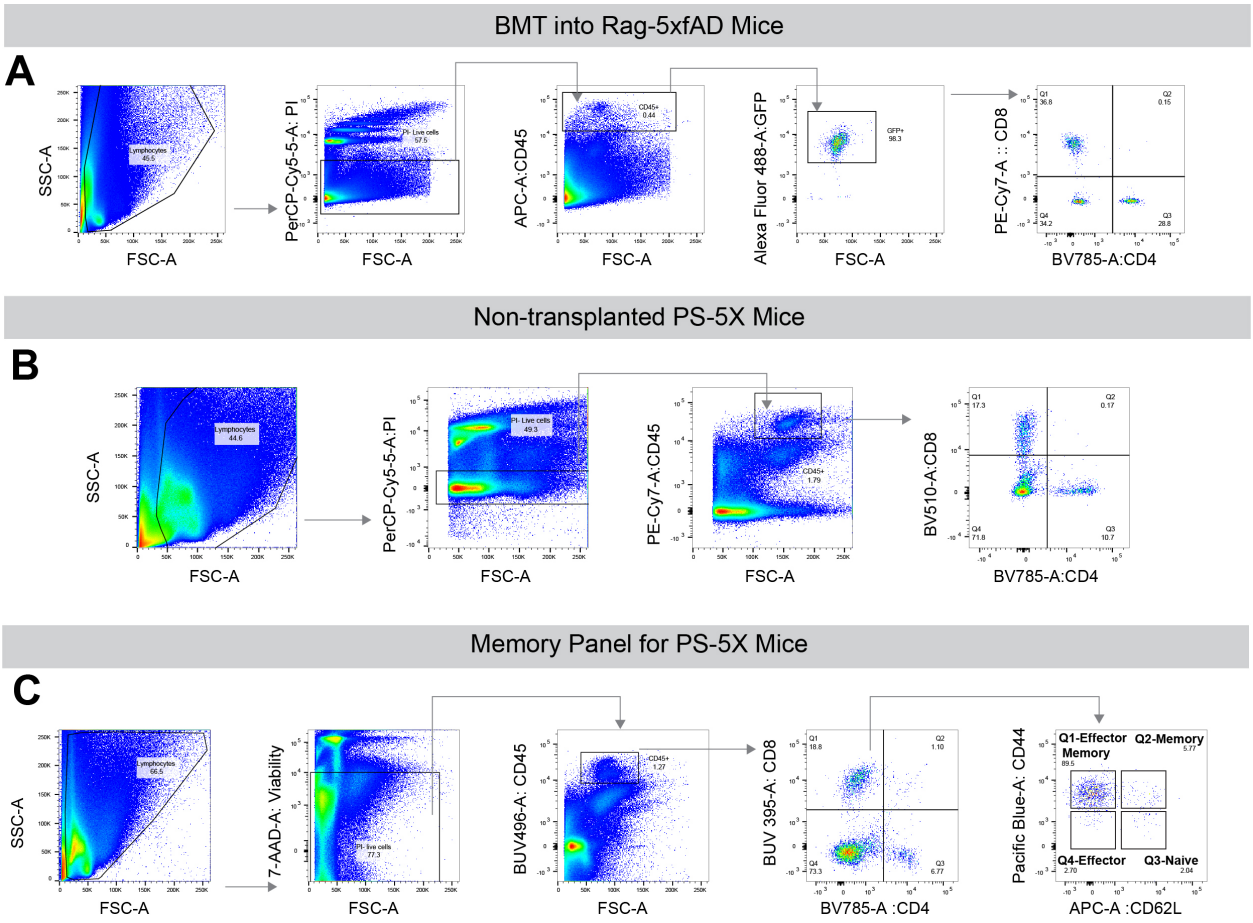

Figure S.1: Flow cytometry gating strategy for different T cells panels. (A) GFP+ T cells in the BMT immune-deficient Rag-5xfAD mice were gated on as lymphocytes that are singlet, live, CD45hi, GFP+, CD4+ or CD8+ T cells. (B) Non-transplanted T cells from immune-intact PS-5X mice were gated on as lymphocytes that are singlet, live, CD45hi, CD4+ or CD8+ T cells. (C) PS-5X mice were analyzed with memory markers CD44 and CD62L.. These cells are lymphocytes, singlet, live, CD45hi, CD8+ that are either central memory (CD44+,CD62L+), effector memory (CD44+, CD62L-), effector (CD44-, CD62L-), or naive (CD44-, CD62L+) T cells.

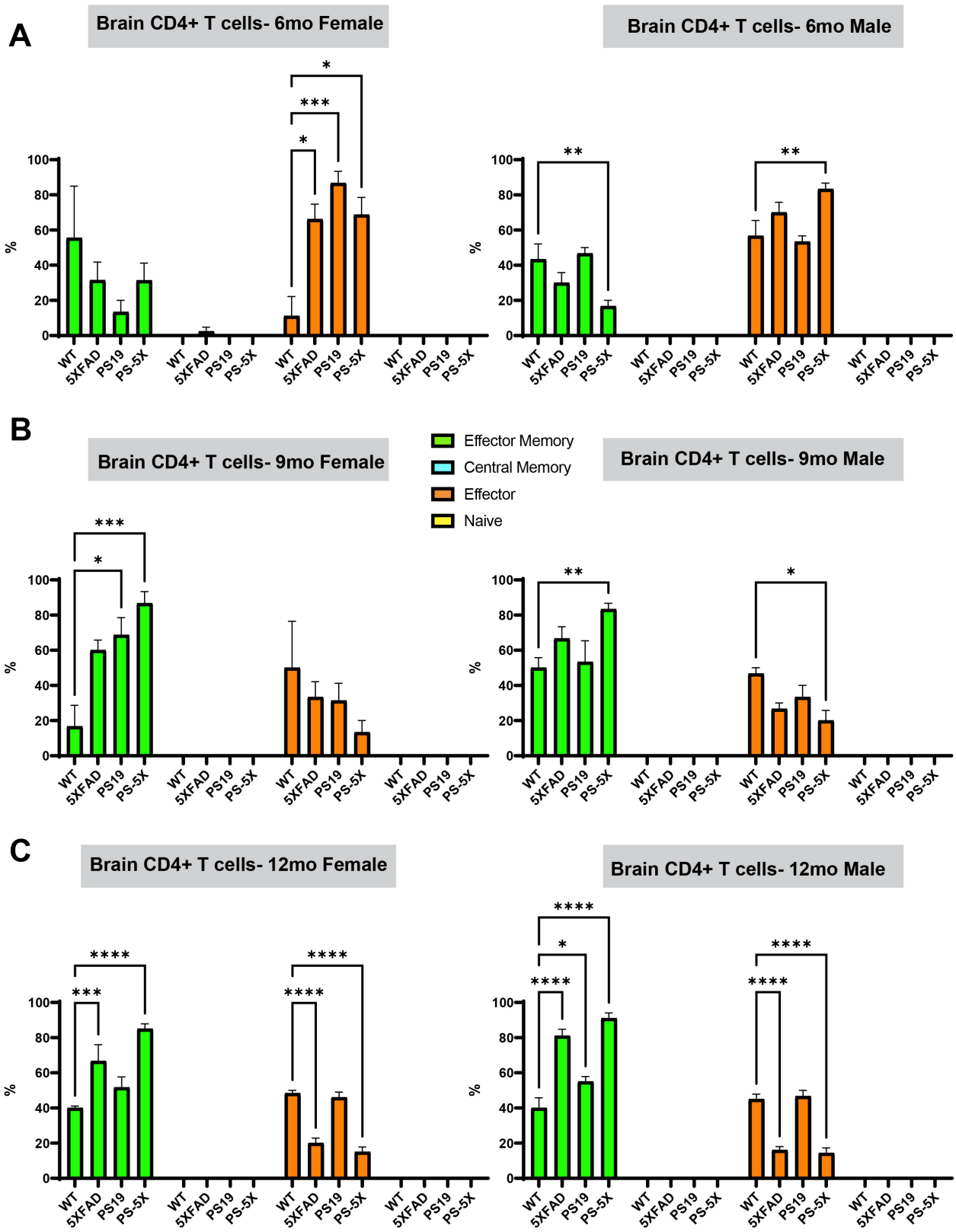

Figure S.2: Brain Memory CD4+ T cells. (Caption at end of appendix.)

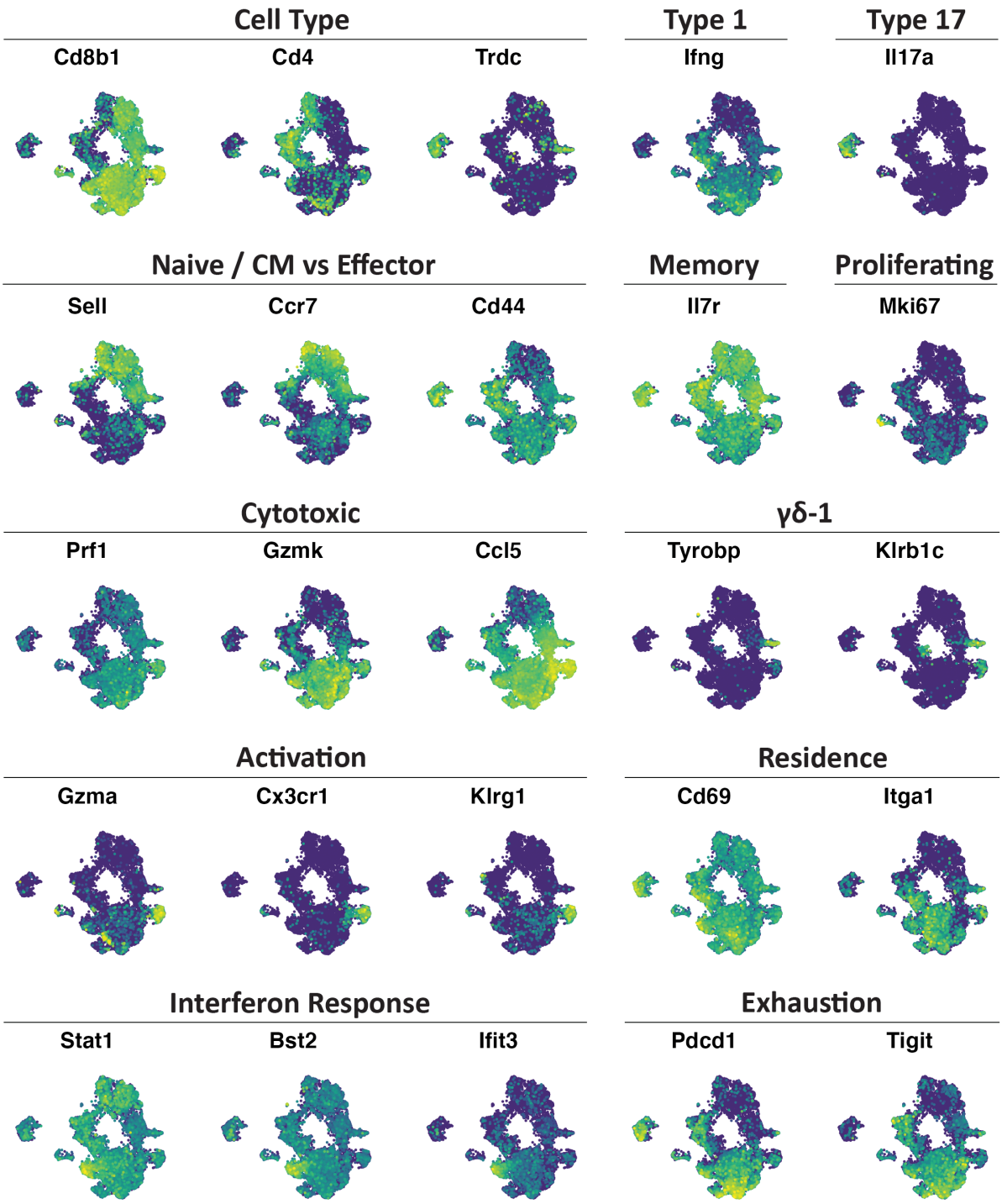

Figure S.3: Gene expression plots of cluster-defining genes. UMAPs of key genes used to annotate clusters, as well as several genes showing regions of tissue residence, interferon response, and proliferative exhaustion.

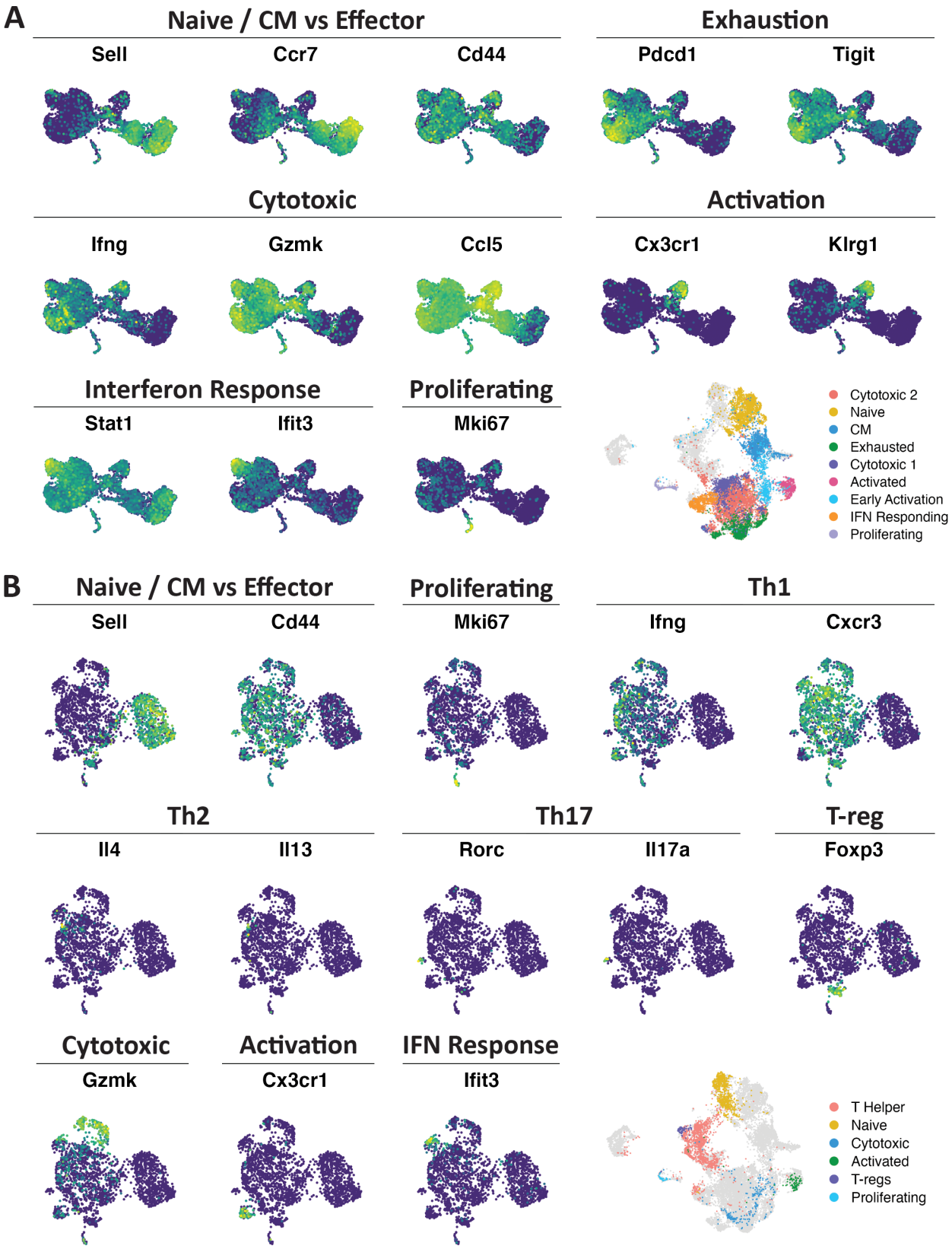

Figure S.4: Gene expression plots of CD8- and CD4-specific clustering. (Caption at end of appendix.)

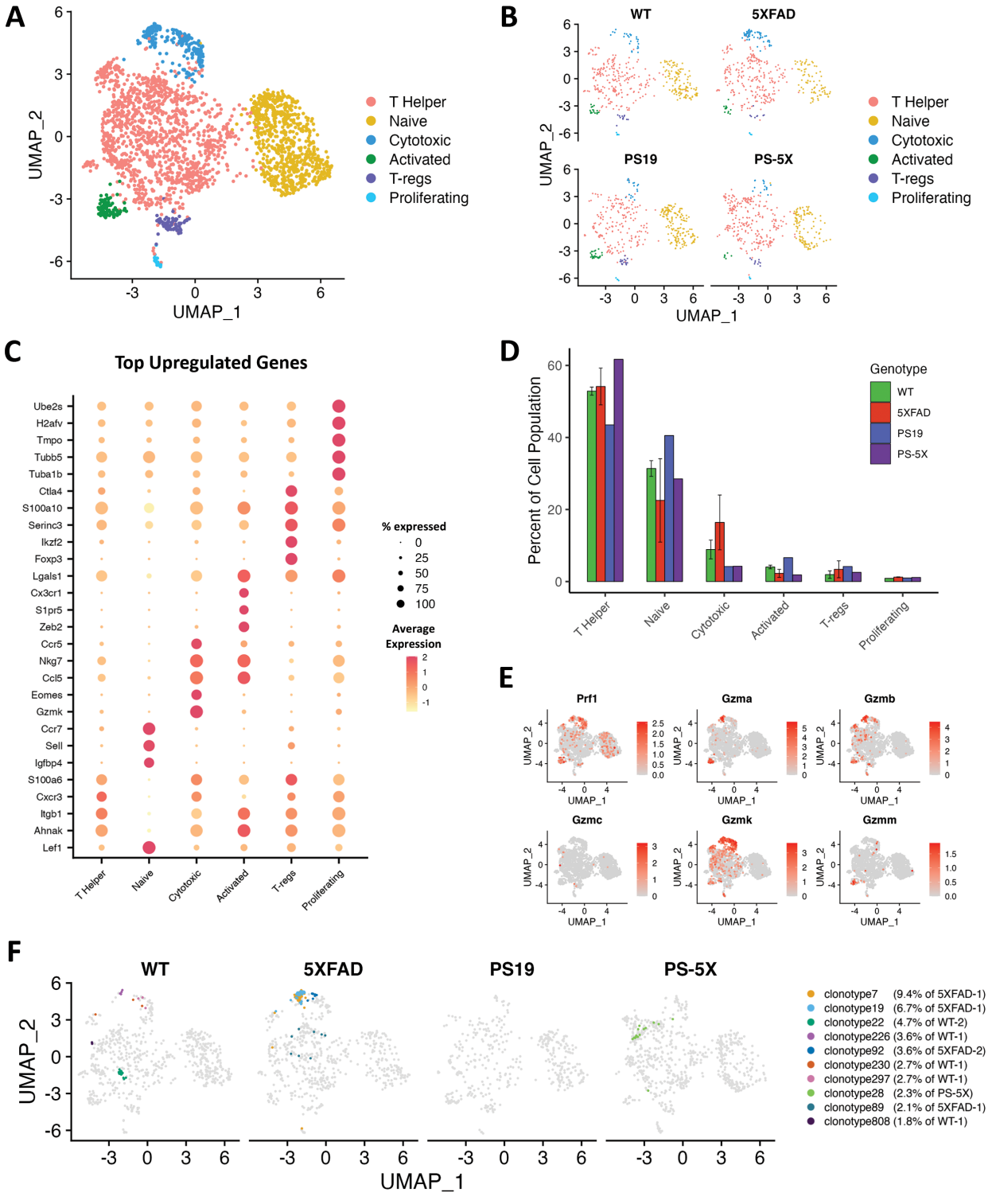

Figure S.5: Analysis of CD4+ T cell RNA and TCR expression. (Caption at end of appendix.)

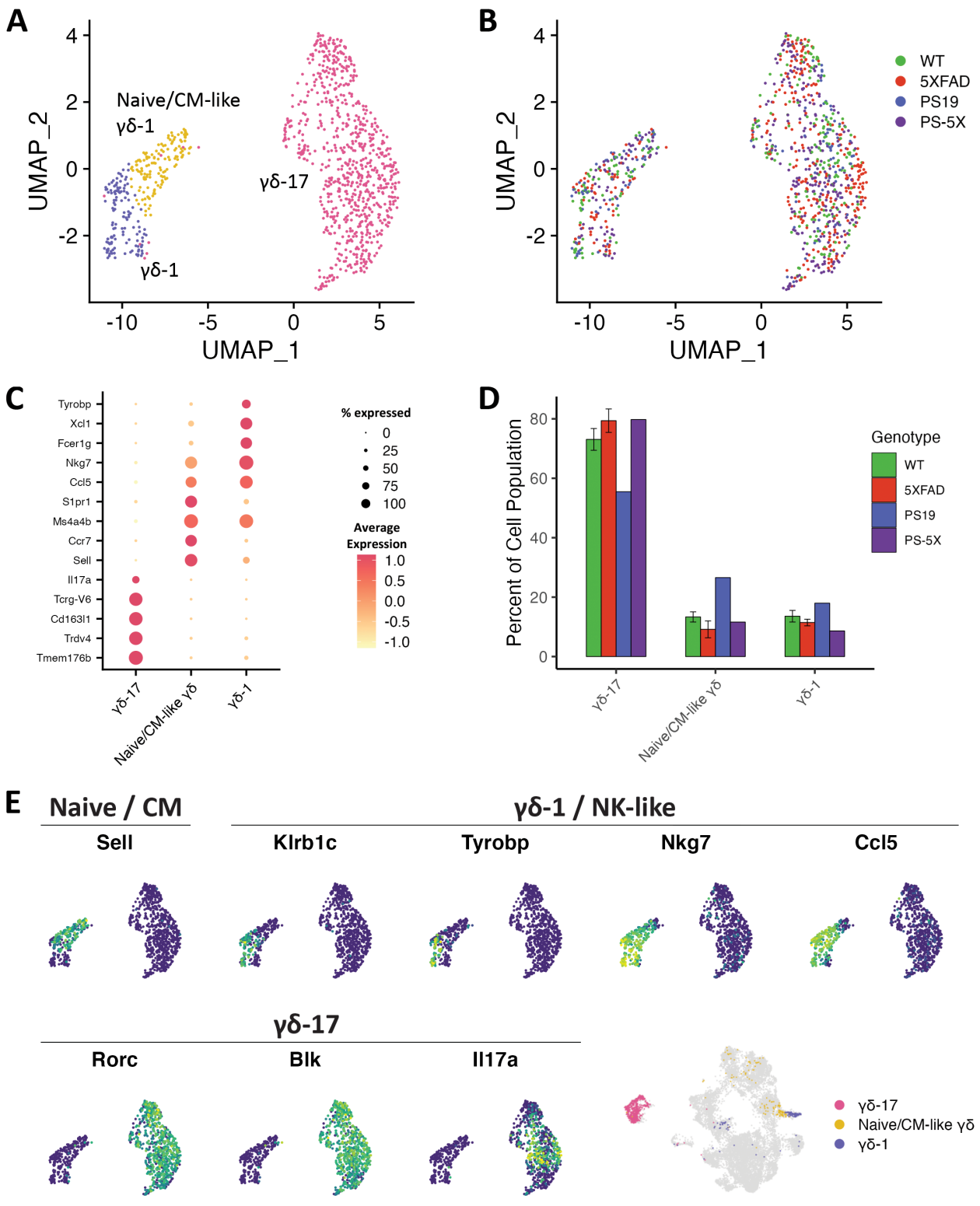

Figure S.6: Analysis of γδ cell RNA expression. (Caption at end of appendix.)

Figure S.2: Brain Memory CD4+ T cells. (A) 6mo female and male PS-5X, PS19, 5XFAD, and WT CD4+ T cells were analyzed via flow with memory markers CD44 and CD62L. Memory T cells were gated on as follows: central memory (CD44+,CD62L+), effector memory (CD44+, CD62L-), effector (CD44-, CD62L-), or naive (CD44-, CD62L+). (B) 9mo female and male PS-5X, PS19, 5XFAD, and WT CD4+ T cells were analyzed via flow with memory markers CD44 and CD62L. Memory T cells were gated on as follows: central memory (CD44+,CD62L+), effector memory (CD44+, CD62L-), effector (CD44-, CD62L-), or naive (CD44-, CD62L+). (C) 12mo female and male PS-5X, PS19, 5XFAD, and WT CD4+ T cells were analyzed via flow with memory markers CD44 and CD62L. Memory T cells were gated on as follows: central memory (CD44+,CD62L+), effector memory (CD44+, CD62L-), effector (CD44-, CD62L-), or naive (CD44-, CD62L+). Statistical significance was determined if $p < 0.05$.

Figure S.4: Gene expression plots of CD8- and CD4-specific clustering. (A) UMAPs of cluster-defining genes used for CD8-specific cluster annotation, followed by a UMAP showing the CD8 cell cluster locations in the full data set. (B) Expression of cluster-defining genes for CD4-specific cluster annotation, followed by a UMAP showing the CD4 cell cluster locations in the full data set.

Figure S.5: Analysis of CD4+ T cell RNA and TCR expression. (A) Clustering of CD4+ T cells after removal of CD8+ cells, γδ cells, and double-positive cells. The six clusters were identified by characteristic markers as T Helper (*Itgb1, Fasl, Tnfrsf4*), Naive (*Sell, Ccr7, Cd44-*), Cytotoxic (*Prf1, Gzmk*), Activated (*Ccl5++, Cx3cr1, Klrg1*), T-regs (*Foxp3, Il2ra, Ikzf2*), and Proliferating (*Mki67, Top2a*). (B) UMAP of clusters split by genotype. Cell populations were randomly downsampled for each genotype to match the smallest sample size, in order to reveal population differences. (C) Dot plot of the top 5 most up-regulated genes in each cluster. Dot color represents average expression value in the cluster, and dot size represents the proportion of cells in the cluster that express each gene. (D) Population analysis did not reveal significant differences in cluster proportions between genotypes. Error bars show maximum and minimum values for genotypes that have two samples. (E) UMAPs showing expression of several cytotoxic genes is high in both the “Cytotoxic” and “Activated” clusters, revealing a population of cytotoxic CD4+ cells. (F) Locations of the top 10 clonally expanded clonotypes assigned to CD4+ cells. Percentages are calculated as the number of CD4+ cells with a given clonotype divided by the total number of the sample’s CD4+ cells with any identified clonotype.

Figure S.6: Analysis of γδ cell RNA expression. (A) Clustering of γδ T cells after removal of CD8+ and CD4+ cells. The three clusters were identified by characteristic markers as γδ-17 (*Il17a, Rorc, Blk*), γδ-1 (*Ccl5, Nkg7, Ifng*), and Naive/CM-like γδ (*Sell, Ccr7, Ccl5, Nkg7*). (B) UMAP colored by genotype. (C) Dot plot of the top 5 most up-regulated genes in each cluster. (D) Population analysis did not reveal significant differences in cluster proportions between genotypes. Error bars show maximum and minimum values for genotypes that have two samples. (E) Expression UMAPs of key genes used for cluster annotation, followed by a UMAP showing the γδ cell cluster locations in the full data set.